The Pennsylvania State University

The Graduate School

Department of Astronomy and Astrophysics

THREE BODY DYNAMICS IN DENSE GRAVITATIONAL SYSTEMS

A Dissertation in

Astronomy and Astrophysics

by

Kenneth Moody

Submitted in Partial Fulfillment
of the Requirements
for the Degree of

Doctor of Philosophy

December 2009

The dissertation of Kenneth Moody was reviewed and approved[1] by the following:

Steinn Sigurdsson
Associate Professor of Astronomy and Astrophysics
Head of the Department of Astronomy Graduate Studies Dissertation Adviser
Chair of Committee

Prof. Donald Schneider
Professor of Astronomy and Astrophysics

Prof. Eric Feigelson
Professor of Astronomy and Astrophysics

Prof. Mercedes Richards
Professor of Astronomy and Astrophysics

Prof. James Kasting
Professor of Geoscience

[1]Signatures on file in the Graduate School.

Abstract

Three body dynamics are of particular interest in clusters where the density of stars provides many opportunities for interactions. Globular clusters, which have had densities of tens to hundreds of thousands of stars per cubic parsec for billions of years, are the ideal laboratory for studying dynamics in systems which at best have solutions in only the mathematical sense of the word. Modelling these systems in a realistic way which includes all stars individually represented, with their evolution and inclusion into a comparable number of binaries as is seen in observed clusters, has driven computer hardware and software for decades (Heggie & Hut 2003). In this thesis, I have used several techniques to answer the following questions: How many black hole binaries will a cluster produce, and will they have the required properties to be seen by our gravitational wave detectors? How often does the crowded environment of star forming cluster allow the exchange of a planet between stars? To answer these questions, I have studied three scenarios: the interaction of black holes in clusters, the effect of the Kozai mechanism on pulsars in clusters, and the effect of an exchanged planetary body on a planetary system.

I have examined the interactions of a system of black holes in a globular cluster in which the black holes have different masses with a more realistic distribution. This is an advance over previous studies which assumed that all black holes have the same mass, and as such when interacting tended to eject all but one or two from the cluster. The previous paradigm for black holes was that all black holes were 10 solar masses. In my thesis, black hole masses are derived from population synthesis models and span a range of a few up to 50 or 80 $M_{\odot}$ depending on metallicity. My new calculations have reduced the efficiency of three-body interactions in ejecting the binary due to their non-equal masses. I also use timescales derived from earlier simulations of clusters (Sigurdsson 1995) to determine the end state of individual binaries interacting with single black holes. While N-body simulations of black hole systems such as in O'Leary et al. (2006) are less model dependent, my method can easily adapt to advances in the understanding of the processes that make black holes and rapidly produce results on rates of binary black hole mergers for gravitational wave observations and the possibilities of intermediate mass black hole seeds.

Numerous black hole binaries are produced by clusters, they are hardened in the potential of the cluster, and the most massive black holes survive the interactions. Interactions with the other black holes preferentially produce binaries with higher eccentricities. I found that as many as one in seven binaries will coalesce within a Hubble time, and with the strength of signal that their higher mass gives they would rival galactic black hole binaries as a background source. Compare this to the more pessimistic forecast in Kulkarni et al. (1993) that they would not be a significant background source. I also found that the binaries are ejected from the cluster with, for the most part, a velocity just above the escape speed of the cluster which is a few tens of km/sec. These gravitational wave sources are thus constrained in their host galaxies as the galactic escape velocity is some hundreds of km/sec which only a very few binaries achieve in special cases (i.e.

originally forming as a tight binary, their first three-body interaction liberates a large amount of kinetic energy). It is therefore fitting to perhaps take a census of galaxies and their clusters within the radius the binaries would be visible to LIGO to estimate the how many sources could be seen, especially considering the first extra-galactic black hole in a globular cluster being recently discovered (Maccarone et al. 2007).

I studied the effect of the Kozai mechanism on two pulsars, one in the globular cluster M4, and the other J1903+0327. The M4 pulsar pulsar was found to have an unusually large orbital eccentricity, given that it is in a binary with a period of nearly 200 days. This unusual behavior led to the conclusion that a planet-like third body of much less than a solar mass was orbiting the binary. Dynamical exchanges can deposit the planet in a highly inclined orbit, which can lead to eccentricity pumping by the Kozai effect. The Kozai effect requires a minimum inclination of the two orbits of about 40 degrees. I used my own code to integrate the secular evolution equations with a broad set of initial conditions to determine the first detailed properties of the third body; namely that the mass of the planet is about that of Jupiter. The second pulsar J1903+0327 consists of a 2.15ms pulsar and a near solar mass companion in an $e = 0.44$ orbit. A preliminary study of this pulsar showed that the high eccentricity can be reproduced by my models, and there are three candidate clusters from which this pulsar could have originated.

My third project was a study of the effect of a planet at 50 AU on the inner solar system. The origin of this planet is assumed to be from an exchange with another solar system in the early stages of the sun's life while it was still in the dense star forming region where it was born. Similar studies have been done with the exchange of stars among binaries by Malmberg et al. (2007b). The exchange once again allows the Kozai effect to bring about drastic change in the inner system. A planet is chosen as the outer object as, unlike a stellar companion, it would remain unseen by current radial velocity and direct observation methods, although it could be detected by upcoming astrometric missions. My study uses an outer body from the size of a super Earth to a brown dwarf, in various inclinations, and exerting its influence on an inner object modelled on the Earth or Jupiter. The 50 AU size of the outer orbit corresponds with the sharp drop off in Kuiper Belt objects. This result represents the first step in a much larger project to fully explore the parameter space. I found that the size of the outer orbit drastically affects the eccentricity obtained by the inner object due to the beating of the Kozai and general relativistic precessions. I also found that four-body calculation are needed for a full understanding of how the change in the outer native object's eccentricity is propagated to the inner native object, native planets being those which are formed along with their host star. Simulations of young dense star forming clusters should illustrate how planetary sized objects are exchanged between stars.

I explored the dynamics of exchanges between objects and the workings of the Kozai mechanism in my first two projects. These tools prepared me for work on a crucial issue in planet formation, that of how a peculiar subset of observed planets were formed. I have shown that exchanges and the Kozai mechanism can work together to produce the observed eccentricities of exoplanets. This is a new approach to the study of the dynamics of planet formation.

TABLE OF CONTENTS

List of Tables

List of Figures

Acknowledgments

I would like to thank my advisor for discssions regarding some of the work in this thesis, including suggesting a well-defined project and helping me to understand some of the more subtle issues involved. I would like to thank my committee for their comments which helped to make this project more widely accessable. Finally, I would like to thank my mom, without whose support this would not have been possible. Her palpable relief when I finished this is almost as much a reward as my doctorate.

Chapter 1

Introduction

1.1 A History of the 3-Body Problem

1.1.1 Analytical Solutions and Partial Solutions

The problem of the motion of two bodies interacting by gravitation was solved as far back as Newton's *Principia* (1756). The common method for solving it today (such as found in Landau & Lifshitz (1969)) is to transform coordinates to the center of mass frame so that the two bodies are connected by the vector $\mathbf{r}$, use the total mass M and the reduced mass $m = m_1 m_2/(m_1 + m_2)$, and find constants of the motion. One of these is the angular momentum per unit mass

$$\mathbf{L} = \mathbf{v} \times \mathbf{r} \tag{1.1}$$

The constancy of the direction of $\mathbf{L}$ implies that the motion of the orbit is in a plane. The energy must also be constant and is given by

$$E = \frac{1}{2} m |\dot{\mathbf{r}}|^2 - \frac{GMm}{r} \tag{1.2}$$

These two constants reduce the problem to two first-order differential equations for the radial motion and the azimuthal motion. The radial motion is governed by a 1-D effective potential V(r) such that

$$V(r) = -\frac{GMm}{r} + \frac{L^2}{2mr^2}. \tag{1.3}$$

The shape of this potential is shown in Figure 1.1. The azimuthal motion shows that these orbits are closed, and the polar coordinate form of $r(\theta)$ shows they have the form of conic sections. At the minimum energy for a particular value of the angular momentum, $\dot{r} = 0$ and the orbit is circular. For energies approaching zero from below, the orbit becomes more eccentric. For $E \geq 0$, the orbit becomes open, at zero energy the orbit is a parabola, above that the orbit is a hyperbola.

The solution becomes much harder when one introduces a third body. The number of parameters jumps from 12 to 18 (three objects, three dimensions, both velocity and position). The barycenter motion provides six constraints, the conservation of angular momentum another three, and the conservation of energy provides one more. This leaves 8 unconstrained parameters which cannot be reduced further.

Interest in the astronomical application of the three-body problem began almost immediately after Newton's formulation of gravity. Euler was the first to do work in what was called lunar theory (Euler 1753). The most obvious three-body system is the

Sun-Earth-Moon system. Work on this system progressed by use of the restricted three-body problem. This simplification involves assuming that one of the bodies is massless, while the other two have a circular orbit. At around the same time, Lagrange (1772) came up with perhaps the most famous solution to the restricted three-body problem. Following the derivation and notation used in Valtonen & Karttunen (2006), the origin of the coordinate system is placed at the center of mass. The total mass of the two major bodies as well as the distance between them is normalized to 1, the secondary is given a mass of μ, which is also the distance of the primary from the origin. The term μ is called the reduced mass, and is defined in terms of the two large masses by the relation $\mu = m_1 m_2/(m_1 + m_2)$. The reduced mass is used to define other dynamical variables such as the chirp mass, which is related to the strength of gravitational radiation from a binary and is defined by $M_{ch} = \mu^{2/5} M^{3/5}$. The stationary system has axes labeled by $\underline{\xi}, \underline{\eta}$, while the rotating coordinate axes are called ξ and η. The transformation between the two systems is given by

$$\underline{\xi} = \xi \cos t - \eta \sin t \tag{1.4}$$

$$\underline{\eta} = \xi \sin t + \eta \cos t \tag{1.5}$$

assuming that the angular velocity of the rotating frame is alos normalized to 1. The Hamiltonian for the third object in the rotating frame is

$$H = \frac{1}{2}(P_\xi^2 + P_\eta^2) + P_\xi \eta - P_\eta \xi - \frac{1-\mu}{\rho_1} - \frac{\mu}{\rho_2} \tag{1.6}$$

with ρ_1 and ρ_2 being the distance from the third body to the primary and secondary respectively. The equations of motion determined from the Hamiltonian for the third body are

$$\ddot{\xi} - 2\dot{\eta} = \frac{\partial \Omega}{\partial \xi} \tag{1.7}$$

$$\ddot{\eta} + 2\dot{\xi} = \frac{\partial \Omega}{\partial \eta} \tag{1.8}$$

with the $2\dot{\xi}$ and $2\dot{\eta}$ terms representing the Coriolis force. The term Ω is the effective potential which determines the motion of the third object and is given by

$$\Omega = \frac{1}{2}(\xi^2 + \eta^2) + \frac{1-\mu}{\rho_1} + \frac{\mu}{\rho_2} \tag{1.9}$$

Combining the two equations of motion, one finds that the requirement that the square of the velocity of the third body $v^2 = \dot{\xi}^2 + \dot{\eta}^2$ being positive constrains its location. Five points are extrema or saddle points of the co-rotating potential Ω. Three lie along the line connecting the two main bodies and are unstable to perturbations in the plane of the orbit (see Figure 1.2. Two other points form equilateral triangles in the co-rotating frame and are stable for a small enough second body ($\mu < 0.0385$, Szebehely 1967). Instances of objects in Lagrangian points include the Trojan asteroids 60 degrees ahead

and behind Jupiter, and artificial objects such as the WMAP and soon to arrive Herschel satellites at the Sun-Earth L2 point.

The other planets also provide modification from the simple interaction of the Sun and Earth. There was concern over the stability of the solar system at a time when the system was thought to be young enough such that not all possible configurations could have occured. Stability was examined by expanding the dependence of the semimajor axes as a function in time as a series in the mass and check for terms which grew with time. Laplace et al. (1829) performed this expansion and found that, for small eccentricities and up to terms proportional to m^2, the semimajor axes of the orbits are bounded. Lagrange (1776) proved the same for general eccentricities but also only to terms proportional to m^2. Poisson (1808) expanded the series to include terms of m^3, and found that there are terms for the semimajor axis that do explicitly depend on time. This implies that instead of being limited to an annulus, a body may drift in space over long periods of time.

Comets also provided an interesting problem for celestial mechanics. Halley was the first to predict the return of his eponymous comet in 1758 based on calculations of its orbit using Newton's theory of gravity. But, as calculated by Clairaut (1760), interactions with Jupiter delayed the comet until later that year. Encounters with Jupiter were also proposed for the conversion of comets from long periods to short periods, this process being called the capture hypothesis. A comet discovered by Messier in 1770 was calculated by Lexell (1778); Lexell & Maskelyne (1779) to have been put on a 5.6 year orbit by a close passage by Jupiter. Another close passage was speculated to have removed it from the inner solar system. More on the capture hypothesis was developed by Laplace and Leverrier and Tisserand (1889). The first detailed calculations of probabilities of Jupiter converting comets to short periods was done by Newton (1893).

An ultimate solution to the three body problem was the challenge made by Swedish King Oscar II. It was to take the form of a power series, and was to describe for all time the position and velocity of the three bodies. Poincaré came close enough to a solution to be awarded the prize with his work as published in *Les Méthodes nouvelles de la mécanique céleste* in 1892, 1896, and 1899. It was Sundman (1912) who actually put forth the correct final solution. However, this series solution converges so slowly as to require millions of terms to obtain reasonable accuracy. It was therefore to numerical integration of the trajectories that most attention turned.

1.1.2 Numerical Integration of the Three-body Problem

Instead of searching for (and not finding) a workable analytic solution to the movement of three bodies under the influence of gravity, one could just use Newton's first law and just integrate the equations of motion

$$\ddot{\mathbf{r}}_\mathbf{i} = \frac{Gm_j}{r_{ij}^3}\mathbf{r}_{ij} + \frac{Gm_k}{r_{ik}^3}\mathbf{r}_{ik} \tag{1.10}$$

for each of the three objects, with the indices i, j, k running from 1 to 3, and $\mathbf{r}_{ij}$ and $\mathbf{r}_{ik}$ being the vectors from the first to the second objects, and first to the third objects

respectively. Unlike the computational challenges of a large system of particles, integration of three-body systems is a easily manageable task, and can be even done even without use of today's fast computers. Early attempts at numerical integration of three-body motion were done on specific initial conditions. One such example is the problem studied by Burrau (1913) where the three bodies were set at the corners of a 3-4-5 right triangle with the mass of each body corresponding to the length of the side opposite it. The positions and velocities are calculated from the forces on them, each being moved in turn by a time step. The late stages of the paths of the three objects with this starting point calculated by Szebehely & Peters (1967) are shown in Figure 1.3.

Initial conditions for starting the integration need to be considered carefully in order to properly explore the parameter space. These conditions include six values for the velocities of the objects (three of the nine being able to be reduced by moving to the center of mass frame), two values describing which direction the third object is coming from, and two values for the mass ratios between the objects. By proper scaling, rotations, and translations, the three objects can be placed so that two sit at either end of a line segment of length 1 centered at the origin, while the third object is somewhere in the region defined as the part of the circle of radius 1 and centered at the left object that lies within the first quadrant.

This generator for the initial conditions is shown in Figure 1.4. Such conditions were set up by Anosova et al. (1994) (with zero velocity conditions) and Anosova (1990) (with non-zero velocities). Of greatest interest in starting conditions are those provided by context within a larger simulation. Simulations such as those by Aarseth (1963); Aarseth & Zare (1974) often have a close passage of a binary with a field star, which requires what is called regularization. Regularization is the process by which the equations of motion for two bodies which includes a singularity for zero distance between the bodies is smoothed into a easily integrable system which also includes the perturbation from the third body. In the process of integrating three-body motions as well, sometimes close passages between two of the objects must be regularized as well. The standard regularization technique now used is that formulated by Kustaanheimo & Stiefel (1965), which is viewed as a watershed moment for simulations of three or more body systems.

The interaction of three bodies is most often expressed in astrophysical situations as the interaction of a binary with a single object. Heggie (1975) did an early comprehensive study of this crucial issue in dynamics which explored the most common outcomes. Hut (1983) explored the qualitative states that three body systems originally consisting of a binary and a third object may undergo in the process of their interaction. At all energies, scattering can occur when a binary and the third object may come together, interact for a while, and then recede, with or without the binary having exchanged membership. For positive total energy, the binary may even be broken up in a process called ionization. If the system has negative energy, the three bodies may exist in a resonant state for many orbital times of the inner binary before decaying into a binary and single star. Of course there exist bound states where all three objects have stable widely separated orbits. Trajectories that start as a free binary and single object and end with a bound stable triple are highly unlikely to occur from random initial conditions, as are direct collisions between objects; these are said to belong to a set with zero measure in the parameter space of initial conditions. Some work was started by Hills (1975)

and Valtonen & Aarseth (1977) on the interactions of binaries with single stars, then Hut & Bahcall (1983) began a multi-part series (continued in Hut (1993) and Heggie et al. (1996)). The goal of Hut's project was to systematically explore via Monte Carlo methods the parameter space of possible binary-single star interactions and compute cross-sections for the possible types of outcomes. These cross-sections can then in turn be used in more aggressive simulations of dense clusters where binary-single interactions are expected to be common (c.f. Sigurdsson & Phinney (1993) and Figure 1.5).

1.2 Compact Objects in Dense Clusters

Interest in compact objects in globular clusters began with the launch of a generation of X-ray telescopes in the early to mid 70's (e.g. Uhuru 1971, COS-B 1975). These telescopes found numerous sources in globular clusters such as NGC 1851, 6441, 6624, and M15 (Clark 1975; Clark et al. 1975). Two models evolved to explain the source of the x-rays in these clusters. Bahcall & Ostriker (1975), Silk & Arons (1975), and Grindlay & Gursky (1976) proposed that the source was a black hole accreting gas ejected from stars late in their evolution. Their calculation showed that for the observed flux the mass of the black hole had to be in the $100 - 1000 M_{\odot}$ range, what today would be referred to as an intermediate mass black hole, although they were not called such back then. M15 was particularly interesting for this theory as its light density profile showed a cusp in the center (King 1966, 1975). Dynamical simulations of clusters showed that the inner regions tended to collapse and, in the limit of point masses with no binaries, reach infinite density. The considerably more massive stellar remnants are found to sink to the centers of clusters, and from there were expected to coalesce through 3-body interactions and gravitational radiation. It was therefore previously theorized that there would be massive black holes in the centers of globular clusters (Spitzer (1975) and Wyller (1970) but for different reasons).

An alternate explanation of the X-ray sources proposed that they were much smaller accreting compact objects in binaries. Bursts from these X-ray sources were an early indication that the accreting compact object model was the correct one. Swank et al. (1977) made an analogy between long bursts seen in the Crab Nebula and the short ones seen in globular clusters, suggesting that they shared the same mechanism, namely matter accreting onto a neutron star. Another one of the primary tests for which model was correct was to see if the x-ray sources were centered in the clusters. That would have to wait for the next generation of telescopes, such as the Einstein satellite, with higher resolution. Such measurements were made by Grindlay et al. (1984), who found that the X-ray sources were at a radial distance consistent with objects of 0.9-1.9$M_{\odot}$ which imply a neutron star with a low-mass companion.

Alpar et al. (1982) first suggested that a moderately spinning neutron star could be brought up to a period of milliseconds by gaining angular momentum from an accretion disk, provided it had a low enough magnetic field. Starting in 1987 with the confirmation of pulsations from a steep spectrum radio source in M28 by Lyne et al. (1987), radio observations of globular clusters turned up a population of pulsars. Periods of under half a second found for the pulsars and the ancient age of the clusters point to the fact that these pulsars had been spun-up. Scenarios for the transformation of cluster LMXBs into

millisecond pulsars were developed, such as ablation of the secondary star by Fruchter et al. (1988) (aka the "Black Widow" pulsar) or by dynamical interactions in the cluster (Rappaport et al. 1989). The ratio of X-ray binaries in globular cluster versus in the field per unit stellar mass is 100. This suggests that the density of the globular cluster environment may have something to do with their formation.

The discovery of pulsars in globular clusters has so far been driven by the sensitivity of the detectors available; as indicated in Bailyn (1991) the lower limit on flux for the then known 21 pulsars was consistent with detector limits. With the commissioning of new radio telescopes, and particularly of the GBT and its associated state of the art reduction techniques, the discovery rate of pulsars in globular clusters quickened considerably. Ransom (2008) (from which Figure 1.6 was derived) reviews some of the more exotic pulsars, including the fastest spinning pulsar at 716Hz (Hessels et al. 2006) and very heavy pulsars (Freire et al. 2008a,b).

With the discovery that X-ray sources in globular clusters were consistent with being powered by neutron stars, the idea of globular clusters containing black holes was passed over for a while. One major concern for producing compact objects in clusters is their shallow potential well ($v_{esc} \sim 30 - 50$km/sec). The natal kick of neutron stars is determined from the current space velocities of pulsars (c.f. Cordes (1986); Lyne & Lorimer (1994); Harrison et al. (1993)) to be around 150km/sec with a tail to a few hundred km/sec. This implies that only a fraction (15% to 30% from Verbunt & Hut (1987); Hut et al. (1991), 4% to 15% from Ivanova et al. (2008)) of compact stars from supernovae could be retained. With the discovery of numerous pulsars in globular clusters through the 80's and early 90's, however, the lack of observed black holes started to be revisited. Given a standard Salpeter IMF, the number of neutron stars seen today would indicate that hundreds of black holes were produced in each cluster. Other opinions stated that the observed IMF of globular clusters is not Salpeter (McClure et al. 1986), and that the high mass stars produced by a Salpeter mass function would, upon their deaths, unbind the cluster through mass loss (Grindlay 1987; Chernoff & Weinberg 1990). The origin of the observed neutron stars is then due to the accretion induced collapse of white dwarfs (Bailyn & Grindlay 1990). Kulkarni et al. (1993) and Sigurdsson & Hernquist (1993) prefer the explanation that the clusters had a standard mass function, including the formation of black holes, which then ejected themselves through dynamical processes. The black holes, being much heavier than the average star, sink very quickly (core relaxation timescale) to the center and begin, by three-body interactions to form binaries. Binary black holes interacting with single black holes tend to harden the binary and the potential energy liberated is used to eject the single object and possibly the binary as well. The result is that, except for a single or binary object, the black holes are expelled.

These discussions assume that all black holes form with a mass of $10M_{\odot}$. Miller & Hamilton (2002a) used four-body interactions to produce a triple system which induced a merger. The threshold mass for a black hole to be retained is set by Miller & Hamilton (2002b) to be $50M_{\odot}$. With $10M_{\odot}$ black holes, this would require a few successful mergers to obtain this size. Other ways a merger might be more successful would be if the black holes were not of identical mass. Sigurdsson (1995) found that more unequal mass ratio binaries were less likely to be ejected by superelastic recoil that equal mass ones. Recent

population synthesis models, such as Belczynski et al. (2008) have shown that not all black holes are created equal, and some exceptional ones such as those formed during the merger of a common envelope binary can already exceed the threshold mass derived by Miller & Hamilton (2002b). Once it has come to dominate the center of the cluster, such a black hole could accrete other black holes (Miller & Hamilton 2002b) and grow to $10^3 M_\odot$. There are a few ways a massive object is expected to affect the dynamics of the cluster. A cusp in the center of M15's velocity dispersion seen by Larson (1984) and later by van den Bosch et al. (2006) as evidence of extra non-luminous matter (many light objects in the first case, a single large object in the second case), while the lack of the cusp in observations by Lauer et al. (1991) is used as evidence against a massive object at the center of M15. Trenti et al. (2007); Heggie et al. (2007) suggest an increase in the ratio of the core radius to the half-mass radius could be due to the influence of a massive central object, but Hurley (2007) gives a note of caution about this suggestion. Finally, if a massive binary is present in the center of the cluster, perhaps rotation of the cluster could be caused by transfer of angular momentum as modeled by Mapelli et al. (2005) with possible observations by Gerssen et al. (2002); van der Marel et al. (2002); Gebhardt et al. (2005). In any of these cases, along with the sole case of an ultraluminous x-ray source in a globular cluster in NGC 4472 (Maccarone et al. 2007), the evidence for a bona fide intermediate mass black hole is still thin.

1.3 Eccentric Exoplanets

1.3.1 Extrasolar Planet Discoveries

The extrasolar planet (exoplanet) revolution was kicked off by the discovery of the 4.23 day variation in radial velocity by Mayor & Queloz (1995) attributed to the pull of a Jupiter-mass planet going around 51 Pegasi, although there had been a precursor by Wolszczan & Frail (1992) of planets around a pulsar. The location of these large planets very close to their host stars, although making them easy to find, proved a puzzle to planet formation models. Normally, Jovian planets were expected to form far from their central star where gas was plentiful and cold so that it could be easily accreted. Because of the discovery of these "hot Jupiters", models began to be proposed (e.g. Papaloizou & Terquem (2006)) that would cause the newly formed massive planets to migrate from where they formed to where we see them today. These close in planets have the almost zero eccentricities one would expect for planets for which tidal circularization is expected to be efficient, with some exceptions addressed by Matsumura et al. (2008).

The next puzzling class of exoplanets are those called "eccentric warm Jupiters" typified by the discovery of the planet around 70 Vir by Marcy & Butler (1996), whose radial velocity curve is seen in Figure 1.7. Formation scenarios tend to place planets in circular orbits, so the large observed eccentricities are due to perturbations that may come early in the history of the system such as interactions with the planetesimal system (Murray et al. 1998) or while the protoplanetary disk was still extant (Goldreich & Tremaine 1980; Papaloizou et al. 2001; Cresswell et al. 2007), or later on. The later influences that have been suggested are, in order of increasing intimacy to the planetary system, close passages by a star that excite the eccentricity (Laughlin & Adams 1998;

Hurley & Shara 2002; Zakamska & Tremaine 2004), continuous disturbance to the orbit by a distant planet or stellar companion (Holman et al. 1997; Mazeh et al. 1997; Ford et al. 2000b; Takeda & Rasio 2005), or planet-planet scattering among a few (Rasio & Ford 1996; Weidenschilling & Marzari 1996a; Veras & Armitage 2004, 2005) or 10 to 100 planets (Papaloizou & Terquem 2001; Adams & Laughlin 2003; Jurić & Tremaine 2008). The goal of the simulations is to be able to reproduce the distributions of eccentricities with semimajor axis. Jurić & Tremaine (2008) obtained too few planets with $e \leq 0.2$, and so a mechanism which, while efficiently producing planets with eccentricities as high as that observed for HD80606b, can still leave some planetary systems unmolested, including our own solar system which oddly contains planets in co-planar nearly circular orbits.

The reaction of planets to the interaction of stars in dense clusters is an ongoing problem of interest. Interactions of stars, besides increasing the eccentricity of planet around stars in open clusters, as found by Laughlin & Adams (1998), can also go so far as to remove planets from their host star entirely in the densest clusters (Hurley & Shara 2002). Malmberg et al. (2007b); Malmberg & Davies (2009) study how in dense star forming regions, stars may interact, exchange binary members, and explain how that goes on to affect the eccentricities of native planets. Five percent of stars like the sun have had a close pass of a couple hundred AU while in the dense environment of the star forming region. This is close enough for stellar encounters to swap stars and create a situation where the new star's (likely) inclined orbit can induce a large eccentricity on the planets of the inner system. They manage to reproduce, for low to moderate eccentricity systems, the distribution of eccentricities for planets situated a few AU from its host star. This is a good start, but a complete understanding should cover a broader area of parameter space.

1.3.2 The Kozai Mechanism

A hierarchical triple system can be thought of for the purpose of dynamics as two separate orbits that have some crosstalk. The name of the Kozai mechanism came from Kozai (1962), a study of Jupiter's perturbation of asteroid orbits. Since then, it has been invoked in such widely ranging topics as supermassive black hole mergers (Blaes et al. 2002), stellar mass black hole mergers (Miller & Hamilton 2002a), and planet-planet scattering (Ford et al. 2005). The Hamiltonian for the system is given by the following (Harrington 1968)

$$\mathcal{F} = \frac{k^2 m_0 m_1}{2a_1} + \frac{k^2 m_2 (m_0 + m_1)}{2a_2} + \frac{k^2}{a_2} \sum_{j=2}^{\infty} \alpha^j M_j \left(\frac{r_1}{a_1}\right)^j \left(\frac{a_2}{r_2}\right)^{j+1} P_j(\cos\Phi) \qquad (1.11)$$

with k^2 the gravitational constant. As is shown in the schematic in Figure 1.8, m_0 and m_1 are the masses of the inner objects, m_2 the mass of the outer object, a_1 and a_2 the inner and outer semimajor axes, α the ratio a_1/a_2, r_1 the separation of the inner objects, r_2 the distance from the inner object's center of mass to the outer object, P_j the Legendre polynomial, Φ the angle between r_1 and r_2, and

$$M_j = m_0 m_1 m_2 \frac{m_0^{j-1} - (-m_1)^{j-1}}{(m_0 + m_1)^j} \tag{1.12}$$

The angular momenta L_i, reduced angular momenta G_i, and harmonic angular momenta H_i are given by the following

$$L_1 = \frac{m_0 m_1}{m_0 + m_1} \sqrt{k^2 (m_0 + m_1) a_1} \tag{1.13}$$

$$L_2 = \frac{m_2 (m_0 + m_1)}{m_0 + m_1 + m_2} \sqrt{k^2 (m_0 + m_1 + m_2) a_2} \tag{1.14}$$

$$G_j = L_j \sqrt{1 - e_j^2} \tag{1.15}$$

$$H_j = G_j \cos i_j \tag{1.16}$$

with the conjugate angles for the momenta being the mean anomaly l_i, the argument of periastron g_i, and the angle of the nodes h_i. The nodes are eliminated by the method of Jefferys & Moser (1966), then the Hamiltonian is transformed by the von Zeipel method so that the short term variations represented by the dependence on the l_i are removed as is demonstrated in Hagihara (1972). Here are given the equations governing the evolution of the arguments of periastron and eccentricities of the two orbits as given by equations (29)-(32) of Ford et al. (2000b) with the correction to the sign of C_3 as found by Blaes et al. (2002). An example of the evolution for various initial conditions, see Figure 1.9. For the quadrupole equations, only the C_2 term of dg_1/dt and de_1/dt survive, and $de_2/dt = dg_2/dt = 0$.

$$\theta = \cos i = \frac{H^2 - G_1^2 - G_2^2}{2 G_1 G_2}$$

$$\cos(\phi) = -\cos(g1)\cos(g2) - \theta \sin(g1)\sin(g2)$$

$$C_2 = \frac{k_2^2}{16} \frac{(m_0 + m_1)^7}{(m_0 + m_1 + m_2)^3} \frac{m_2^7}{(m_0 m_1)^3} \frac{L_1^4}{L_2^3 G_2^3}$$

$$C_3 = -\frac{15}{16} \frac{k_2^2}{4} \frac{(m_0 + m_1)^9}{(m_0 + m_1 + m_2)^4} \frac{m_2^9 (m_0 - m_1)}{(m_0 m_1)^5} \frac{L_1^6}{L_2^3 G_2^5}$$

$$B = 2 + 5e_1^2 - 7e_1^2 \cos(2g_1)$$

$$A = 4 + 3e_1^2 - \frac{5}{2}(1 - \theta^2) B$$

$$\frac{dg_1}{dt} = 6C_2(\frac{1}{G_1}(4\theta^2+(5\cos 2g_1-1)(1-e1^2-\theta^2))+\frac{\theta}{G_2}(2+e1^2(3-5\cos 2g_1)))-5\theta B\cos\phi)$$
$$-C_3e_2(e_1(\frac{1}{G_2}+\frac{\theta}{G_1})(\sin g_1\sin g_2(A+10(3\theta^2-1)(1-e_1^2))$$
$$-\frac{(1-e_1^2)}{(e_1G_1)}(\sin g_1\sin g_2 10\theta(1-\theta^2)(1-3e_1^2)+\cos\phi(3A-10\theta^2+2))) \quad (1.17)$$

$$\frac{de_1}{dt} = C_2\frac{1-e_1^2}{G_1}30e_1(1-\theta^2)\sin 2g_1+C_3e_2\frac{1-e_1^2}{G_1}(35\cos\phi(1-\theta^2)e_1^2\sin 2g_1)$$
$$-10\theta(1-e_1^2)(1-\theta^2)\cos g_1\sin g_2-A(\sin g_1\cos g_2-\theta\cos g_1\sin g_2)) \quad (1.18)$$

$$\frac{dg_2}{dt} = 3C_2(\frac{2\theta}{G_1}(2+e_1^2(3-5\cos 2g_1))+\frac{1}{G_2}(4+6e_1^2+(5\theta^2-3)(2+e_1^2(3-5\cos 2g_1))))$$
$$+C_3e_1(\sin g_1\sin g_2(\frac{4e_2^2+1}{e_2G_2}10\theta(1-\theta^2)(1-e_1^2)$$
$$-e_2(\frac{1}{G_1}+\frac{\theta}{G_2})(A+10(3\theta^2-1)(1-e_1^2)))+\cos\phi(5B\theta e_2(\frac{1}{G_1}+\frac{\theta}{G_2})+\frac{4e_2^2+1}{e_2G_2}A)) \quad (1.19)$$

$$\frac{de_2}{dt} = -C_3e_1\frac{1-e_2^2}{G_2}(10\theta(1-\theta^2)(1-e_1^2)\sin g_1\cos g_2+A(\cos g_1\sin g_2-\theta\sin g_1\cos g_2)) \quad (1.20)$$

Qualitatively, the Kozai mechanism transfers angular momentum from the mutual inclination of the orbits to the eccentricity of the inner orbit. In the case of the quadrupole, where only the first term of the power series of the Hamiltonian is used, the eccentricity and inclination relative to the total angular momentum of the outer orbit remain fixed, so that the inner orbit responds to the perturbation of the outer body. The constancy of e_2 leads to an integral of the motion $\sqrt{1-e_1^2}\cos i$ remaining constant as well. For the octupole description, where the second term of the power series in the Hamiltonian is considered, the outer orbit is free to respond to changes in the inner orbit. Since the octupole description includes terms to order α^3, precession of the orbit due to general relativity must also be included as it depends on $\alpha^{5/2}$. Precession due to GR, or to some other source, can, if it is faster than the precession induced by the Kozai mechanism, wash out the resonance needed to pump the eccentricity.

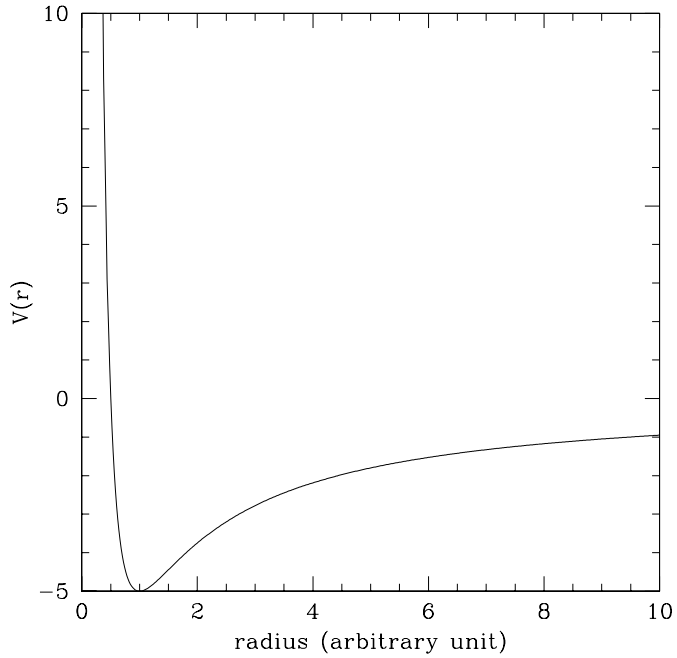

Fig. 1.1 Effective potential of the two-body system.

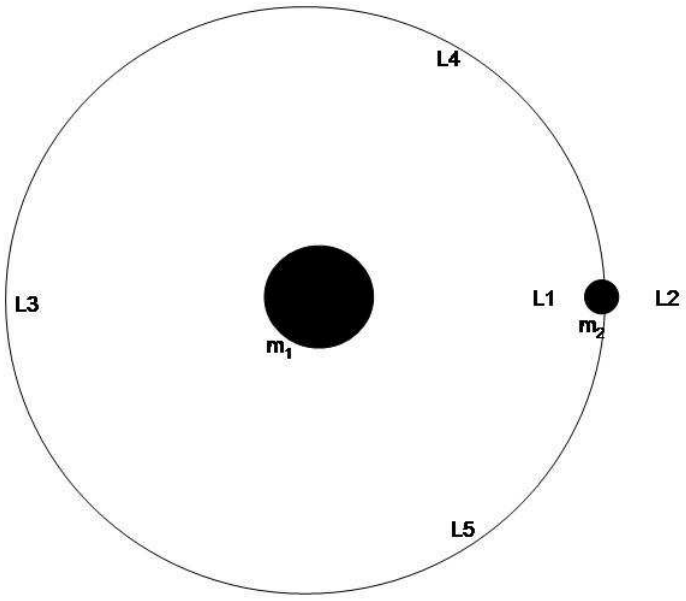

Fig. 1.2 Positions of the Lagrangian points in the restricted 3-body problem. L4 and L5 are stable, while L1-3 are only stable to vertical perturbations.

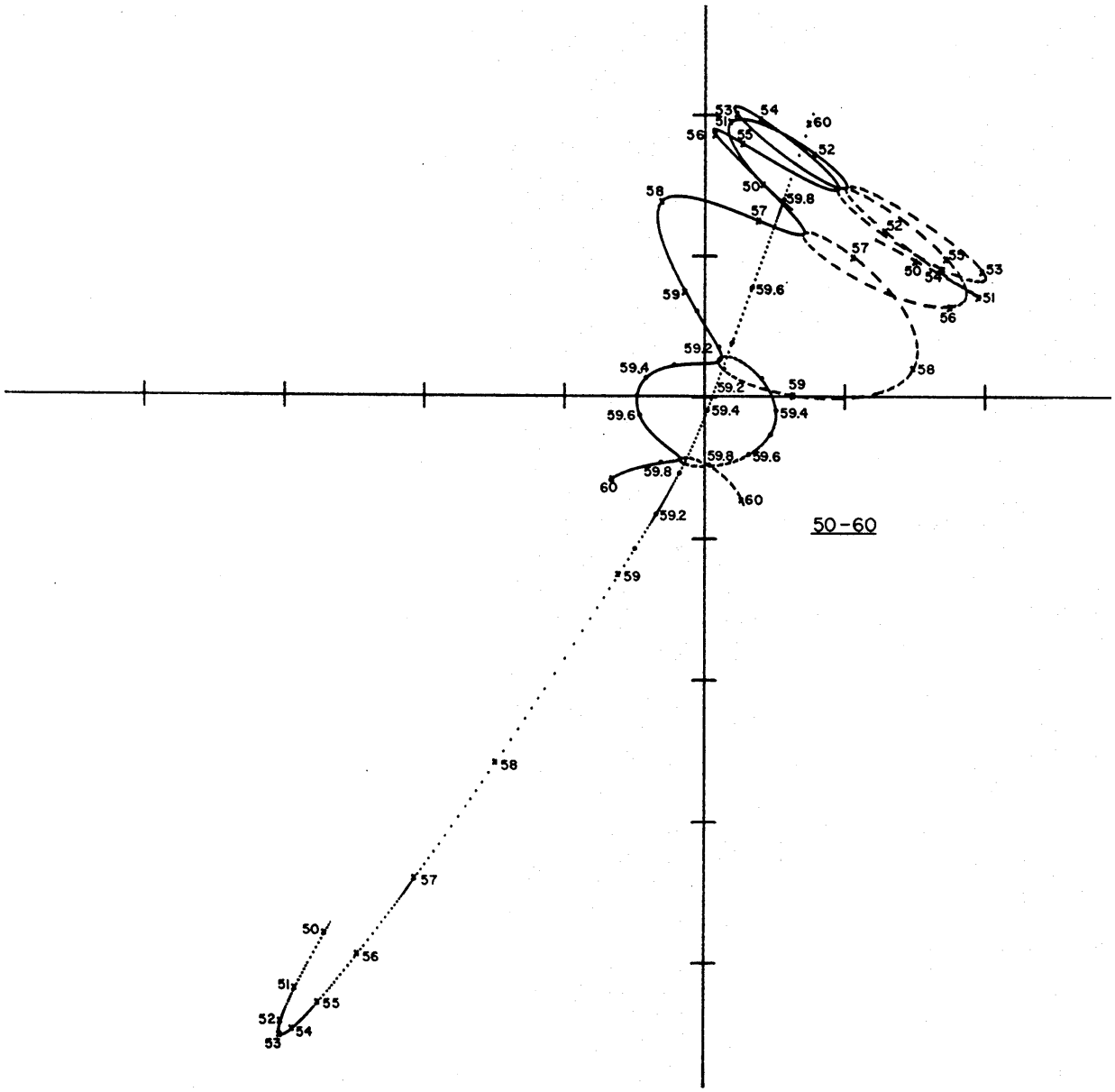

Fig. 1.3 Early numerical integration attempt on a special set of initial conditions. General behavior of one binary and one escaped body in the final state is evident. From Szebehely & Peters (1967).

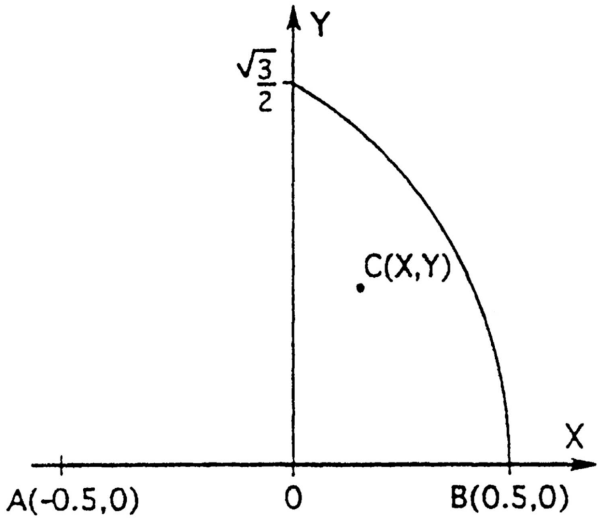

Fig. 1.4 Allowed region for picking three-body integration initial conditions. Besides its location, ten other initial conditions for describing the masses, orientation, and velocities are needed to fully describe the set up for a particular interaction. From Anosova et al. (1994).

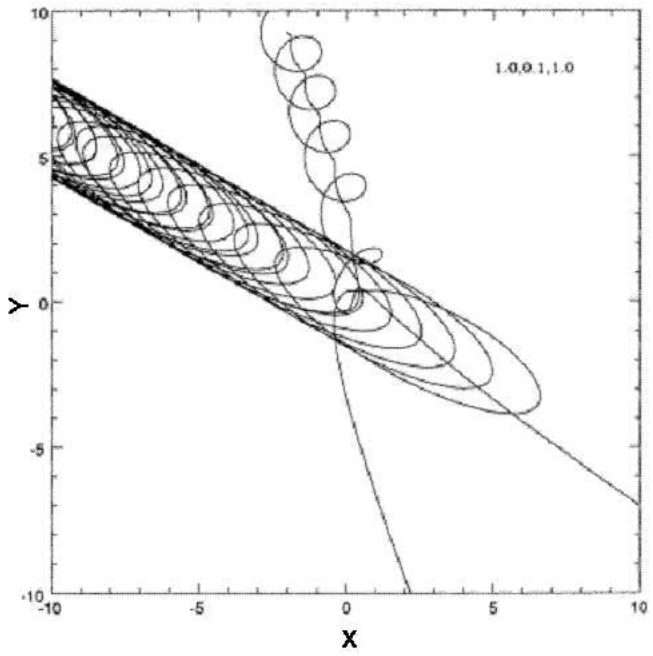

Fig. 1.5 An example of modern numerical integration techniques. This figure shows a three-body interaction between a large mass ratio binary (0.1:1.0) and a heavy third object (1.0) which ejects the light object and forms a wide binary with the other heavy object. Figure 5b from Sigurdsson & Phinney (1993).

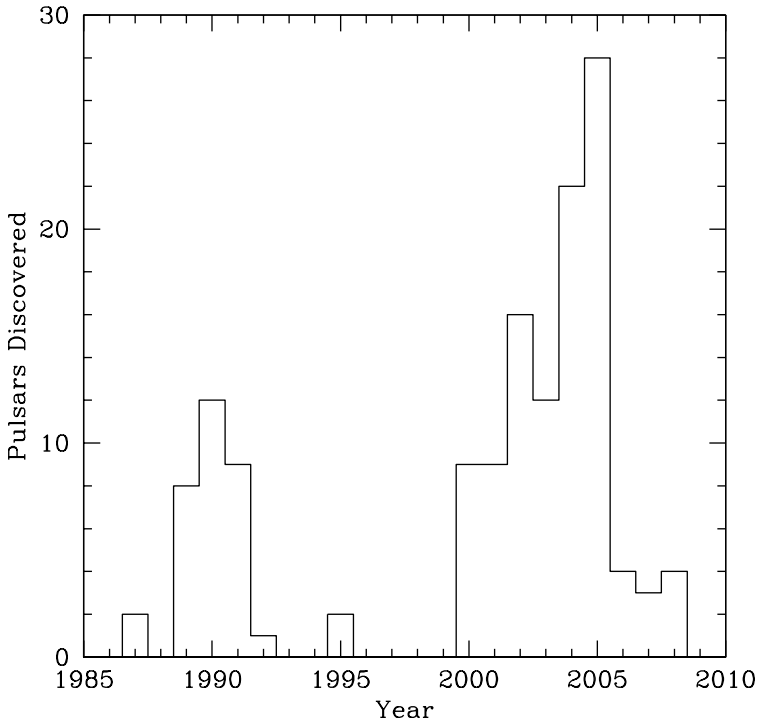

Fig. 1.6 Discovery history of radio pulsars. From Ransom (2008)

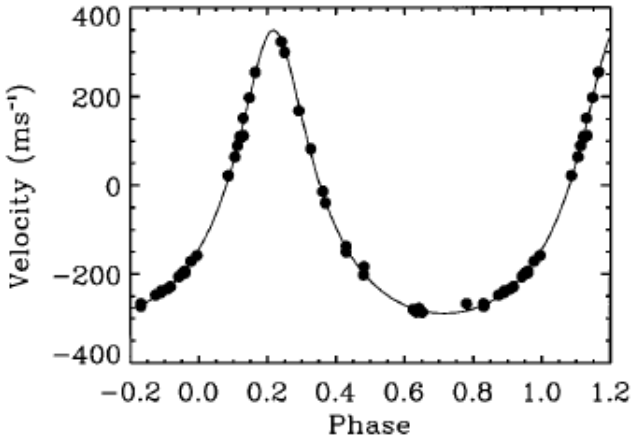

Fig. 1.7 Radial velocity profile for the 70 Virginis system from Marcy & Butler (1996). The peaked nature of the curve shows that the planet has an appreciable eccentricity, in this case 0.4. A circular orbit would give a sinusoidal curve in the radial velocity.

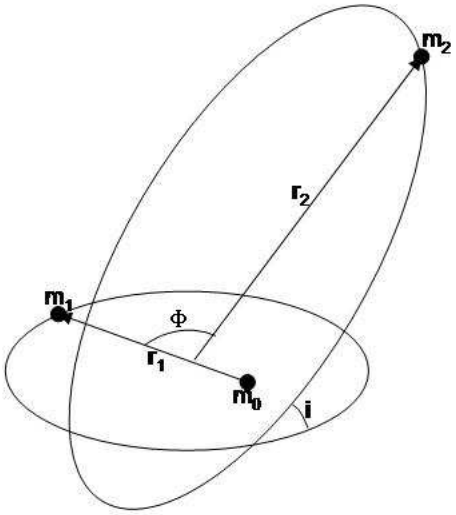

Fig. 1.8 Coordinate system for the three-body problem which produces the Kozai resonance.

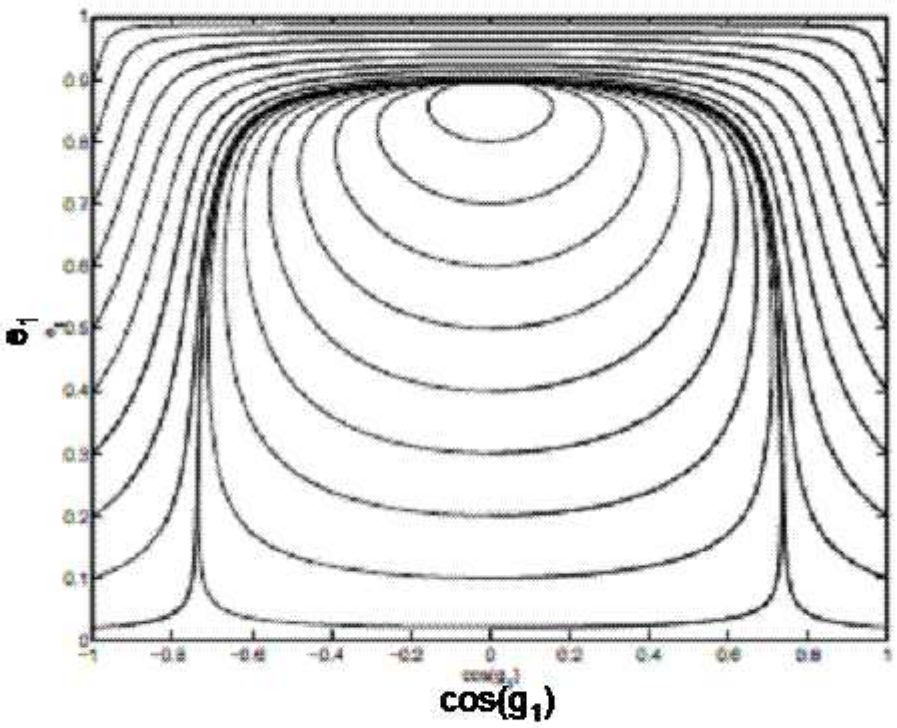

Fig. 1.9 Diagram of trajectories for the eccentricity and orientation of a system with the primary mass 1000 times the other two masses ($m_0 = 10^3 m_1 = 10^3 m_2$), equivalent to the Sun with two Jupiters. The ratio of the semimajor axes $a_2/a_1 = 100$, the initial value of $e_2 = 0.9$, and e_1 range from 0.02 to 0.9. This figure is for the quadrupole formulation, in the octupole formulation the trajectories are not closed. Figure from Ford et al. (2000b).

Chapter 2

Binary Black Hole Mergers

2.1 Previous Studies and Observations of Black Holes in Clusters

This chapter was published as Moody & Sigurdsson, 2009, ApJ, 690, 1370.

Observed black hole masses occupy two regimes, $M_{BH} \lesssim 100 M_\odot$ for black holes formed from core collapse supernova, and supermassive black holes with $M_{BH} \gtrsim 10^6 M_\odot$ which reside in the centers of galaxies. Observations of some objects, however have suggested that a middle regime of intermediate mass black holes (IMBH, review by Miller & Colbert (2004)) could exist with masses between stellar and supermassive black holes. Ultraluminous X-ray sources ($L_X > 10^{39}$ ergs sec^{-1}) have been found in intense star forming regions outside the nuclei of some galaxies (Kaaret et al. 2001; Matsumoto et al. 2001; Fabbiano et al. 2001), and recently even in one globular cluster in another galaxy (Maccarone et al. 2007). The lower limit on the mass for these objects, assuming isotropic emission at the Eddington limit, is a few hundred solar masses. A stellar mass black hole would require special geometry of its accretion disk for sufficient beaming to occur and the accretion to be sub-Eddington (King et al. 2001), or need special conditions on the gas to provide a super-Eddington accretion rate (Begelman 2001). Conversely, a supermassive black hole ($M \gtrsim 10^6 M_\odot$) would experience dynamical friction and sink to the center of its galaxy in too short a time to be plausibly observed at locations within the host galaxies where the IMBH candidates are projected to be seen today (Kaaret et al. 2001). An intermediate mass for these objects would seem to be indicated. (Filippenko & Ho 2003) found in the nearly bulgeless galaxy NGC4395 an AGN for which $M_{BH} \lesssim 10^5 M_\odot$, which is in the upper range of IMBH masses. An object with a similar mass may also exist in the galaxy POX 52 (Barth et al. 2004).

Another possible place to look for IMBHs besides in starburst regions in galaxies is in the centers of globular clusters. Observations have shown an increase in the mass-to-light ratio towards the centers of a few globular clusters that might be consistent with a massive object. There is a $M > 10^4 M_\odot$ object in the Andromeda Galaxy cluster G1 (Gebhardt et al. 2002, 2005) and a $4 \times 10^4 M_\odot$ object found by Noyola et al. (2008) in the cluster ω Cen. A few thousand solar mass object in M15 is seen by van der Marel et al. (2002) and Gerssen et al. (2002), although in this case, Baumgardt et al. (2003) are able to simulate the observations without an IMBH using smaller compact objects. The velocity dispersion of the central stars in the cores of these globular clusters as compared to the conjectured mass of the IMBH put these clusters on the same M-σ relation as the bulges of galaxies with supermassive black holes (Gebhardt et al. 2002; van der Marel et al. 2002; Gerssen et al. 2002). While the theory of the origin of the M-σ relation for supermassive black holes would probably not apply to globular clusters, it is intriguing that, at least in these two cases, the IMBHs in these clusters are consistent with it.

Two possible scenarios for the formation of IMBHs within a globular cluster have been proposed recently. The first involves the process of core collapse, by which the heavier stars in a cluster first sink to the middle through mass segregation. The stellar density reaches very high values which might be sufficient such that several stars collide forming a very large star (mass a few hundred solar masses), which collapses directly to an IMBH (Begelman & Rees 1978; Portegies Zwart & McMillan 2002; Freitag et al. 2007). Otherwise, stellar evolution causes the high mass stars to form black holes, which can become binaries through exchange into existing binaries of lower mass main sequence or neutron stars (Sigurdsson & Phinney 1993). We assume that formation of an IMBH by runaway merger does not occur in this case. Three-body interactions, which in the cores of clusters are dominated by interactions with all three objects being black holes, can then begin to work to harden binaries to the point where they merge. It is this scenario we intend to investigate.

Previous studies of dynamical formation of a IMBH from stellar mass black holes have been performed. Black holes have been shown to be dynamically important in such aspects as the radius-age relation of Magellanic Cloud clusters (Mackey et al. 2007, 2008), and even in galactic nuclei (Lee 1995). Portegies Zwart & McMillan (2000) include a study of how important black hole binaries in clusters are to gravitational wave research. Recently, Holley-Bockelmann et al. (2008) studied mergers of black holes in a system already containing a $100M_{\odot}$ black hole, which represents the next step in IMBH formation after our work. Kulkarni et al. (1993) and Sigurdsson & Hernquist (1993) used only 10 $M_{\odot}$ black holes, and determined that the formation of 10^3 $M_{\odot}$ objects is possible. On the other hand, Miller & Hamilton (2002b) showed that these binaries tend to be ejected before reaching a size at which recoil becomes unimportant, precluding further growth.

Since black holes are produced from progenitors with a wide range of masses (20-100 $M_{\odot}$) and have varied evolution histories (wind losses and mass transfer) just prior to becoming black holes, a distribution in masses may better reflect the actual situation in globular clusters. O'Leary et al. (2006) did a study using the distribution of black hole masses and binary periods as given in Belczynski et al. (2004) and a more complicated method of computing interactions than our semi-analytic model. They use the old prescription for gravitational radiation recoil similar to that found in Favata et al. (2004). González et al. (2007) has done numerical simulations which track all stages of gravitational radiation emission until that emission ceases, and they have calculated definitive recoil velocities, so that the sole remaining uncertainty in determining the circumstances of black hole mergers is the initial distributions of their masses. Our semi-analytic method can more quickly respond to updates in stellar population synthesis models than direct many-body integration.

We describe the conditions under which the simulations were done, including initial conditions of the binary and the analytical form of the 3-body interactions and relevant time scales, then report results from several simulation runs, with a few parameters (e.g. metallicity) adjusted after each one. Finally, we discuss what the results imply for observed systems and suggest two systems that fall in the higher probability category for harboring an IMBH.

2.2 Semi-Analytic Simulations of Binary-Single Star Encounters

We simulate the history of 100,000 binaries for each set of initial conditions. The ensemble of initial conditions includes two values each for metallicity and escape velocity. An examination of Belczynski et al. (2004) shows that there exist two distinct shapes of the period and mass distributions based on metallicity, therefore only a qualitative distinction with the changeover coming at $\log[Fe/H] = -1.3$ for observed clusters is included. The escape velocities were chosen as a proxy for several properties to represent moderately sized clusters and heavy clusters; smaller clusters which might have had a lower value for the escape velocity are not expected to retain any binaries that interact due to their extremely shallow potentials. The models' initial conditions are described in Table 2.1. Model A has a low metallicity and 30km/sec escape velocity, model B has a high metallicity and 30km/sec escape velocity, model C has a low metallicity and a 50 km/sec escape velocity, and model D has a high metallicity and a 50km/sec escape velocity. Each binary history is run until one of three fates is determined: ejection as a binary through 3-body superelastic recoil (Fate 1), ejection as a single object upon merger from gravitational radiation recoil (Fate 2), or a retained merged single object (Fate 3). For those systems which come under Fate 1, the gravitational radiation merger timescale is calculated for the ejected binary and determine the fraction of those in the simulation that coalesce within a Hubble time. Results for the runs are in Table 2.2. For model A, 95.7% of binaries are ejected by 3-body interactions, 3.8% are ejected upon merger, and 0.5% are retained after merger. For model B 98.2% of binaries are ejected by 3-body interactions, 1.0% are ejected upon merger, and 0.8% are retained after merger. For model C, 94.1% of binaries are ejected by 3-body interactions, 4.5% are ejected upon merger, and 1.4% are retained. For model D, 92.7% of binaries are ejected by 3-body interactions, 3.8% are ejected upon merger, and 3.5% are retained.

Whereas previously (c.f. Sigurdsson & Hernquist (1993)) the distribution of black hole masses has been assumed to be single-valued at $10M_{\odot}$, we start with a multi-valued initial mass function (IMF) for black holes. Based on Figure 3 of Fryer & Kalogera (2001) for f=1 (fully efficient supernova) and stellar IMF power-law index γ=2.0, we propose using for our low metallicity distribution a smooth power law, which gives the probability of a black hole having mass M proportional to $10^{-.05M/M_{\odot}}$ for masses in the range $3M_{\odot}$ to $80M_{\odot}$. This is the same analytic form as the low metallicity (Z=0.001) IMF found by Belczynski et al. (2004) for his standard model parameters. Fryer & Kalogera (2001) calculate a black hole IMF for single progenitor stars, and are used by Belczynski et al. (2004) to predict black hole masses from a range of progenitor masses, while also considering binary evolution effects such as common envelope phases. The most uncertainty in determining mass functions from binary evolution models comes during the common envelope phase and in calculating mass loss. These are common to any attempt to use a distribution of masses.

The IMFs in Belczynski et al. (2004) are presented as histograms, but these are converted to analytical probability distributions for ease of use with computer-based simulations. Binaries are constructed using the IMF to pick both masses, a distribution in periods taken from Belczynski et al. (2004) as appropriate for the metallicity studied and also converted to an analytical form, and an eccentricity from a thermal distribution

(P(e)=2e). We chose the masses independently as we expect the stars to have, for the most part, developed independently in well separated binaries.

The center of a dense cluster where the simulations take place is expected to be an environment free of main sequence stars through the action of the gravitational instability described by Spitzer (1969) and because the simulations start late enough such that all stars of comparable mass to the stellar remnants have evolved. Other studies such as Portegies Zwart & McMillan (2002) start at a time prior to 100Myr, and so have rapidly evolving massive stars which have settled to the center of their cluster simulations. This means we do not track stellar interactions, implicitly we assume that we are in a regime where there are multiple black holes which have formed a dense sub-core in the cluster, and that the interactions of these black holes dominates the fate of any binary. In general, interactions of the sub-core with stars are not important. They become very important in late stages, particularly for the "last" black hole binary. Discussion of stellar interactions with the binary is beyond the scope of this thesis. The forms for both the IMF $P(M)$ and periods $P(T)$ are as follows (Belczynski et al. 2004):

$$P_{\mathrm{lowZ}}(M) = 0.152 \cdot 10^{-0.05M/M_\odot}, \text{ all M.}$$

$$P_{\mathrm{highZ}}(M) = \begin{cases} 0.028, & 3M_\odot \geq M \geq 15M_\odot, \\ 10^{0.6M/M_\odot}, & 15M_\odot \geq M \geq 55M_\odot, \\ 0, & 55M_\odot \geq M \geq 80M_\odot. \end{cases}$$

$$P(T) = \begin{cases} \sqrt{1-(T-1)^2}, & 0 \geq \log T(\mathrm{days}) \geq 2 \text{ low Z only}, \\ (T-2), & 2 \geq \log T(\mathrm{days}) \geq 6 \text{ all Z}. \end{cases}$$

Binaries are subjected to encounters with a third black hole whose mass is randomly drawn from the IMF. The time scale for the encounter t_{enc}

$$t_{enc} = 1.5 \times 10^9 \mathrm{years} \frac{m_3 v_{10}}{\mu_{1\,2} m_T a_{AU} n_4} \tag{2.1}$$

is calculated from equation (2.9) of Sigurdsson & Phinney (1993) with m_3 the mass of the third black hole, $\mu_{1\,2}$ the reduced mass of the binary, m_T the total mass of all three objects, the masses being expressed in terms of $M_\odot$, a_{AU} the binary's semimajor axis, n_4 the density of stars $n/10^4$ pc^{-3}, and v_{10} the relative velocity of the third object $v/10$ km/s, which is taken to be 1 for typical globular clusters, which have velocity dispersions on the order of 10 km/sec. For this work the value of the dimensionless cross section $\tilde{\sigma} = 10$ as defined in equation (2.7) is used, as this value is broadly consistent with interacting systems having mass ratios in the range of those in our simulations as given in tables 3A and 3B of Sigurdsson & Phinney (1993). This time scale is compared to the time for merger by emission of gravitational radiation (Peters 1964)

$$t_{GW} = 3.151 \times 10^{17} \mathrm{years}\ g(e) \left(\frac{a}{AU}\right)^4 \left(\frac{M_\odot}{m_1}\right) \left(\frac{M_\odot}{m_2}\right) \left(\frac{M_\odot}{m_1+m_2}\right) \tag{2.2}$$

$$g(e) = \left(1 - e^2\right)^{7/2} \left(1 + \frac{73}{24}e^2 + \frac{37}{96}e^4\right) \tag{2.3}$$

For $t_{enc} < t_{GW}$, the encounter takes place. This entails choosing a new eccentricity from the thermal distribution and a change in the semimajor axis a such that the binding energy of the binary is changed by

$$\Delta = 1 - \frac{a_{in}}{a_{out}} \frac{m_a m_b}{m_1 m_2} \tag{2.4}$$

where a_{in} and a_{out} are the starting and ending semimajor axes of the binary for the encounter, m_1 and m_2 are the masses of the two original objects in the binary, and m_a and m_b are the masses of the two new objects. Based on the results in Sigurdsson & Phinney (1993), the two most massive of the three interacting objects form the new binary, leading to the possibility of membership change. If there is not a change, a is simply reduced by a factor $(1 - \Delta)$. With an exchange in membership, it is possible for a to increase dramatically. For simplicity, we choose a fixed value of $\Delta = 0.4$, characteristic of the mean energy transferred in the same encounters from Sigurdsson & Phinney (1993) that gave us our value for $\tilde{\sigma}$. This is warranted, if there are multiple encounters per system before ejection. For a check on the adequacy of a single value of Δ, a set of simulations was run allowing Δ for each interaction to vary in a normal distribution around 0.4. Even with a variance of 0.2, the effect was negligible.

Besides changes in the internal dynamics of the binary, the conservation of momentum among the two systems requires the binary to recoil. The magnitude of the recoil is

$$v_{rec} = \frac{m_e}{m_T} \sqrt{\frac{m_3(m_1 + m_2)}{m_e(m_a + m_b)} \sigma_{GC} + \frac{2\Delta m_T G m_1 m_2}{m_e(m_a + m_b) a_{in}}} \tag{2.5}$$

If the recoil is smaller than the assumed escape velocity of the globular cluster, the time is incremented by t_{enc}, and the run continues by choosing a black hole mass independently from the mass distribution. The dynamical friction timescale for the binary is approximately $\langle m \rangle / M_{BH} t_r$ (O'Leary et al. 2006), where $\langle m \rangle$ is the average stellar mass, and t_r is the relaxation timescale. Very few binaries are kicked with the narrow range of velocity required to have a turning point of several half-mass radii, and these are highly radial orbits. On those radial orbits the binaries still interact with the core, and so the core relaxation time applies. The core relaxation times for most clusters are $10^7 - 10^8$ years (Harris 1996), so most binaries will return to the core in less than a million years. If the binary is ejected, the run is stopped and t_{GW} is calculated for the binary. Those for which t_{GW} is less than 10^{10} years may be field gravitational radiation sources. The run will also be stopped once $t_{enc} > t_{GW}$, at which time the recoil velocity from asymmetric emission of gravitational radiation is calculated. We used the zero spin expression for the gravitational radiation recoil from González et al. (2007)

$$v_{GW} = 1.20 \times 10^4 \eta^2 \sqrt{1 - 4\eta}(1 - 0.93\eta) \text{ km/sec} \tag{2.6}$$

where η is the symmetric mass ratio defined using $\eta = q/(1+q)^2$, q being the mass ratio of the two objects in the binary ($0 \geq q \geq 1, 0 \geq \eta \geq 0.25$). Stellar mass black holes,

unlike supermassive black holes in galaxy centers which have accreted most of their mass from a thin disk where the spin goes to 0.98, are not likely to have a large spin parameter. The exceptions, the so called microquasars such as that observed by McClintock et al. (2006), are expected to be rare. O'Shaughnessy et al. (2005b) find by analogy with neutron star birth spins (Lorimer et al. 2005; Kramer et al. 2003; Migliazzo et al. 2002) that expected spins should be less than 0.1, unless otherwise spun up by fallback from the supernova explosion. Burrows et al. (2007) find that only rapidly spinning cores may produce the phenomena called hypernovae. Since these types of objects are rare, it can be inferred that most supernovae that produce black holes make slowly spinning ones. Any accretion that does occur while the black hole is in a binary with a mass donor is expected by Belczynski et al. (2008) to increase the spin parameter $a = J/M^2$ beyond 0.5. From the fully spin dependent form of the recoil velocity (Campanelli et al. 2007) and using the approximation of $1/\sqrt{2}$ for the values of the sine and cosine of the angles, it is found that $v_{GW}(a)/v_{GW}(a = 0)$ goes above 2 for values of $a >\sim 0.4$ except for extreme mass ratios which are more sensitive to spin. The merged object is then ejected or retained in the globular cluster depending on the magnitude of v_{GW}.

2.3 Results

As seen in Table 2.2, the most likely conditions for a black hole to be retained are in massive, metal-rich clusters. The change in mass distribution with metallicity, which affects the mass ratio distribution of binaries, is the main driver of whether or not a binary may be retained. As seen in Figure 2.1, the initial distribution of mass ratios for metal poor binaries is nearly constant above 0.2, which is the condition O'Leary et al. (2006) place on their binaries *a priori*. For the distribution of initial mass ratios for high metallicity binaries, there is a peak at $q = 0.25$ due to systems with one member from each of the two parts of the distribution (centered at 10 and $40M_{\odot}$). The mass ratio distribution of ejected binaries is shifted toward higher values of q for both high and low metallicity distributions, because equal mass binaries are more likely to be ejected. This follows from previous attempts at this problem (Kulkarni et al. 1993; Sigurdsson & Phinney 1993) with the failure of equal mass binaries to produce a retained object.

We compare our results of ejected binaries to those of O'Leary et al. (2006) by collecting enough of our runs within a single model to create an N=512 cluster. The models of theirs most similar to our were the e5e5king11, v2e5k11, and v3e5k11 models for low escape velocity, and the e5e5king7, v2e5k7, and v3e5k7 models for high escape velocity. All of these fall into low metallicity models, as that corresponds to the models of Belczynski et al. (2004) that O'Leary et al. (2006) used. In the models indicated, O'Leary et al. (2006) find the ejection fraction of black holes in binaries in low v_{esc} clusters is 0.14, and a fraction of 0.1 in high v_{esc} clusters. A similar value exists for the fraction of ejected black holes in binaries.

The large numbers of ejected binaries produced in each cluster make them an interesting target of investigation. Some fraction of these have a t_{GW} less than 10Gyr, and so would make a background source for gravitational radiation detectors (Portegies Zwart & McMillan 2000). High mass metal rich clusters produce the most binaries that merge in less than 10Gyr. The next highest number come from high mass metal poor

clusters. Low mass metal poor clusters produce more binaries that merge in less than 10Gyr than low mass metal rich clusters. The change in Hubble time mergers with mass is expected since a heavier cluster would allow the binary to become harder before ejecting it. The size of the orbit of the binary upon ejection is proportional to $v_{esc}^{(-1/2)}$, while the time for merger by gravitational radiation emission is proportional to a^4, so that a factor of 2.5 smaller t_{GW} is expected for similar systems in our high mass clusters versus our low mass clusters. The difference in the number of binaries that merge within a Hubble time with respect to metallicity is harder to understand. The binaries for the most part stay within their host galaxy. Figure 2.2 shows the distribution of velocities of the ejected binaries. The high velocity tail for models A and C is due to binaries from the low metallicity period distribution which have small initial separations since v_{rec} is inversely proportional to a. This also is the reason why the high mass cluster models are shifted to higher velocities (at least for v_{rec} between 50 and 200 km/sec), since the binaries are able to become more tightly bound before being ejected. The fraction of binaries at each point covers a 5 km/sec bin. For the two low metallicity models, which have binaries that start with tight orbits having $\log T(days) < 2$, there are a few systems ($\sim 1\%$) that are ejected with a velocity higher than 300 km/sec, but most binaries (and all of the high metallicity ones) have $v_{rec} < 200$km/sec. This means that while they leave their parent cluster, they are still confined to their parent galaxy unless it is a dwarf galaxy.

The distributions of masses for the retained and ejected merged objects are in Figure 2.3. Both of these plots are normalized to the number of black holes that undergo fate 2 (ejection) or fate 3 (retention), the number of which for each model is given. For low metallicity systems, the distribution is flat up to $60M_{\odot}$, after which it drops. High metallicity systems show one peak of 20-30$M_{\odot}$, and another between 80 and $100M_{\odot}$, which reflects the underlying initial mass distribution. There is a substantial fraction (1% to 5%) of black holes that are retained which have masses above $100M_{\odot}$, which is a common definition for the lower boundary IMBH masses. For ejected objects, the low metallicity systems show a monotonic decline from $15M_{\odot}$ to the maximum mass seen at $120M_{\odot}$, with a slight break downward at $60M_{\odot}$. For the high metallicity systems, there is a peak around 40-60$M_{\odot}$ where the distribution of masses for retained objects has a deficit. These objects show a "complimentary" distribution to the retained objects, especially for the metal rich clusters where the peak mass of ejected objects fits nicely into the deficit of retained objects. The currently used recoil velocity function has its peak at a mass ratio of about a third, so that if a binary in the high metallicity model consists of one member from each of the two regions, it will have a total mass of about 40-60$M_{\odot}$ and a mass ratio of 0.3-0.4 which will most likely be ejected, whereas a binary with both members from the same region will have a mass of either 20 or 80-100$M_{\odot}$ and q close to one and be retained (if it survives 3-body interactions of course).

The plots for the number of binaries that exist at high separations for the time indicated are in Figure 2.4. While the binaries are in the globular cluster, they may go through short-lived phases with large semi-major axes due to exchanges of membership. These stages may be important in transferring angular momentum from the binary to the cluster as a whole through interactions with stars as shown in Mapelli et al. (2005). For a fraction of the binaries, the histories of a are recorded and examined to determine

how much time they spend with $a > 10^2$, 10^3, and 10^4 AU. The distributions of the two high metallicity samples are the same, but the low mass metal poor model shows fewer binaries that get to high separations. The low metallicity low and high mass models have 34.2% and 16.2% that never have $a > 10$AU respectively, while for high metallicity this percentage is 41.6%. Other than this difference, the distributions of time spent at high separations is similar.

2.4 Discussion

The event rate from merging black hole binaries can be calculated from the fraction of systems that merge within a Hubble time and the relative contributions from low and high metallicity systems and light or massive clusters. To conservatively estimate the event rate, we assume 100 globular clusters per galaxy (e.g. the Milky Way is currently thought to have about 150) and 100 BH per globular cluster ($N_{BH} \sim 10^{-4} N_\star$). We assume that the break between high versus low metallicity is at an [Fe/H] of -1.3 and that light globulars have v_{esc} of less than 30 km sec^{-1} and heavy globulars above this value. The escape velocity for a globular cluster is given by $v_{esc} = \sqrt{2\Phi_0}$, where Φ_0 is the central potential of the cluster, $W = \Phi_0/\sigma^2$ is the King parameter and is correlated with the cluster concentration, and σ is approximately equal to the velocity dispersion except in the case for shallow globulars. The concentration and thus W is determined from the catalog of Harris (1996), while 1D velocity dispersion data were obtained from Pryor & Meylan (1993). For the 56 Milky Way clusters for which the escape velocity could be determined, the percentage of clusters in each of our models is as follows: A 45% (25), B 21% (12), C 20% (11), and D 14% (8). Including data from Table 2.2 on the number of mergers within a Hubble time, the ejected binaries account for ∼640 mergers per galaxy in a Hubble time, with another 335 coming from those binaries that merge while still in the cluster. Over a Hubble time this gives a rate of 10^{-7} per year per galaxy. These are very conservative estimates for the rate, as the Milky Way is assumed to have about 150 globular clusters, and giant ellipticals can have on the order of 10^3. Assuming a value of 300 globular clusters per galaxy and 300 black hole binaries per cluster, there would be an order of magnitude jump in the rate to 10^{-6} per year per galaxy. A further increase in rate is expected from the additional mergers produced by black holes that are retained after their first merger. Galactic binary BH merger rates are estimated at 10^{-6} per year (O'Shaughnessy et al. 2005a). Based on a similar calculation to determine the number of clusters in the Milky Way which could have a merged object retained, it is found to be 0.655. This means there may be 1 globular cluster which has a merged object, but not many.

The mergers are expected to be delayed from the formation of the clusters, which in the case of globulars is close to the beginning of the universe. The last interaction before the binary is ejected typically happens when the semimajor axis is 0.1-1 AU, giving a t_{enc} of $10^8 - 10^9$ years. The timescales for the gravitational merger of the ejected binaries spans a wide range of values ($5 < \log t_{GW}(\mathrm{yr}) < 20$). Figure 2.5 shows the distribution of merger timescales for ejected binaries for each of the models. The percentage of binaries which merge between 1 and 10 Gyr is 2.6% for model A, 2.3% for model B, 4.3% for model C, and 8.2% for model D. While we have used a thermal

distribution ($P(e) = 2e$, $\langle e \rangle = 0.67$) for the eccentricity after an exchange, the 3-body study by Sigurdsson & Phinney (1993) found that this works for equal mass exchanges, but for non-equal masses, the eccentricities may be higher ($\langle e \rangle \approx 1 - 1.3(m_3/m_2)$). This does not affect recoil velocities, but the t_{GW} would be shortened, and the expected rates of black hole mergers would increase by a factor of a few. If we choose black hole binaries as we do for the simulation runs and determine their t_{GW} without any interactions, it is found that for metal rich systems, only 0.1% merge in less that a Hubble time, whereas 7% of low metallicity binaries do so. This is explained as a model dependent result, the low metallicity period distribution includes systems which have periods shorter than 100 days while the metal rich distribution does not. Because the metal poor system already produce binaries with small a and thus shorter t_{GW}, they are less reliant than high metallicity systems on interactions to reduce the semimajor axis. This result also explains the above statement that, for low mass clusters, metal poor systems make more quickly merging binaries than metal rich systems. In lower mass systems, the binaries undergo fewer interactions before being ejected, and so the metallicity deppendence is more important.

The chirp mass of a binary is defined by $M_{ch} = \mu^{3/5} M^{2/5}$ where $\mu = m_1 m_2/(m_1 + m_2)$ is the reduced mass and M is the total mass of the binary. The strain from gravitational radiation is proportional to the chirp mass. The chirp masses for cluster binary mergers are much higher due to exchanges undergone while the binary was in the cluster. While galactic mergers have chirp masses of 3-8$M_\odot$ (Belczynski et al. 2007), the chirp masses for the ejected binaries are 15-25$M_\odot$ in the metal rich case and 20-40$M_\odot$ in metal poor clusters. The higher chirp masses, while dependent on the models used for the initial mass function of the black holes, is a distinct prediction characteristic of the globular cluster binaries, and easily observable by gravitational radiation instruments. Since the strain due to gravitational radiation scales as M/r, the factor of 4-6 increase in mass of the cluster binaries makes them visible over a factor of 60-200 larger volume, which makes them almost as important source as galactic binaries for the conservative values of GC/galaxy and binaries/GC. If we assume the less conservative numbers, the cluster binary inspirals would dominate the signal. LIGO will have an abundance of targets from the ejected binaries.

My work in this project provides a first step from population synthesis to the possible formation of an IMBH in the center of a globular cluster. Examining a second merger once the merged object has exchanged into a new binary is beyond the scope of this work, but has been studies by Holley-Bockelmann et al. (2008). To connect our theoretical models to observed clusters, a plot of metallicity versus v_{esc} is given in Figure 2.6 using metallicity data from the catalog by Harris (1996) and the escape velocity as described above.

Two clusters that have both high metallicity and $v_{esc} > 50$ km sec^{-1} are NGC 6388 and NGC 6441. Both of these clusters lie within 4 kpc of the galactic center. These clusters are most well known for their contribution to the "second parameter" problem in that they have more extended blue horizontal branches than their metallicity would indicate. It is speculated that this might be due to dynamical interactions in the clusters (Rich et al. 1997; Miocchi 2007). They note that the M31 cluster G1, a cluster suspected of having an IMBH by Gebhardt et al. (2002), also shows an extended blue horizontal

branch. These clusters may have been at one point the nuclei of dwarf galaxies, as a couple of other suspected nuclei appear in interesting regions of the metallicity-v_{esc} plot. Other clusters suspected of being dwarf galaxy nuclei are M54 (due to its association with the Sagittarius dwarf galaxy) by Ibata et al. (1994) and ω Cen (Norris et al. 1996, 1997). The presence of extended blue horizontal branch stars in the metal-rich clusters NGC 6388 and NGC 6441 is thought to give a similar argument for their being formed in a similar manner (Piotto et al. 1997). Two other clusters which are less outstanding but still in the upper right part of the diagram are NGC 2808 and M62. Observations of variability in the recently discovered ULX in a globular cluster of NGC 4472 by Maccarone et al. (2007) lead to estimates of a $300M_{\odot}$ IMBH, though their other solution gives a mass of $30M_{\odot}$. They find a metallicity of the cluster of -1.7 from color-metallicity relations, and the luminosity gives it a absolute magnitude of -9.2. When compared to analogous clusters in the Milky Way (e.g. NGC 6273), this cluster fits into category C, low metallicity high mass. Figure 2.6 places NGC 6388 and NGC 6441 in context with other massive, well studied globular clusters.

2.5 Conclusion

In conclusion, within our simplified model assumptions, most black hole binaries are ejected through gravitational 3-body interaction from the cluster into the general potential of the galaxy. Of those binaries that survive to merge by gravitational radiation, about 2/3 to half are ejected through gravitational radiation recoil. Between 0.5% and 3.5%, depending on metallicity and cluster escape velocity, of all black hole binaries in clusters are predicted to be retained upon merger of the binary, with typical final masses of 20-50 $M_{\odot}$, but in some instances over $100M_{\odot}$. Of course if other formation channels dominate, or there is significant gas accretion after the dynamical interaction phase, then the final black hole masses may be very different (higher if there is significant accretion). The rate per galaxy of black hole binary mergers through gravitational radiation from the globular cluster population is competitive with the total merger rate from the parent galaxy, but biased towards higher masses. While most globular clusters in massive galaxies probably form at high redshift, this suggests that black hole binary coalescence from clusters in low mass, nearby star forming galaxies may be a significant contributor to the total high frequency gravitational radiation signal in the local universe. The current results are dependent on the exact form of the initial conditions of mass distributions and period distributions obtained from population synthesis. As the formation mechanisms for black holes become more well understood, it would be appropriate and easy to refine the results obtained in this paper.

Table 2.1. Initial conditions of the models.

Model	metallicity	v_{esc}(km/sec)
A	low	30
B	high	30
C	low	50
D	high	50

Note. — All runs used σ_{GC}=10 km/sec and Δ=0.4 as described in text.

Table 2.2. Results of simulations.

Model	Fate(%)			% ejected binaries
	1	2	3	with $t_{GW} < t_H$
A	95.7 (95744)	3.8 (3790)	0.5 (466)	5.3 (5071)
B	98.2 (98242)	1.0 (997)	0.8 (761)	4.1 (4023)
C	94.1 (94069)	4.5 (4530)	1.4 (1401)	8.3 (7799)
D	92.7 (92666)	3.8 (3842)	3.5 (3492)	13.3 (12362)

Note. — Percentages given, absolute number out of 10^5 in parentheses. Fate: 1–binary ejected by 3-body interaction, 2–binary ejected upon merger by gravitational radiation recoil, 3–merged binary retained in globular cluster. Column (5) shows percentage (number) of binaries in Fate 1 with $t_{GW} < 10^{10}$ years.

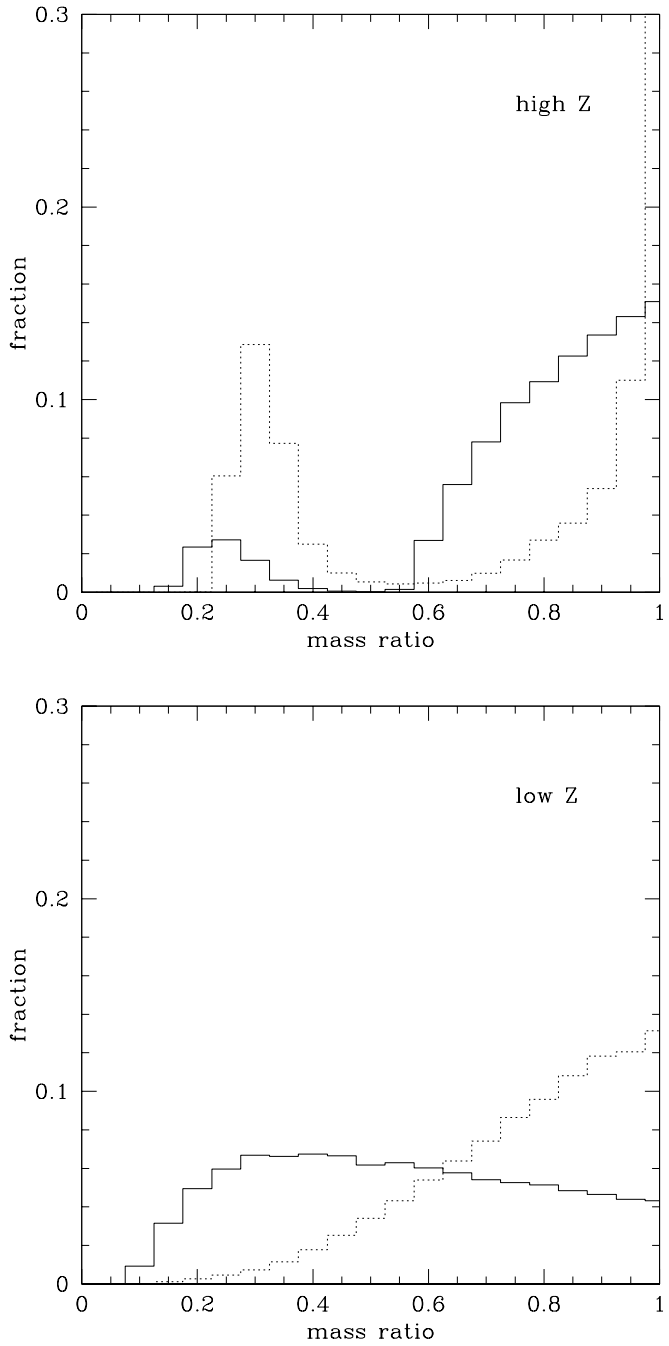

Fig. 2.1 Histogram showing distributions of mass ratios. The top panel shows the metal rich initial condition, the bottom panel has the metal poor condition. The solid line in each plot is the distribution obtained by randomly selecting two black holes from the indicated distribution, as is done initially in each simulation. The dotted line shows the distribution of mass ratios for ejected binaries. The initial high metallicity mass ratio distribution is bimodal due to the black hole IMF having two peaks near 10 and 45 $M_{\odot}$, giving a q of 0.25. Three body recoil is efficient at ejecting binaries with mass ratios $q \gtrsim 0.3$, therefore the distribution of the mass ratios of ejected binaries is skewed closer to 1. In the high metallicity case, this includes the lower q peak shifting to 0.3.

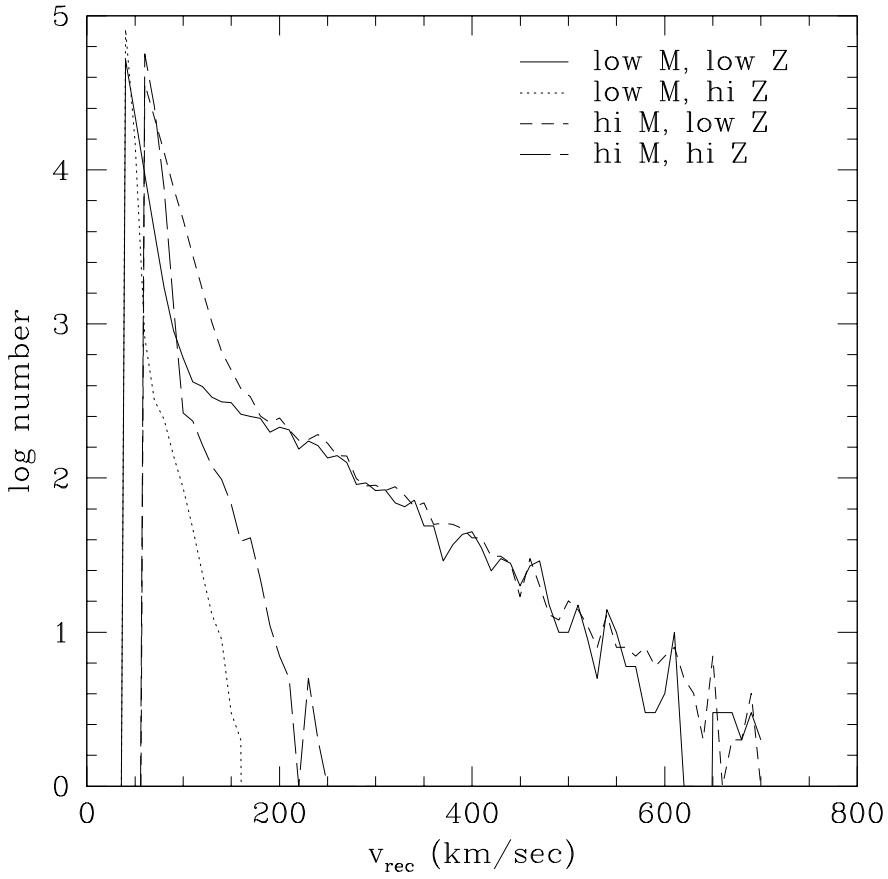

Fig. 2.2 Plot of the recoil velocities of ejected binaries. The solid line is for model A (low mass, low metallicity). The dotted line shows model B (low mass, high metallicity). The short dashed line is for model C (high mass, low metallicity). The long dashed line is for model D (high mass, high metallicity). The plots start at the escape velocity for the cluster. The high velocity tail for models A and C is due to binaries from the low metallicity period distribution which have small initial separations since v_{rec} is inversely proportional to a. This also is the reason why the high mass cluster models are shifted to higher velocities (at least for v_{rec} between 50 and 200 km/sec), since the binaries are able to become more tightly bound before being ejected. The fraction of binaries at each point covers a 5 km/sec bin.

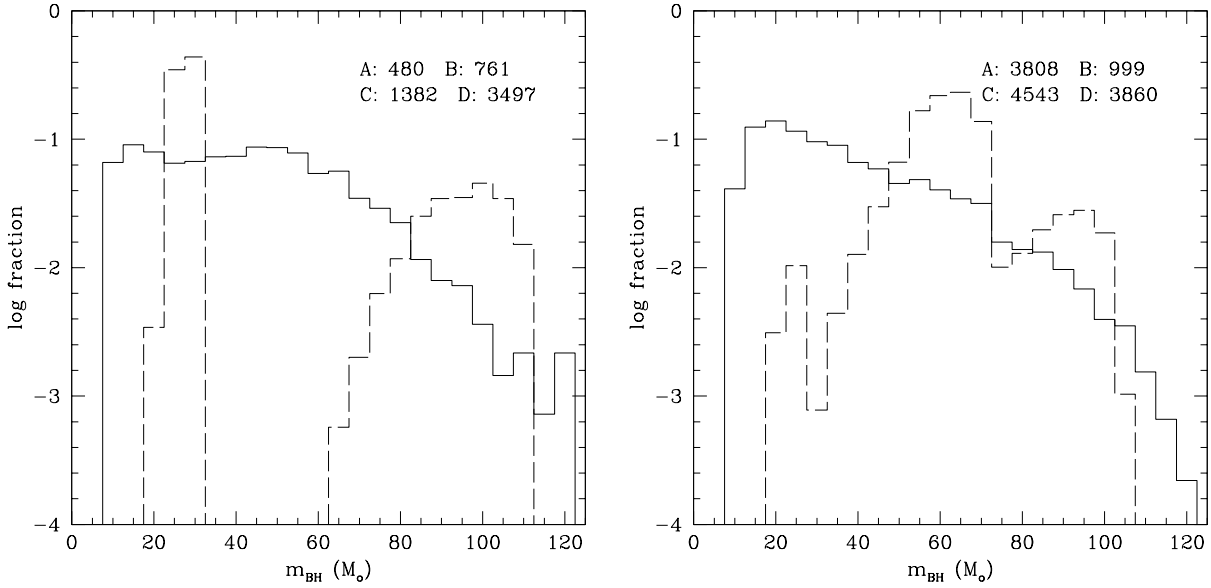

Fig. 2.3 The left histogram showing distribution of masses for the black holes retained upon merger. The bins are $5M_{\odot}$ wide and show the log of the fraction in each bin. The solid line is for metal poor systems, while the dashed line is for metal rich systems. The model dependence is most visible in the second of these with the lack of merged black holes at 40 to $60M_{\odot}$ and the sharp dropoff above $110M_{\odot}$. There is a substantial fraction (1% to 5%) of black holes that remain which have masses above $100M_{\odot}$, which is a common definition for the lower boundary IMBH masses. The plot on the right shows the mass distribution for those objects ejected upon merger by gravitational radiation, with the same convention for the lines. Both of these plots are normalized to the number of black holes that undergo fate 2 (ejection) or fate 3 (retention), the number of which for each model is given. These objects show a "complimentary" distribution to the retained objects, especially for the metal rich clusters where the peak mass of ejected objects fits nicely into the deficit of retained objects.

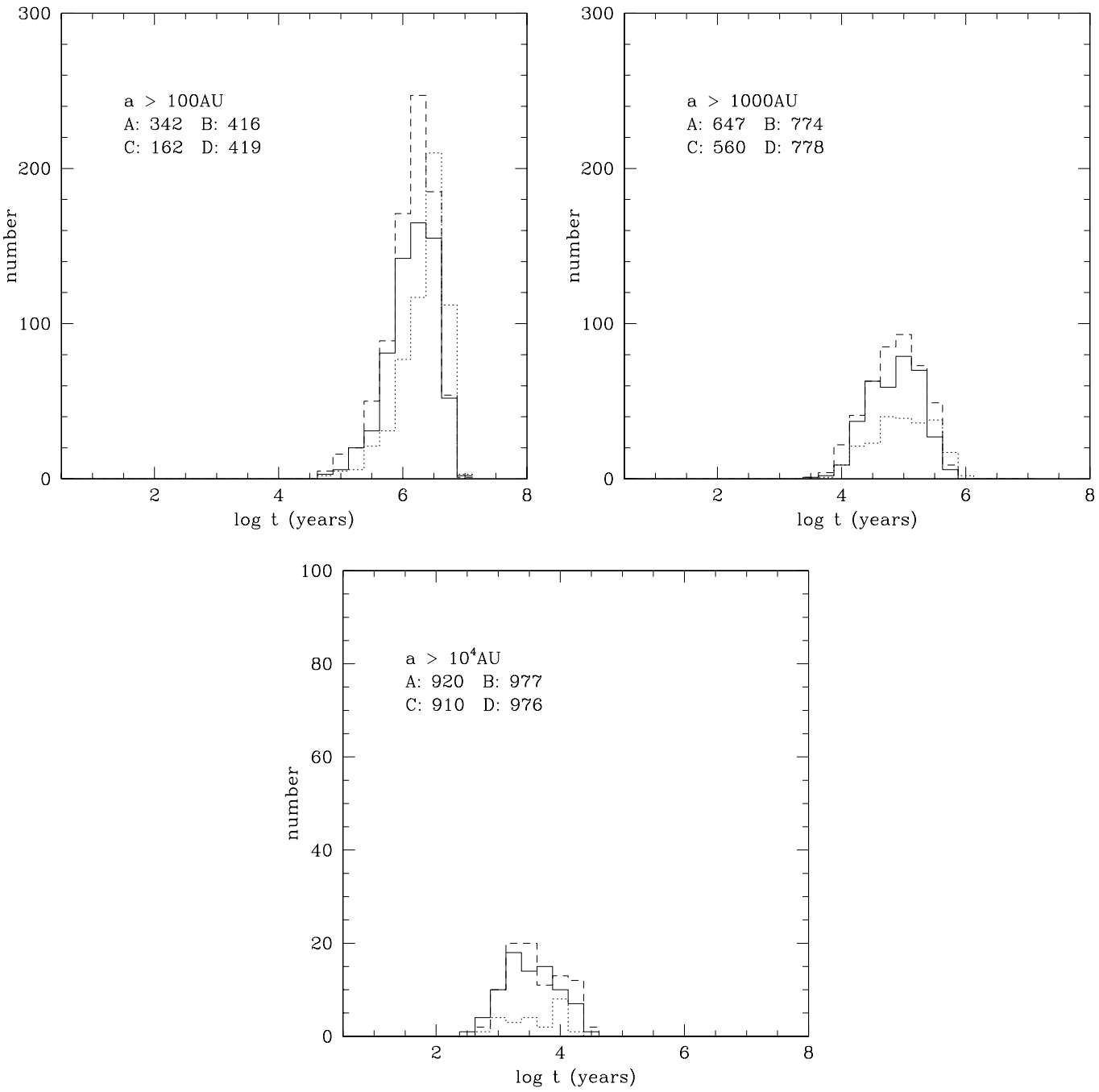

Fig. 2.4 Distributions of time spent at large a by the 1000 binaries for which detailed histories are kept. The solid line is for model A, the dotted for model B (which is identical to the distributions for model D), and the dashed line for model C. The top left plot show the number of binaries that exist at an $a > 10^2$ in 0.25 dex bins, the top right shows the same for $a > 10^3$, and the bottom plot shows those which had $a > 10^4$. Numbers in the plot show the number of binaries for each model which never have the semimajor axis indicated. The time spent by the binaries at semimajor axes of $a \gtrsim 10^{3.5}$ is small due to 3-body interactions hardening the binary.

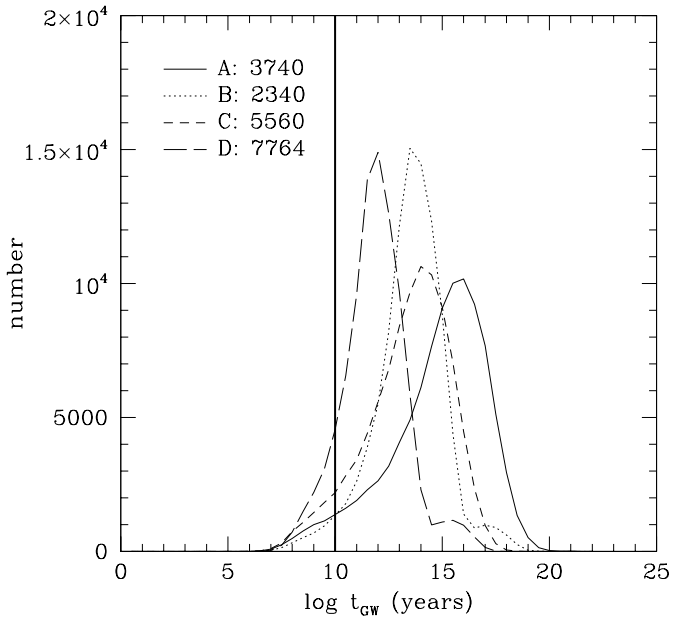

Fig. 2.5 Distributions of t_{GW} for the ejected binaries. The solid line is for the low mass, low metallicity model (model A), the dotted line is for the high mass, low metallicity model (B), the short dashed line is the low mass, high metallicity model (C), and the long dashed line is the high mass, high metallicity model (D). The thick vertical line indicates a Hubble time $t_H = 10^{10}$ years. I find the effect of both increasing mass and higher metallicity is to shift the distribution to shorter times. The distributions at lower metallicity are broader, as indicated by the lower peak value. The peak values for the models are at 10^{16}, $10^{13.5}$, 10^{14}, and 10^{12} years for models A,B,C, and D respectively. The number of binaries with $t_{GW} < 10^{10}$ is given in the plot.

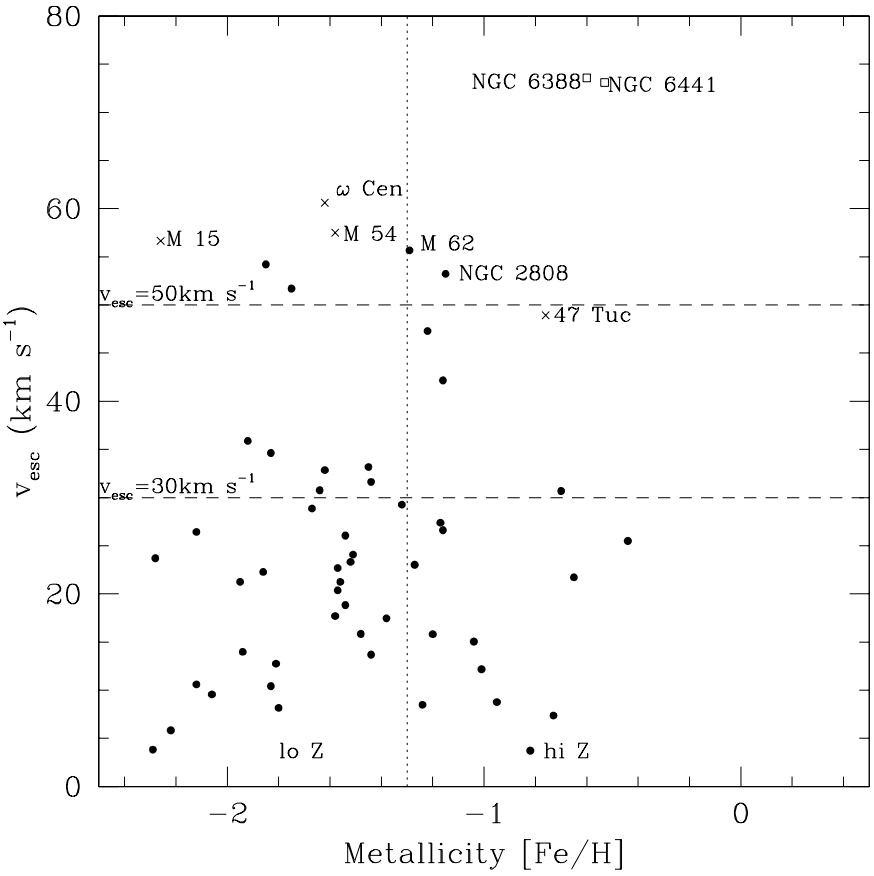

Fig. 2.6 Metallicity versus escape velocity for Milky Way globular clusters. This plot is shown to compare observed globular cluster properties to the models used. The horizontal lines show the two escape velocities examined. The larger escape velocity passes through many of the most massive clusters, while the lower escape velocity is a good upper bound to the lighter globular clusters. The vertical line is set at the dividing line between the metallicity regimes used in determining distributions (Z=0.001). The two objects in the upper right section (open squares) are NGC 6388 and NGC 6441. Crosses are large well studied globular clusters as labeled. Suspected dwarf galaxy nuclei are M54/Sgr (Ibata et al. 1994) and ω Cen Norris et al. (1996, 1997).

Chapter 3

Eccentricity Perturbation via the Kozai Mechanism From Jovian Mass Objects

3.1 Introduction

The modification of orbits through the influence of a third body is an old and almost wholly intractable problem. Although some special solutions have been found (e.g. Lagrange points), the general solution is for the most part useless in its full form. Certain approximations can be made which allow examination of certain behaviors of the three-body system. Kozai (1962) treated the perturbation of asteroids by the influence of Jupiter. Other applications for the three-body perturbation are the merger of supermassive black hole binaries (Blaes et al. 2002), eccentric protoplanetary disks (Quintana et al. 2002), and planets around main sequence stars having eccentric orbits (Innanen et al. 1997; Holman et al. 1997; Ford et al. 2000b).

An example of a system where this perturbation is demonstrated is the pulsar PSR1620-26 in M4, discovered by Lyne et al. (1988). It was found to have a 11ms period and a low mass white dwarf as a companion in a 191 day orbit (Rappaport et al. 1995; Sigurdsson et al. 2003). Such a white dwarf-neutron star binary is expected to have a nearly circular orbit with an eccentricity proportional to the period ($e_1 \approx 10^{-4}(P_b/100 \text{ days})$) established by tidal dissipation during the mass transfer phase when the low mass white dwarf was a red giant (Phinney 1992). The observed eccentricity of the binary $e_1 = 0.025$ (McKenna & Lyne 1988)) is a couple orders of magnitude larger than expected for the binary's orbital period. The possibility that other stars in the cluster could have perturbed the eccentricity up to its observed value has been examined (Rasio 1994; Sigurdsson 1993). Rasio (1994) found that the number of necessary encounters would most likely have destroyed the binary. The eccentricity and the peculiarly large second derivative found for the frequency (Backer et al. 1993; Thorsett et al. 1993) indicated that a third body is likely to be perturbing the inner binary, the third object being either a stellar mass $M \lesssim 1M_\odot$ companion with a period $P \sim 10^3$ years (Rasio 1994), or a planet-sized one having $P \sim 10^2$ years (Sigurdsson 1995). Subsequent timing observations (Thorsett et al. 1999; Sigurdsson & Thorsett 2005) have reduced the possible range of values for the size and orientation of the orbit of the third object and its mass.

With an HST observation of the field by Sigurdsson et al. (2003) that identified the white dwarf companion to the pulsar, the mass of the third body was constrained to a few Jupiter masses for most orientations of its orbit. This made it the second post-main sequence object having a planet sized companion, since the planets around PSR1257+12 being the first (Wolszczan & Frail 1992), and challenged theories about the necessity of metals for planet formation (Ward & Brownlee 2000; Lineweaver 2001). I have investigated the possibility that a Jupiter-mass third object in the PSR1620-26

system might be causing the observed eccentricity of the inner binary through the Kozai resonance.

Another example of eccentric orbits that are expectd to be circular are the class of planets called eccentric warm Jupiters typified by 70 Vir (Marcy & Butler 1996). These are planets which have eccentricities of 0.2-0.7. Studies have been done where there is more than one planet visible in the standard radial velocity method (υ And in particular by Ford et al. (2005)). For a sufficiently distant planet, the gravitational effects on other planets of the system might still be present without a sufficiently large reflex motion of the star to be detected (or at least over too long a time to be observed). Astrometric observation of these could be fruitful as the longer baseline would provide a larger angular movement especially for closer examples.

We briefly discuss the secular evolution equations and how they are implemented to obtain variations in the orbital elements of the PSR1620-26 system. We then show our results and compare them to observed properties of the system. Finally, we discuss other applications for this dynamical mechanism to interesting astrophysical problems such as extrasolar planets having eccentric orbits. We give a brief example of a distant third body affecting a Sun-Jupiter analog system.

3.2 Numerical Procedure

The equations for the evolution of the eccentricities (e_1 and e_2) and arguments of periastron (g_1 and g_2) for the two orbits are derived from the three-body Hamiltonian (Harrington 1968)

$$\mathcal{F} = \frac{k^2 m_0 m_1}{2a_1} + \frac{k^2 m_2 (m_0 + m_1)}{2a_2} + \frac{k^2}{a_2} \sum_{j=2}^{\infty} \alpha^j M_j \left(\frac{r_1}{a_1}\right)^j \left(\frac{a_2}{r_2}\right)^{j+1} P_j(\cos\Phi) \qquad (3.1)$$

with k^2 the gravitational constant, m_0 and m_1 the masses of the inner objects, m_2 the mass of the outer object, a_1 and a_2 the inner and outer semimajor axes, α the ratio a_1/a_2, r_1 the separation of the inner objects, r_2 the distance from the inner object's center of mass to the outer object, P_j the Legendre polynomial, Φ the angle between r_1 and r_2, and

$$M_j = m_0 m_1 m_2 \frac{m_0^{j-1} - (-m_1)^{j-1}}{(m_0 + m_1)^j} \qquad (3.2)$$

The first term of the Hamiltonian is the interaction of the two inner bodies, while the second is the interaction of the outer body with the combined inner system. The power series represents the coupling between the two orbits. The first term (proportional to α^2) is what produces the Kozai mechanism whereby the inner orbit is perturbed by the outer orbit. The second term, called the octupole because it is proportional to α^3, represents the effect that the changing inner orbit has on the outer orbit. Differentiating the Hamiltonian and averaging over some short-term variations, as has been done previously (Harrington 1968; Soderhjelm 1984; Marchal 1990), leads to equations that give the secular perturbations of the eccentricity and orientation of the two orbits.

The coupled differential equations for the eccentricities and orientations of the two orbits, which are equations (29)-(32) in Ford et al. (2000b) with the correction as indicated in Blaes et al. (2002), are integrated using the fourth order Runge-Kutta method. Initial conditions for the case of PSR 1620-26 were obtained from Thorsett et al. (1999). The parameters that were kept the same for all runs were the separation and masses of the inner binary ($m_0 = 1.4M_\odot$, $m_1 = 0.3M_\odot$, $P_1 = 191$ days). The solutions are insensitive to small changes in the masses of the inner binary (m_0 and m_1). The inner binary was started with an eccentricity of 10^{-4}, which is caused by the tidal circularization described in Phinney (1992). The three parameters varied among the different runs were the mass of the third object m_2, and the eccentricity e_2 and initial inclination i_0 of the outer orbit. The conditions used for the runs are described in Table 3.1. Each set of initial conditions was integrated for $5{\times}10^8$ years, which reflects the expected lifetime of the system based on the age of the white dwarf (Sigurdsson et al. 2003).

3.3 Simulation Results

3.3.1 Simulations of the B1620-26 system

We ran various series of initial parameters, the extent of which can be found in Table 3.1. A scematic of the sizes of the orbits to scale for the pulsar binary system is given in Figure 3.1. We started with a dense grid in the high inclination regime $80^\circ < i < 100^\circ$ with $m_2 = 1.5, 1.8, 2.1, 2.5, 3.5, 5\mathrm{M}_\odot$ and $e_2 = 0.15$. Changes in the outer eccentricity affect the period of oscillation of the inner eccentricity slightly for values of e_2 within 0.05 to 0.3, but it does not affect the maximum eccentricity achieved by the inner system. The maximum eccentricities are given in table form in Table 3.2 and displayed in Figure 3.2. These curves show a smooth monotonic increase in $e_{1,max}$ with inclination until a sharp drop at a specific vallue related to m_2. The value of the dropoff is related to the value at which i_2, the angle between the outer angular momentum vector and the total angular momentum vector becomes greater than 90 degrees. A set of low inclination models with $m_2 = 2M_{Jup}$ was run to reproduce the peak in maximum eccentricity around 45 and 135 degrees that is expected to be found based on work by Ford et al. (2000b). As is seen in Figure 3.3, there is a peak in $e_{1,max}$ near these two inclinations, but it is much lower than values obtained in the high inclination regime, and so would require a much more massive planet to produce the observed value of e_1. Figure 3.5 shows the family of solutions which produce a value of $e_1 > 0.025$. From other observations of the system (Ford et al. 2000a), upper limits on the mass of the outer body are at about $5\mathrm{M}_{Jup}$.

General relativistic (GR) precession of the inner orbit was included by making $(dg_1/dt) = (dg_1/dt)_{Kozai} + (dg_1/dt)_{GR}$, where

$$\left(\frac{dg_1}{dt}\right)_{GR} = \frac{6\pi G m_0}{a_1(1-e_1^2)P_1 c^2}$$

as first derived by Robertson (1938). When this rate is close to that of the precession caused by the Kozai mechanism, it is important to include GR precession, and as Ford

et al. (2000b) showed, GR precession can contribute to increasing the eccentricity. We performed a coarse grid of models without GR precession to determine the difference qualitatively. Non-GR solutions have a smoother behavior, having a longer period of oscillations than GR solutions. There is a larger set of solutions that allow e_1 to grow to the observed value. Figure 3.4 shows the periods of GR precession (fixed with respect to properties of the outer body) versus the Kozai period given by

$$P_e \simeq P_1 \left(\frac{m_0 + m_1}{m_2}\right) \left(\frac{a_2}{a_1}\right)^3 (1 - e_2^2)^{3/2} \tag{3.3}$$

It is seen that the two periods remain within a factor of 3 through the preferred region of the mass of the outer body. Changing the eccentricities of either orbit within reasonable expectations does not alter this conclusion. The GR precession of the inner binary is important.

Each of the points in Figure 3.5 represents a set of initial conditions which at some point reproduce the observed eccentricity of the binary. This constraint gives us a region in the $i_0 - m_2$ plane, but other observable properties would allow a better prediction. In order to predict another observable property of the binary, we generated curves of how the time derivative of the binary at the observed eccentricity varies with initial inclination and mass of the third object. The value of $\dot{e}_1$ is obtained from the difference in the calculated values of the eccentricity divided by the time step. This could also be done directly from the secular evolution equations. Figures 3.6 to 3.11 show the variation of $\dot{e}_1$ with e_1. Each curve represents one set of initial conditions in i_0 and m_2. The curves follow a narrow trajectory for lower mass outer bodies, but become more erratic at higher masses. The growth of $\dot{e}_1$ is approximately linear until about 2/3 $e_{1,max}$. Table 3.3 shows the average values of $\dot{e}_1$ at the current value of e_1. The measured value of $\dot{e_1}$ is consistent with zero (Thorsett et al. 1999), so we conclude that solutions with their maximum value at the observed value are preferred. If $\dot{e}_1 \sim 0$ and the current value of the eccentricity is a maximum, the mass must fall on the boundary of the region in the $i_0 - m_2$ plane where the initial conditions produce $e_{1,max} > 0.025$, specifically

$$m_2(M_{Jup}) \sim 0.039(i_0 - 90)^2 + 1.13$$

. This boundary is reproduced in Figure 3.5.

For the curves for $e_1(t)$, the number of time steps (each time step represents 10^4 yr) spent in intervals in eccentricity of size 10^{-3} is counted and a histogram made of the count. The result is shown in Figures 3.12 to 3.17. It is seen that, as is typical for an oscillating function, there is more time spent at the extremes than in between. The eccentricity is below 0.01 for much of the time for solutions with $m_2 < 3\ M_{Jup}$, and for higher masses it has a floor value of e_1 which can approach 0.025. Had not these higher masses already been excluded by timing, they might also be considered possible conditions for the system. The reason for the asymmetry is that the curves for $e_1(t)$ have a flatter bottom in the low m_2 intial conditions, while for higher masses the frequency of the oscillations of e_1 inreases. For a function which spends an equal amount of time in each bin, the number of time steps in each bin would be $\bar{N} = N_T/(e_{1,max}\epsilon_{bin})$ where N_T is the total number of time steps, and ϵ_{bin} is the bin size. For these simulations,

$N_T = \epsilon_{bin}$. As a general example, in the case of the simulation with $m_2 = 1.8 M_{Jup}$ and $i_0 = 88^\circ$, ($e_{1,max}$ is about 0.07, and so $\bar{N} = 14$. For these conditions, the count at the bin corresponding to the maximum eccentricity is about twice that, and the bins for $e_1 \lesssim 0.01$ have several times $\bar{N}$. For the allowed masses of the outer body, the time derivative of the eccentricity being zero would indicate a maximum, not a minimum, which implies the mass an initial inclination fall on the relation given above.

3.3.2 Simulations with a Solar System-like Inner System

A few realizations using the present Sun-Jupiter system as a basis were done. The parameters used were: $m_0 = 1$ M$_\odot$, $m_1 = 1$ M$_J$, $e_1(0) = 0.048$, and $a_1 = 5.2$AU. The perturbing body used is a $1 M_J$ planet at 100 AU (referred to herein as Persephone). The range of initial inclinations $i(0)$ used is 10 to 80 degrees in 10 degree increments to provide a even but not overly dense grid and 88 degrees as an extreme case. Two possible eccentricities of the outer planet 0.05 and 0.2 were used as a low and high case to simulate immediately post-capture and later after circularization. The last line of Table 3.1 reiterates the parameters used.

The simulations were run for the same 0.5Gyr as the M4 simulations to keep them similar. We do not expect anything qualitatively different to happen in simulations approaching the expected few to several Gyr duration of systems in the field. First, in the case of a Sun-Jupiter inner system, unlike the WD-MSP binary, the effects of GR precession on the maximum eccentricity achieved by the inner planet are minimal. This is mostly due to the longer period of the Sun-Jupiter system versus the half-year period of the M4 binary, although the reduced mass also contributes somewhat. Second, the eccentricity achieved for even moderate mutual inclinations is very high. Table 3.4 shows that the eccentricity approaches 0.5 for inclinations as small as 50 degrees, and there is a significant jump between 40 and 50 degrees. The higher eccentricity outer orbit leads to a higher maximum eccentricity for the inner orbit by a third at the lowest inclinations, but the effect is reduced at higher inclinations (less than 1% at 70 degrees).

3.3.3 Simulations of the J1903 system

The discovery of pulsar J1903+0327 was and described in Champion et al. (2008). It consists of a 2.15ms pulsar and a roughly solar mass secondary in a 95 day orbit with an eccentricity of 0.44. This is another binary which through standard evolution should be expected to have a low eccentricity ($\sim 10^{-4}$). One of the possible formation scenarios for this system involve it being ejected from a globular cluster. Based on the position and the distance of 6.4kpc that Champion et al. (2008) find from the dispersion measure, the binary lies within 1.55kpc of three clusters: NGC 6760 (1.12kpc), NGC 6712 (1.54kpc), and NGC 6749 (1.55kpc).

Simulations were done with paramaters of the system based on the mass of the pulsar ($m_0 = 1.74 M_\odot$) as given in the paper, a $\sim 1 M_\odot$ companion, and a third object at 3AU. There was a large space of solutions found within our grid which gave the observed eccentricity for this system. While a detailed exploration of the parameter space is warranted, it is beyond the scope of this thesis.

3.4 Discussion

The relative inclination of the system i is the difference in inclination of the inner i_1 and outer i_2 orbits, where the inclination is the angle between our line of sight and the angular momentum vector. Normally, this angle is only defined between 0 and 90 degrees. Negative values are degenerate with a change in position angle of 180 degrees, while values greater than 90 have the same radial velocity profile as the supplemental angle. Attempts to determine the inclination of the orbits from the timing alone led Thorsett et al. (1999) to a value of $i_1 = 40^\circ \pm 24^\circ$ at a 95% confidence, but no constraint on i_2. Based on the mass of the white dwarf as determined from the HST observation, Sigurdsson et al. (2003) found the inner binary has an inclination of $i_1 = 55^{+14}_{-8}$ degrees. Based on the necessary inclinations from our models, we predict that $i_2 = 145^{+20}_{-13}$. The range in i_2 is larger to include the range in relative inclination $i = 85 - 96^\circ$ that are determined from the models. This is the most important parameter of the three studied and is the *sine qua non* for whether the Kozai resonance can produce the observed effect as a massive enough value of m_2 to make up for a lower inclination has since been eliminated.

The timing of the M4 pulsar has slowly reduced the upper limit for the mass of the third object m_2. Original solutions had the mass as high as a few tens of Jupiter masses (Thorsett et al. 1999; Rasio 1994) to explain the high eccentricity of the inner binary without resorting to tidal excitation which would have likely destroyed the system. The low-probability tail of low- or sub-stellar mass ($m_2 \approx 0.1 M_\odot$) high e_2 solutions has recently been ruled out as the planet seems to have reached the outer turning point in its orbit. Based on simulations on how well randomly chosen dynamical variables matched observed derivatives of the frequency (Joshi & Rasio 1997), Thorsett et al. (1999) obtain a mass for the third object of (95% confidence) $m_2 = 11.8^{+37.3}_{-7.3} M_J$. Our models provide a lower limit on the mass of the planet of about that of Jupiter for the observed value of e_1.

Our results do not constrain e_2 well, as a factor of three change from 0.1 to 0.3 produced only a few percent difference in $e_{1,max}$. Rasio (1994) showed that significant jumps in $e_{1,max}$ only occur for values of e_2 greater than 0.5, and recent timing has ruled out such a high value. Because of the exquisite timing, we can also observe how e_1 changes with time. The growth in $|(de_1/dt)_{max}|$ is found to be roughly linear with respect to e_1 up to 80% of $e_{1,max}$. The maximum absolute value of the rate of change in e_1 that is determined from our models is 1.6×10^{-15} s^{-1} for the current value of e_1. The limits of the measured value in Thorsett et al. (1999) of $\dot{e}_1$ is $0.2 \pm 1.1 \times 10^{-15}$ per second fall within this range.

3.4.1 Application to Exoplanets

Dense environments, such as globular clusters and star forming regions, increase the probability of exchange. Objects which come to exist in wide inclined orbits can affect objects in tighter orbits and make eccentric orbits out of what should be by theory circular orbits. A possible example of this is the phenomenon of eccentric warm Jupiters. These are planets whose orbits have eccentricities of 0.2–0.7. Formation of planets in

the standard disk model implies that they should, at least at first, have circular orbits. A few mechanisms have been proposed to explain subsequent evolution of orbits to high eccentricity including close stellar passages (de La Fuente Marcos & de La Fuente Marcos 1997; Laughlin & Adams 1998) or a companion to the star (Holman et al. 1997; Mazeh et al. 1997). The gravitational effect from other planets in the same system as the eccentric giant has been suggested as the cause by Weidenschilling & Marzari (1996b), Rasio & Ford (1996), Lin & Ida (1997), and Levison et al. (1998). Indeed, the signature of the Kozai mechanism is the inward migration of angular momentum from a highly inclined outer object to objects in the inner part of the system.

If, while the protoplanetary system was still in the dense cluster where it formed, it could have had an encounter with another star that exchanged a Jovian mass planet into an wide inclined orbit. The outer planet interacting with the inner system via the Kozai mechanism could cause large eccentricities in the inner planet's orbit while not being visible on current radial velocity surveys as the period would be in the hundreds of years for a 40 AU orbit around a 1 $M_\odot$ star. Intensive hydrodynamic simulations have been done by Bate et al. (2003) and Bate (2009) of moderately dense star clusters undergoing star formation. The simulation shows close passages of stars which profoundly affect their protoplanetary discs. If there should be a planet which formed early on in the history of the cluster, it is not unlikely that it would be exchanged in the numerous encounters seen in the simulation. Currently proposed astrometric searches would be best suited for determining the existence of such planets. Direct imaging of planets around Fomalhaut (Kalas et al. 2008) and HR8799 (Marois et al. 2008) show that massive planets can exist for long timescales at ∼100 AU where being exchanged between stars are likely to deposit them. Exchanges of smaller objects between stars still in their dense star-forming cluster have been proposed to explain objects in our solar system such as Sedna (Morbidelli & Levison 2004).

Considering the extreme effects produced by a 1 Jupiter mass planet on a Sun-Jupiter analog system and the small but measurable effect in the 1700:1 mass ratio case of the third body operating on the WD-MSP binary (albeit in the case of nearly perpendicular orbits), even a body with a few tenths of a Jupiter mass could produce observable effects. In the case of the M4 pulsar system, the outer planet has 4% of the angular momentum of the inner binary, assuming a mass of twice Jupiter in a 20 AU orbit. The same ratio of angular momenta for a solar system analog is achieved by a 3 **Earth**-mass planet in a 100 AU orbit, and for a 1 Jupiter-mass object the angular momentum is nearly 4.5 times as great. Even on the small end of the range of possible masses, presently planned astrometric missions could see the reflex motion for the closest stars ($\lesssim$10 pc).

3.5 Conclusion

The Kozai mechanism can be used for transferring angular momentum between the outer and inner parts of a multiple body system. The case of the M4 pulsar planet system is concidered where a $\lesssim 2M_J$ body pumps the eccentricity of the inner system containing a total mass of $1.7M_\odot$ despite the competing effect of GR precession. With the current estimates for the parameters of the M4 pulsar system (a_2=20 AU and e_2=0.15),

the observed value of the eccentricity of the inner system can be achieved for values of the mutual inclination of the orbits of $85 < i < 96$ degrees for masses of the third body of $m_2 > 2M_{Jup}$. The inclination is the more important element in determining whether the model achieves the observed value of e_1. This high value of the inclination, if confirmed by observation, would discriminate sharply among formation scenarios for this system. Less inclined orbits in both the prograde and retrograde directions do not produce the observed eccentricity for values of m_2 of even 5 times Jupiter, which have already been ruled out.

The eccentricity of the outer orbit does not strongly affect the maximum eccentricity of the binary in our models, so we do not constrain it. The rate of change of the inner orbit's eccentricity is consistent with the limits obtained from our simulations. The size of the outer orbit affects the period of the Kozai resonance, and so determines whether the GR precession damps or reinforces the induced eccentricity. The values used ($a_2 = 20, 42$AU) straddle the maximum of $e_{1,max}$ as a_2 varies (cf. figure 14 of Ford et al. (2000b)), and so the size of the outer orbit should fall within that range.

In the case of an inner system consisting of a sun-like star and a Jupiter-like planet, a much less inclined orbit is sufficient to produce dramatic effects ($e_1 \sim 0.5$), and GR precession in this case can be ignored. The outer body need not even be as massive as Jupiter if it were in a sufficiently inclined orbit. While the instigator of this effect would not be detectable with the commonly used radial velocity methods, space based high precision astrometry missions could be used to determine if some of the planets commonly known as eccentric warm Jupiters exist as a result of the Kozai mechanism.

For the prototype system 70 Vir at a distance of 30 pc, a Jupiter mass planet at 100 AU would cause a movement of the star by 20μas per year, easily seen by presently designed space based astrometry missions. The possible production of systems having a massive planet in a wide, highly inclined orbit in the dense star forming regions early in their lifetime could have an effect on how many habitable planets could exist. The Kozai resonance from the outer planet could directly affect a terrestrial planet causing it to have an undesirably eccentric orbit, or an eccentric inner Jovian type planet could cause the orbit of the terrestrial planet to be chaotic, even insofar as to be ejected.

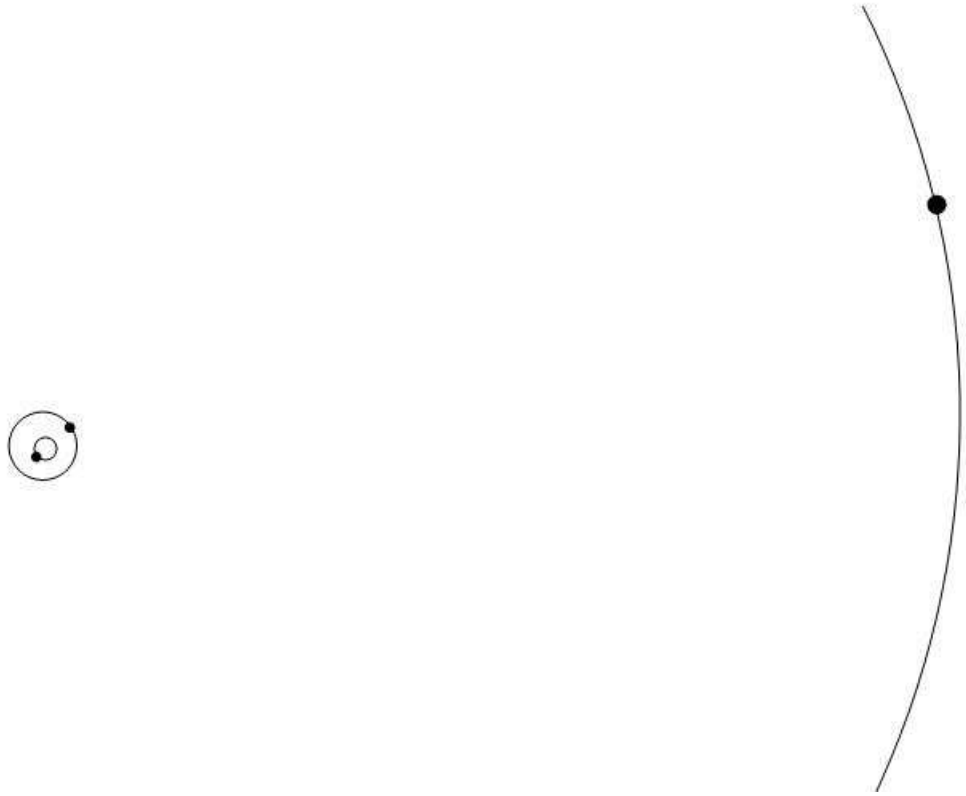

Fig. 3.1 Scale drawing of the PSR 1602-26 system. The inner orbit is approximately 0.75 AU, while the outer body has an orbit of 20 AU. The mass ratio of the inner binary is about 4:1 given a 1.4 solar mass neutron star and a 0.3 $M_{\odot}$ white dwarf. This scematic shows the nature of the system as a heirarchical triple.

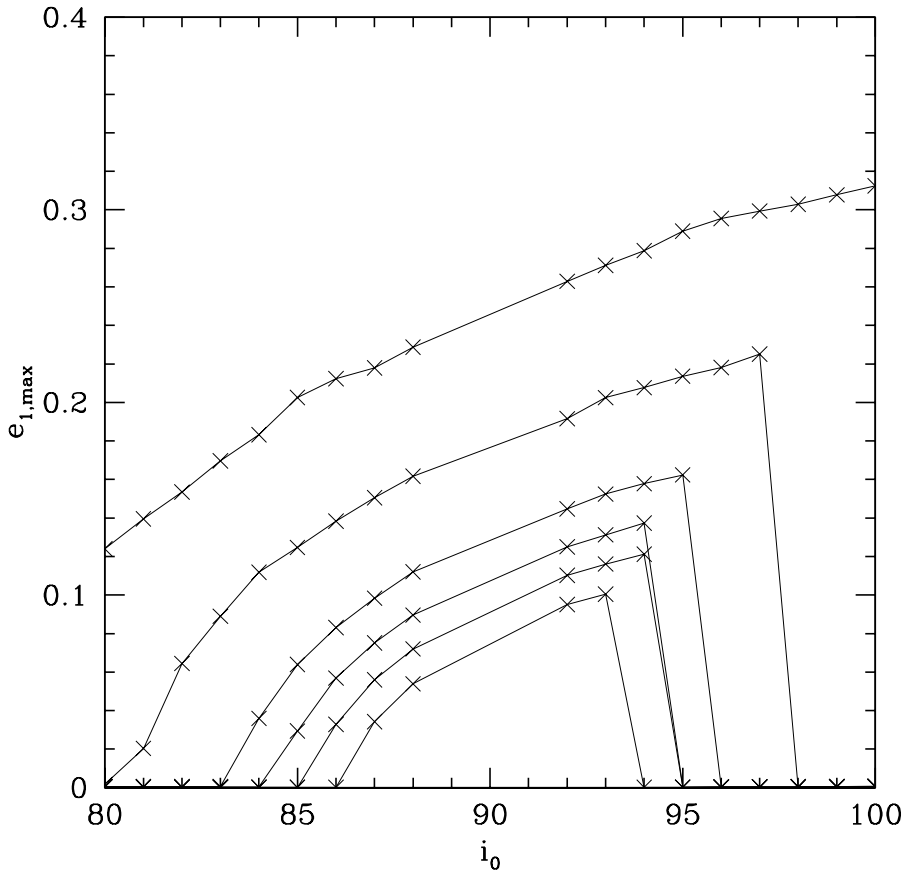

Fig. 3.2 Maximum eccentricity for nearly perpendicular orbits of the third body. The mass $m_2 = \{1.8, 2.1, 2.5, 3.5, 5\}M_\odot$ are shown as having increasingly large eccentricities at all starting inclinations.

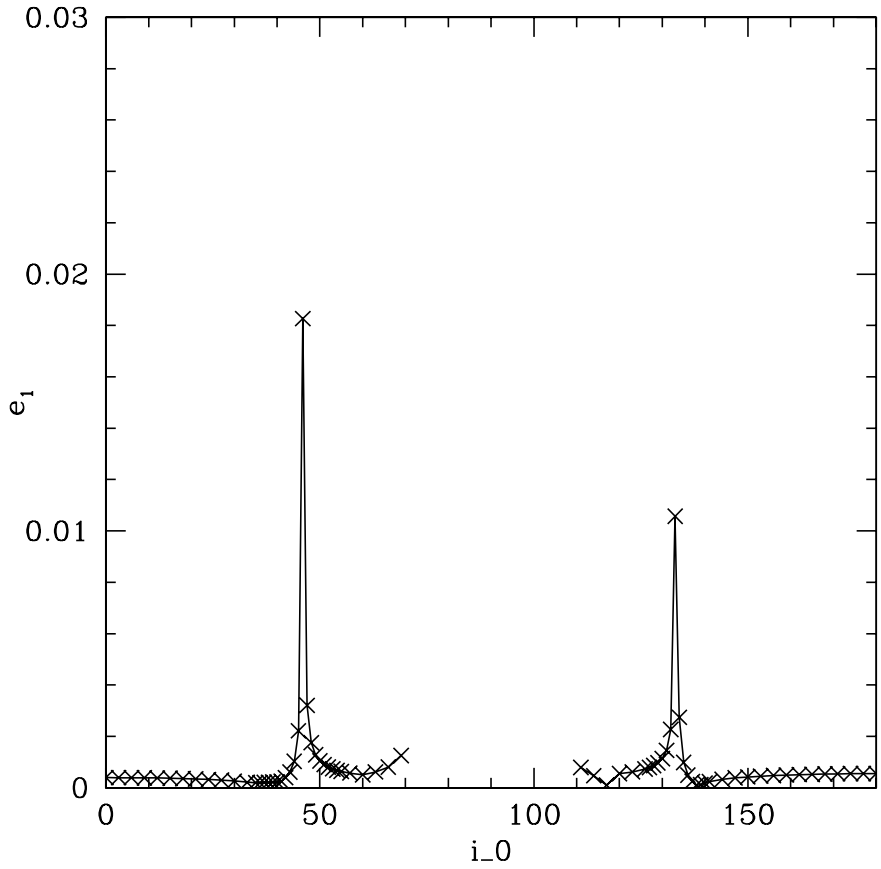

Fig. 3.3 Maximum eccentricity of the pulsar-white dwarf system for low inclination solutions with a 2 Jupiter mass third body. Note that these do not produce the observed value for the binary. The necessary value of m_2 to produce a low inclination solution which does reach the observed eccentricity has been ruled out by observations.

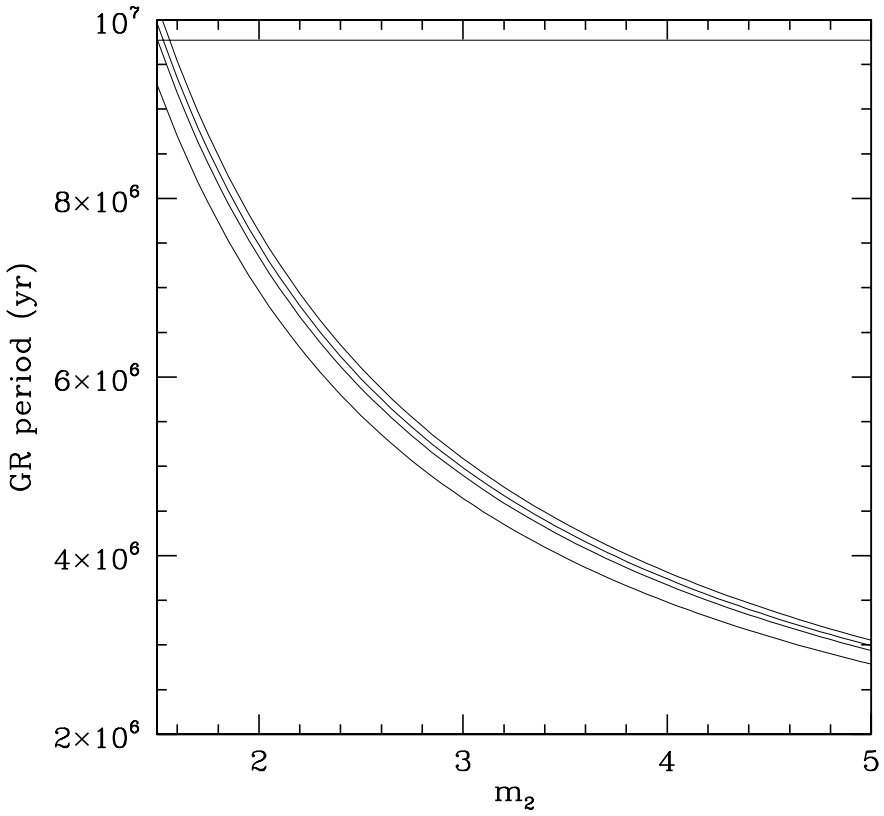

Fig. 3.4 Timescales for general relativistic (GR) and Kozai precession. The horizontal line is the GR precession, which is independent of m_2, while the curves are for $e_2 = \{0.05, 0.1, 0.15, 0.2\}$ from top to bottom. Where the curves are close, the precession from the Kozai mechanism and GR can interfere and so must be taken into account.

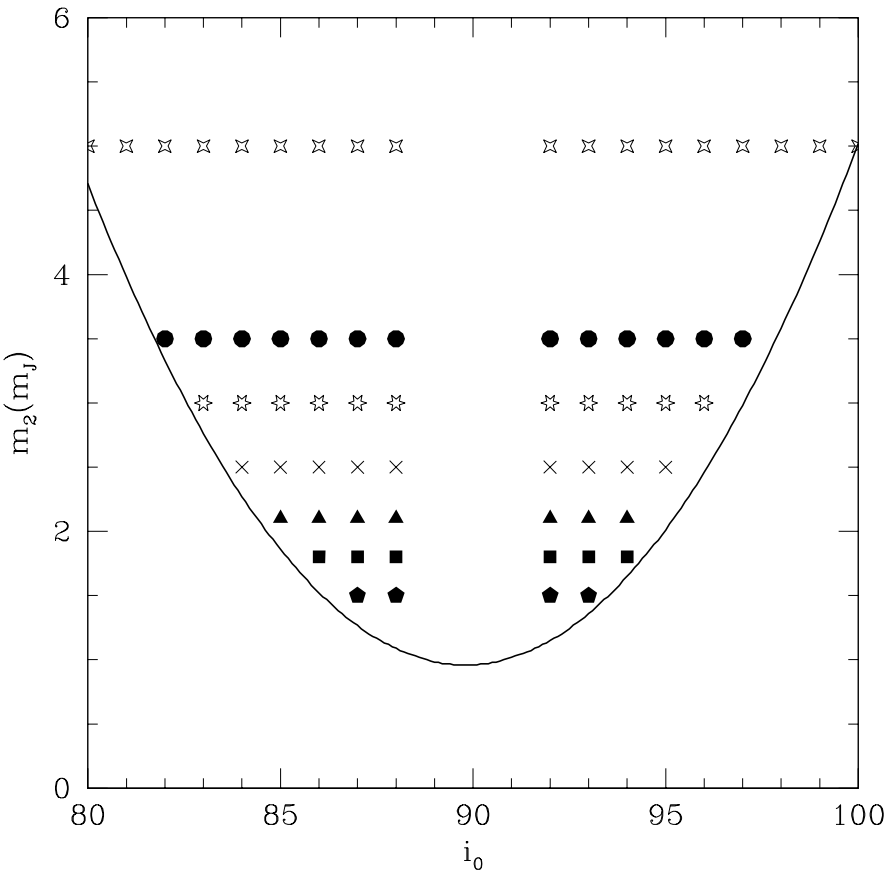

Fig. 3.5 The points show those solutions which have a maximum eccentricity for the binary above the observed value. Each point represents one curve in Figures 3.6 to 3.11 and Figures 3.12 to 3.17. The boundary on this plot shows the set of soultions that have $e_{1,max} = 0.025$ and so are favored by current observations.

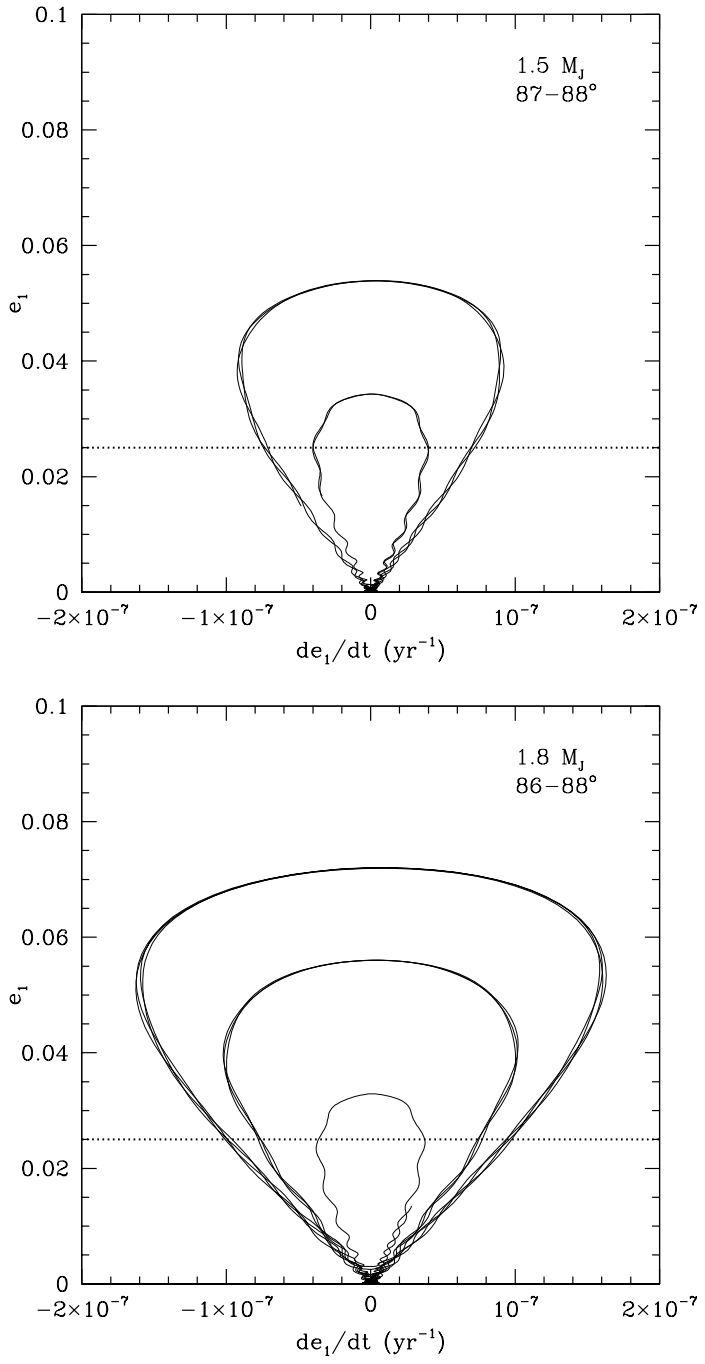

Fig. 3.6 Time derivative of the eccentricity of the binary versus eccentricity. The third body has a mass of $1.5M_{Jup}$ for the top plot, and $1.8M_{Jup}$ for the bottom plot. In the top plot, the curves for 87 (inner) and 88 (outer) degrees are shown. The curves are, by eye, symmetric, well separated, and have a maximum $|de_1/dt|$ of about 10^{-7} yr^{-1} or 3×10^{-15} sec^{-1}. In the bottom plot, the curves are for $i_0 = 88, 87, 86$ degrees from outside to inside. The maximum $|de_1/dt|$ in this plot is 1.5×10^{-7} yr^{-1} or 5.0×10^{-15} sec^{-1}

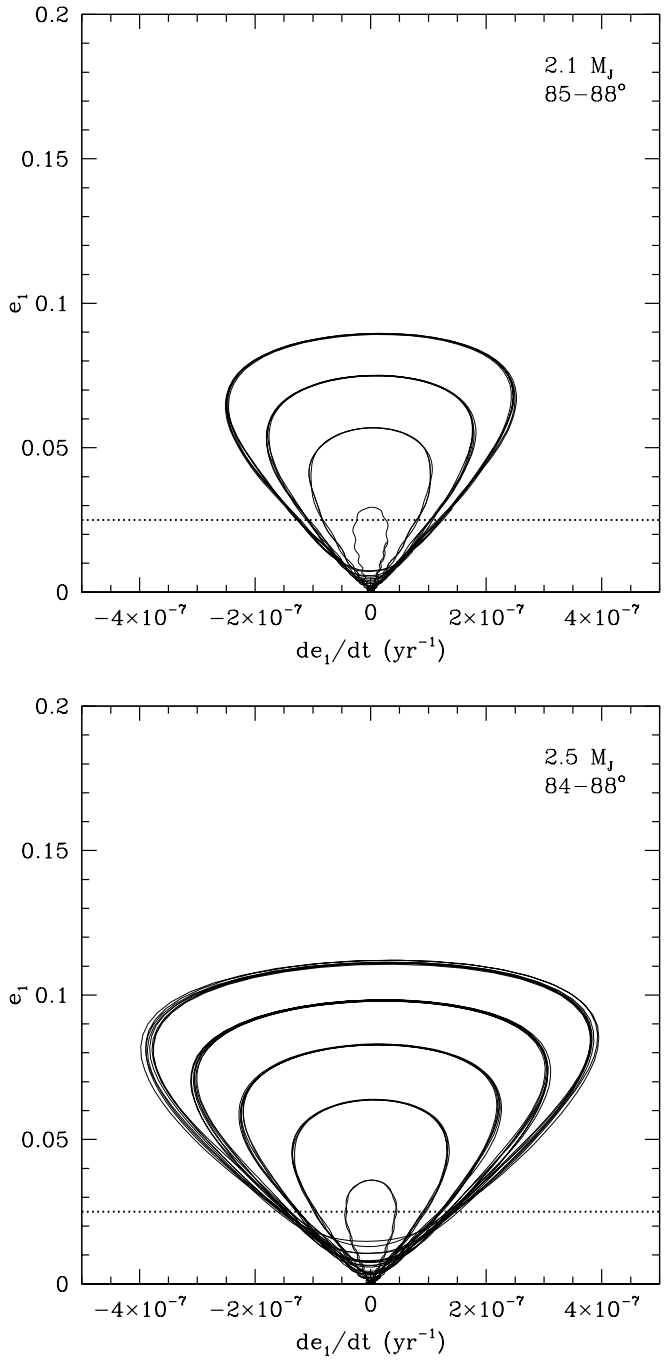

Fig. 3.7 Time derivatives for a 2.1M$_{Jup}$ object with inclinations of 85-88 degrees in the upper plot and a 2.5 M$_{Jup}$ object with inclinations of 84-88 degrees in the bottom plot. Note the change in bottom scale. The curves are still well separated at top, but there is confusion of de_1/dt with inclination for $e_1 < 0.02$. Maximum $|de_1/dt|$ is 2.5×10^{-7} yr^{-1} or 8.0×10^{-15} sec^{-1} for the 2.1M$_{Jup}$ object and 4.0×10^{-7} yr^{-1} or 1.3×10^{-14} sec^{-1} for the 2.5 M$_{Jup}$ object.

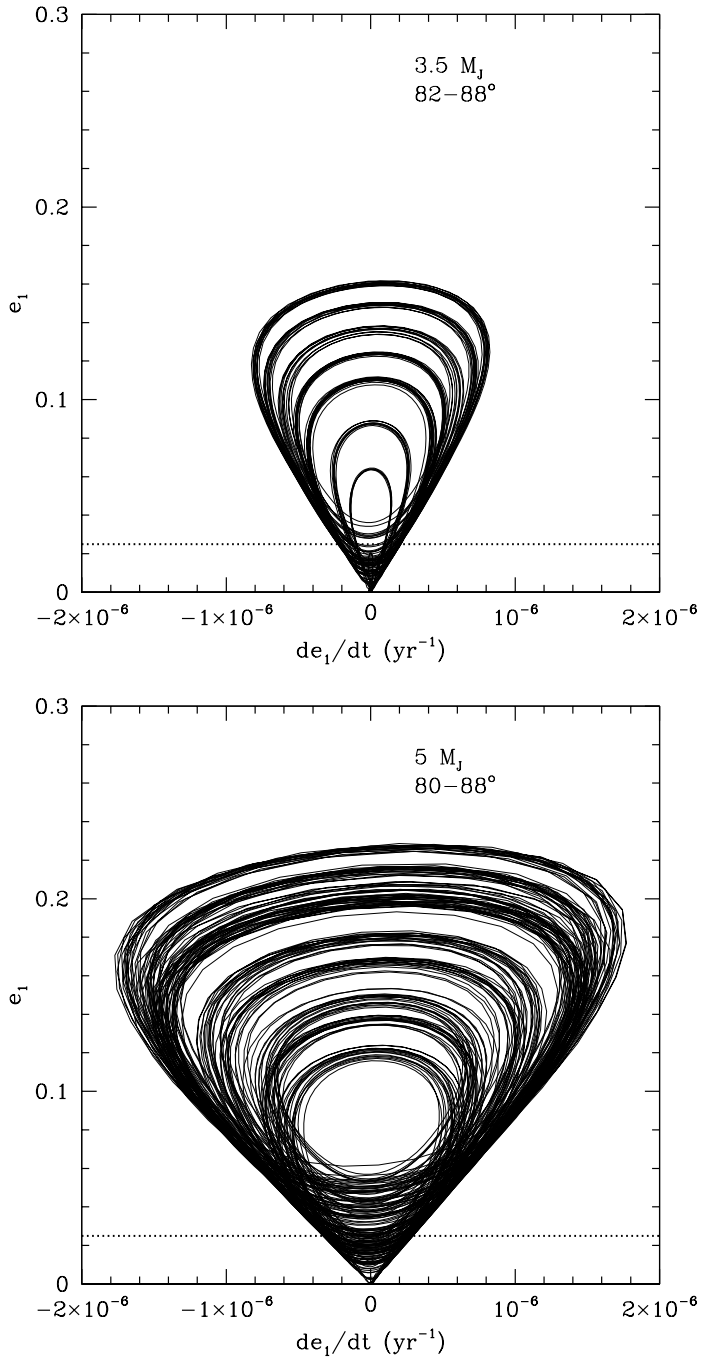

Fig. 3.8 Time derivative of e_1 versus e_1 for a m_2=3.5M_{Jup} object in the top plot, and a 5M_{Jup} object in the bottom plot. Inclinations from 82 to 88 degrees produce visible curves in the top plot, while all inclinations from 80 to 88 show up in the bottom plot. Confusion of mass versus inclination at low e_1 extends up to 0.03 in the top plot, and 0.06 in the bottom plot. The curves are definitely no longer symmetric. For the highest mass objects, $\dot{e_1}(e_1)$ saturates along a linear increase regardless of initial inclination. The scale of the bottom axis has again been increased. Maximum $|de_1/dt|$ is 8.0×10^{-7} yr^{-1} or 2.5×10^{-14} sec^{-1} for the 3.5M$_{Jup}$ object and 1.8×10^{-6} yr^{-1} or 5.7×10^{-14} sec^{-1} for the 5M$_{Jup}$ object.

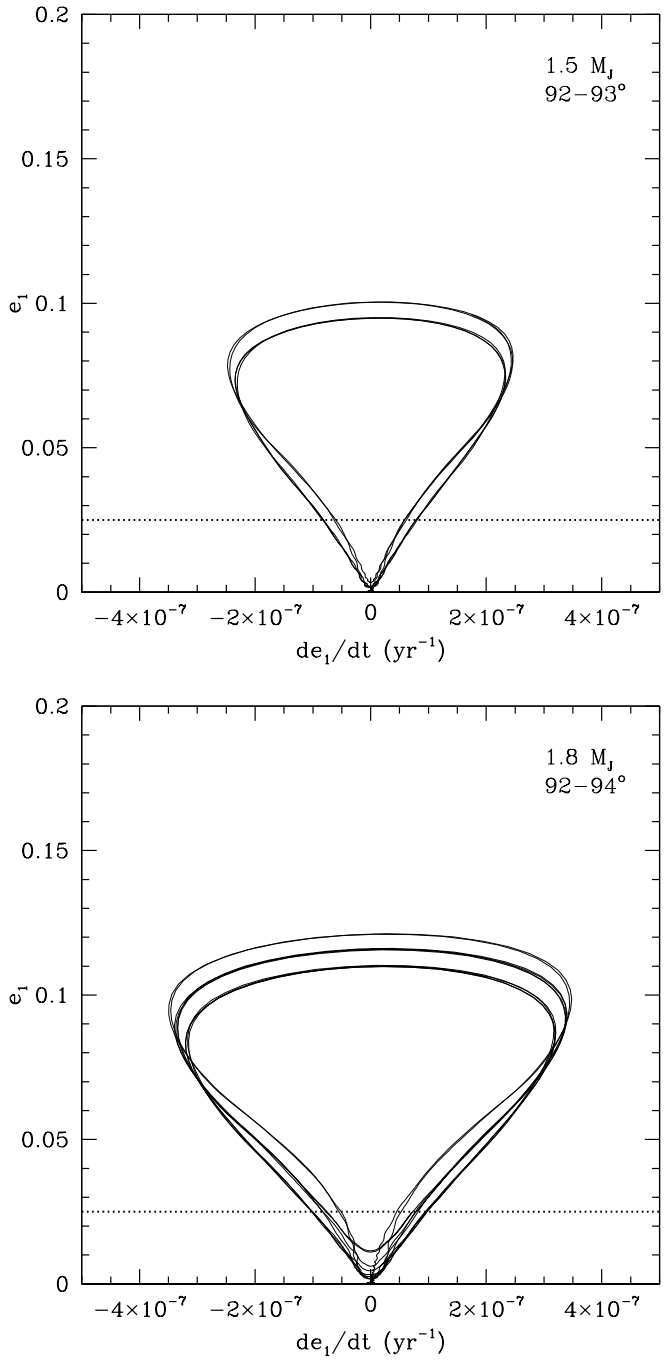

Fig. 3.9 Time derivative of the eccentricity of the binary versus eccentricity. The top plot shows the curves for a $1.5M_{Jup}$ object at an initial inclination of 92 and 93 degrees, while the bottom one plots this for a $1.8M_{Jup}$ object in a 92, 93, and 94 degree initial inclination. For these curves with a lower mass third object, the curves are symmetric across $de_1/dt = 0$. de_1/dt is larger for a given eccentricity for these retrograde solutions than in the prograde case. Maximum $|de_1/dt|$ is 2.5×10^{-7} yr^{-1} or 8.0×10^{-15} sec^{-1} for the $1.5M_{Jup}$ object and 3.5×10^{-7} yr^{-1} or 1.1×10^{-14} sec^{-1} for the $1.8M_{Jup}$ object.

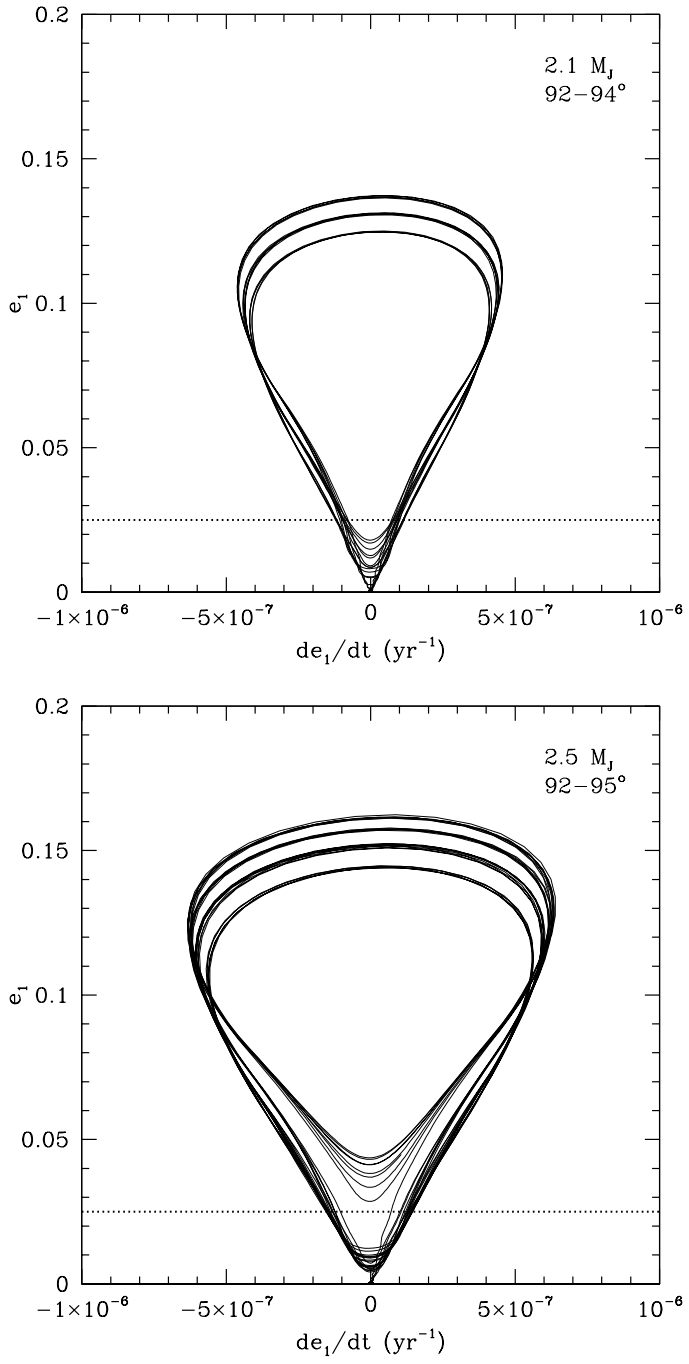

Fig. 3.10 Time derivative of the eccentricity of the binary versus eccentricity for a 2.1M$_{Jup}$ object at 92 to 94 degrees (top plot) and a 2.5M$_{Jup}$ object at 92-95 degrees initial inclination (bottom plot). These curves are not well separated until near their maximum e_1 values. The part of the curve starting from low eccentricity does not seem as linear in $\dot{e_1}(e_1)$ as the prograde solutions. The confusion in starting inclination at low eccentricities can also be seen for $e_1 < 0.02$ in the $m_2 = 2.1 M_{Jup}$ plot. The solution for $m_2 = 2.5 M_{Jup}$ and $i_0 = 92$ degrees shows a minimum of the eccentricity between 0.03 and 0.05 after the first cycle. Maximum $|de_1/dt|$ is 4.5×10^{-7} yr^{-1} or 1.5×10^{-14} sec^{-1} for the 2.1M$_{Jup}$ object and 6.5×10^{-7} yr^{-1} or 2.1×10^{-14} sec^{-1} for the 2.5M$_{Jup}$ object.

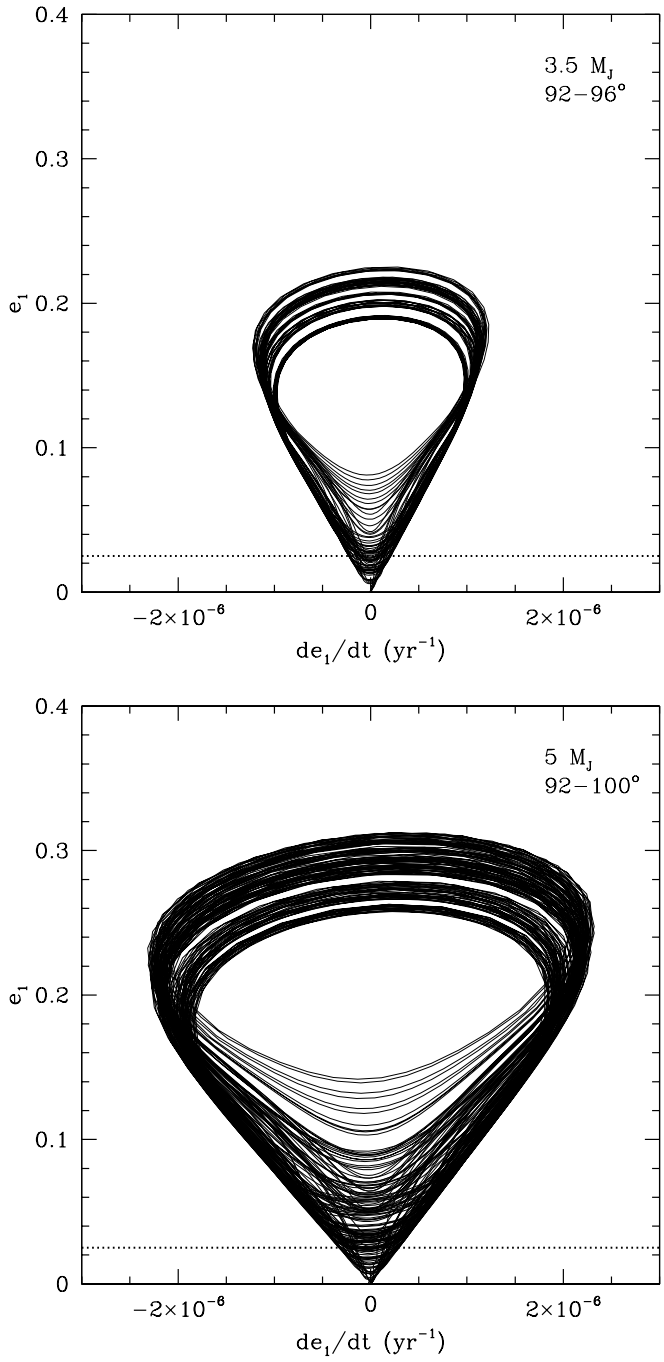

Fig. 3.11 Time derivative of the eccentricity of the binary versus eccentricity for a $3.5M_{Jup}$ object at 92-96 degrees (top plot) and a $5M_{Jup}$ object at 92-100 degrees initial inclination (bottom plot). The asymmetry and saturation of de_1/dt with e_1 can be seen in these high mass retrograde solutions as it was seen in the prograde solutions. For the most part, the curves are well separated only at $e_{1,max}$. Maximum $|de_1/dt|$ is 1.2×10^{-6} yr^{-1} or 3.9×10^{-14} sec^{-1} for the $3.5M_{Jup}$ object and 2.3×10^{-6} yr^{-1} or 7.4×10^{-14} sec^{-1} for the $5M_{Jup}$ object.

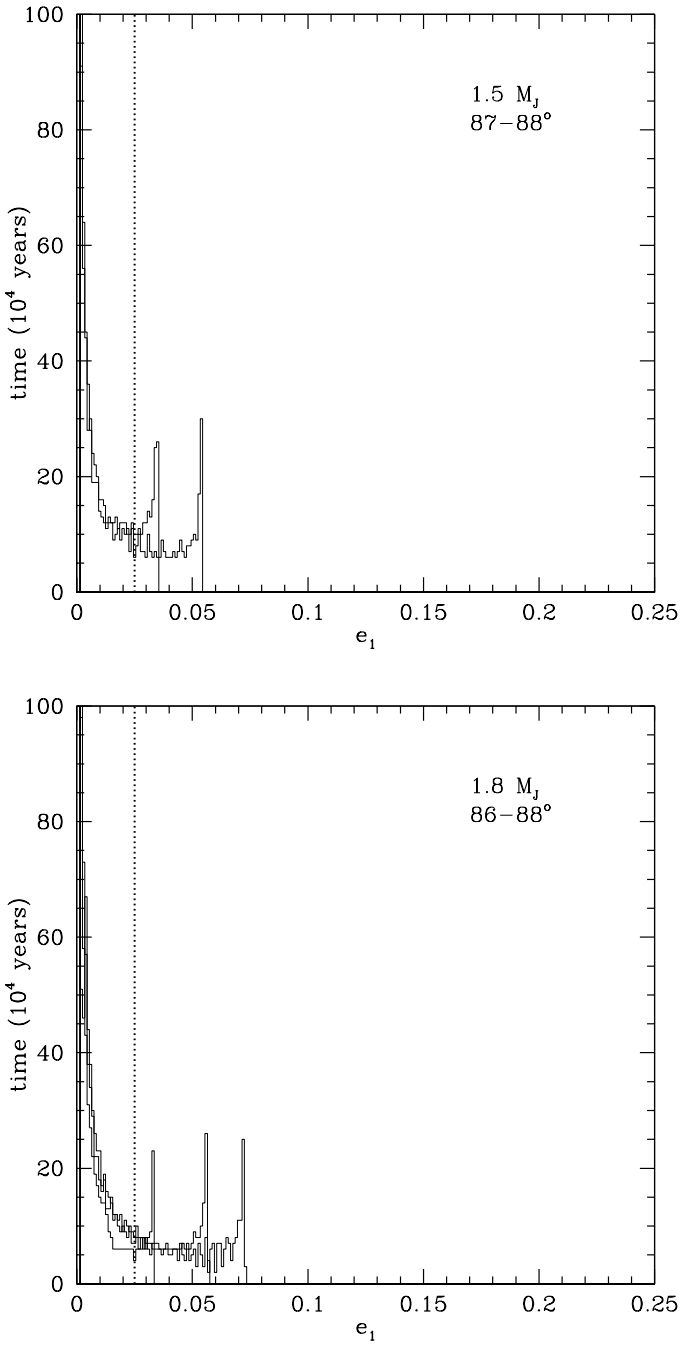

Fig. 3.12 Time distribution of eccentricity in bins of width 10^{-3}. Inclinations shown are 88 and 87 for the top plot, and 88, 87, and 86 for the bottom plot (all others maintained $e_1 < 10^{-3}$). The third body has a mass of $1.5M_{Jup}$ for the top plot, and $1.8M_{Jup}$ for the bottom plot. The eccentricity spends a few times longer near $e_{1,max}$ than at any other eccentricity abover 0.01. This would vindicate the idea that B1620-26 is near its maximum eccentricity as indicated by the time derivative being near zero.

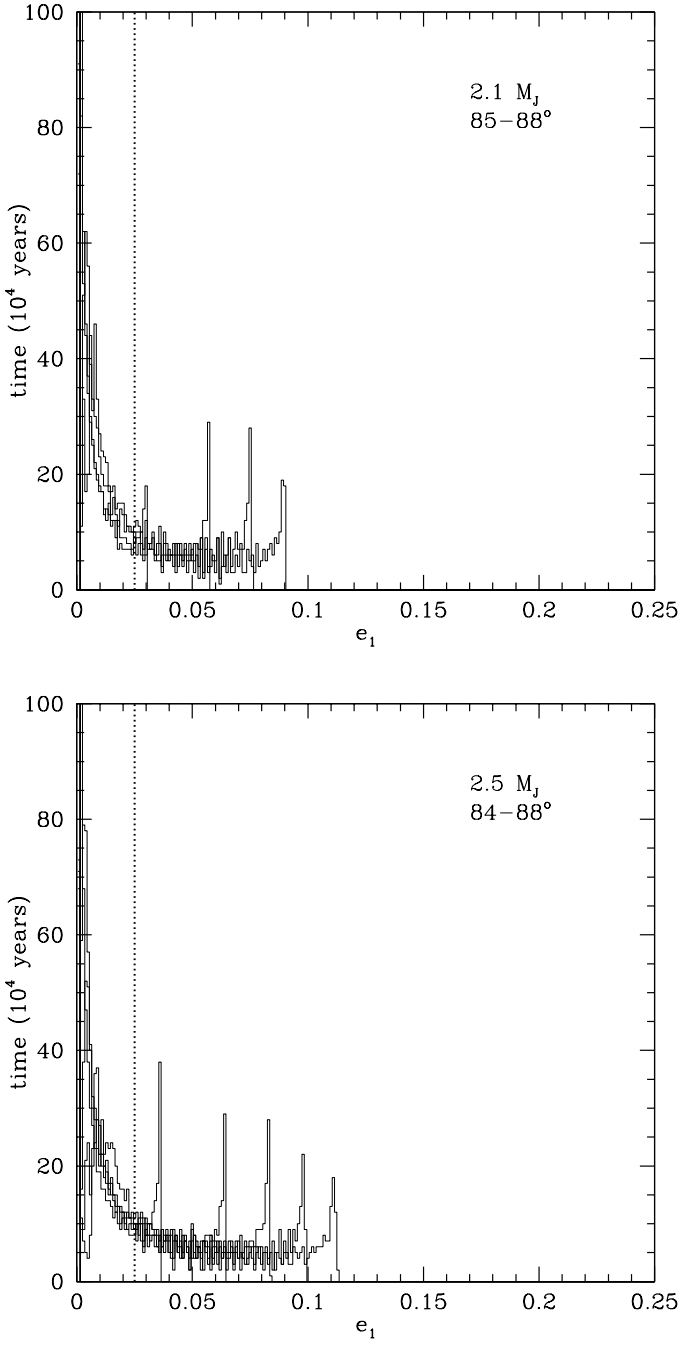

Fig. 3.13 Distribution of time spent at various eccentricities for a 2.1M_{Jup} object at 85-88 degrees (top plot) and a 2.5M_{Jup} object at 84-88 degrees (bottom plot). The behavior is still that the eccentricity spends approximately the average amount of time at most values (i.e. for an $e_{1,max}$ of 0.08, the average time would be 1.25×10^5 years per bin) and 3 or 4 times that near $e_{1,max}$.

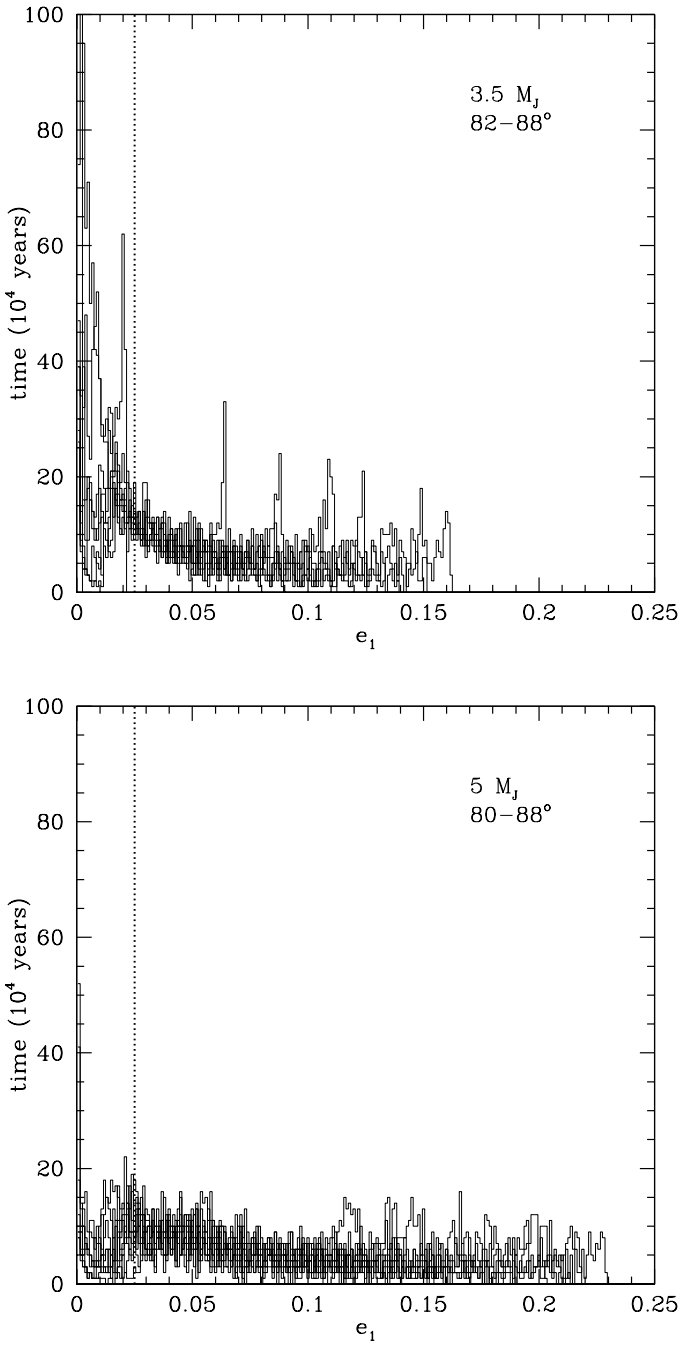

Fig. 3.14 Distribution of time spent at various eccentricities for a $3.5M_{Jup}$ object at 81-88 degrees (top plot) and a $5M_{Jup}$ object at 80-88 degrees (bottom plot). At these high masses and high inclination values, there starts to appear a second maximum in the time distribution at a lower value corresponding to a floor in the eccentricity.

Table 3.1. Initial conditions for simulations

i_0(degrees)	$m_2(M_J)$	$e_2(0)$
Simulations with GR precession		
70, 75, 80	1.3, 1.8, 2.5	0.1, 0.2, 0.3
80-88(1)	1.5,1.8,2.1,2.5,3.5,5	0.15
92-100(1)	1.5,1.8,2.1,2.5,3.5,5	0.15
0-21(3),35-55(1),57-69(3)	2	0.15
111-126(3),127-140(1),141-180(3)	2	0.15
10-80(10), 88	Sun-Jupiter-Persephone system	0.05, 0.2

Note. — Regularly spaced intervals marked as low value-high value(increment). All models have $m_0 = 1.4$ $M_\odot$, $m_1 = 0.3$ $M_\odot$, $e_1(0) = 10^{-4}$, $a_1 = 0.7746$ AU ($P_1 = 191$ days), and $a_2 = 20$AU. Sun-Jupiter-Persephone system is defined by the current Sun-Jupiter system $m_0 = 1$ $M_\odot$, $m_1 = 1$ M_J, $e_1(0) = 0.048$, $a_1 = 5.2$AU and a third body with $m_2 = 1M_J$, $a_2 = 100AU$, and e_2 as given in the table. Each model was run for 5×10^8 years.

Table 3.2. Maximum e_1 values–high inclination. Value only given if $e_{1,max} > 10^{-3}$.

$i(0)$	$m_2 = 1.5M_\odot$	$m_2 = 1.8M_\odot$	$m_2 = 2.1M_\odot$	$m_2 = 2.5M_\odot$	$m_2 = 3.5M_\odot$	$m_2 = 5M_\odot$
80					0.002	0.124
81					0.020	0.140
82					0.064	0.153
83					0.089	0.170
84				0.036	0.112	0.183
85			0.029	0.064	0.125	0.203
86		0.033	0.057	0.083	0.138	0.212
87	0.034	0.056	0.075	0.098	0.150	0.218
88	0.054	0.072	0.090	0.112	0.162	0.229
92	0.095	0.110	0.125	0.145	0.192	0.263
93	0.100	0.116	0.131	0.152	0.202	0.271
94		0.121	0.137	0.158	0.208	0.279
95				0.162	0.214	0.289
96					0.218	0.296
97					0.225	0.299
98						0.303
99						0.308
100						0.312

Table 3.3. de_1/dt values

$i(0)$	$m_2 = 1.5M_\odot$	$m_2 = 1.8M_\odot$	$m_2 = 2.1M_\odot$	$m_2 = 2.5M_\odot$	$m_2 = 3.5M_\odot$	$m_2 = 5M_\odot$
80	0	0	0	0	0	2.73123E-07
81	0	0	0	0	0	2.03146E-07
82	0	0	0	0	9.81281E-08	7.99466E-08
83	0	0	0	0	1.28214E-07	2.1529E-07
84	0	0	0	4.34401E-08	2.02197E-07	2.1699E-07
85	0	0	2.51229E-08	9.44457E-08	2.02585E-07	1.33074E-07
86	0	3.6616E-08	8.15487E-08	1.2431E-07	1.76866E-07	2.50342E-07
87	3.97812E-08	7.62469E-08	1.06392E-07	1.40054E-07	1.9199E-07	1.48663E-07
88	7.18282E-08	9.63179E-08	1.23104E-07	1.51184E-07	1.42855E-07	1.58346E-07
92	8.05786E-08	9.92278E-08	1.16039E-07	1.45455E-07	1.06866E-07	2.45633E-07
93	6.03728E-08	7.72905E-08	8.80645E-08	1.39143E-07	1.69396E-07	1.70005E-07
94	0	5.09071E-08	8.87056E-08	1.22251E-07	1.7579E-07	1.56241E-07
95	0	0	0	7.05992E-08	1.21806E-07	1.55467E-07
96	0	0	0	0	8.52385E-08	2.96465E-07
97	0	0	0	0	1.14265E-07	1.45226E-07
98	0	0	0	0	0	1.28218E-07
99	0	0	0	0	0	1.55596E-07
100	0	0	0	0	0	7.00899E-08

Note. — Time derivative values (yr^{-1}) of e_1 for indicated inclination and outer body mass at the observed value of the inner eccentricity.

Table 3.4. Eccentricities for Sun-Jupiter-Persephone system

i_0(degrees)	$e_2 = 0.05$	$e_2 = 0.2$
10	0.0573	0.0822
20	0.0631	0.0875
30	0.0790	0.1033
40	0.1543	0.1779
50	0.4641	0.4845
60	0.6837	0.7477
70	0.8278	0.8301
80	0.9300	0.9365
88	0.9794	0.9790

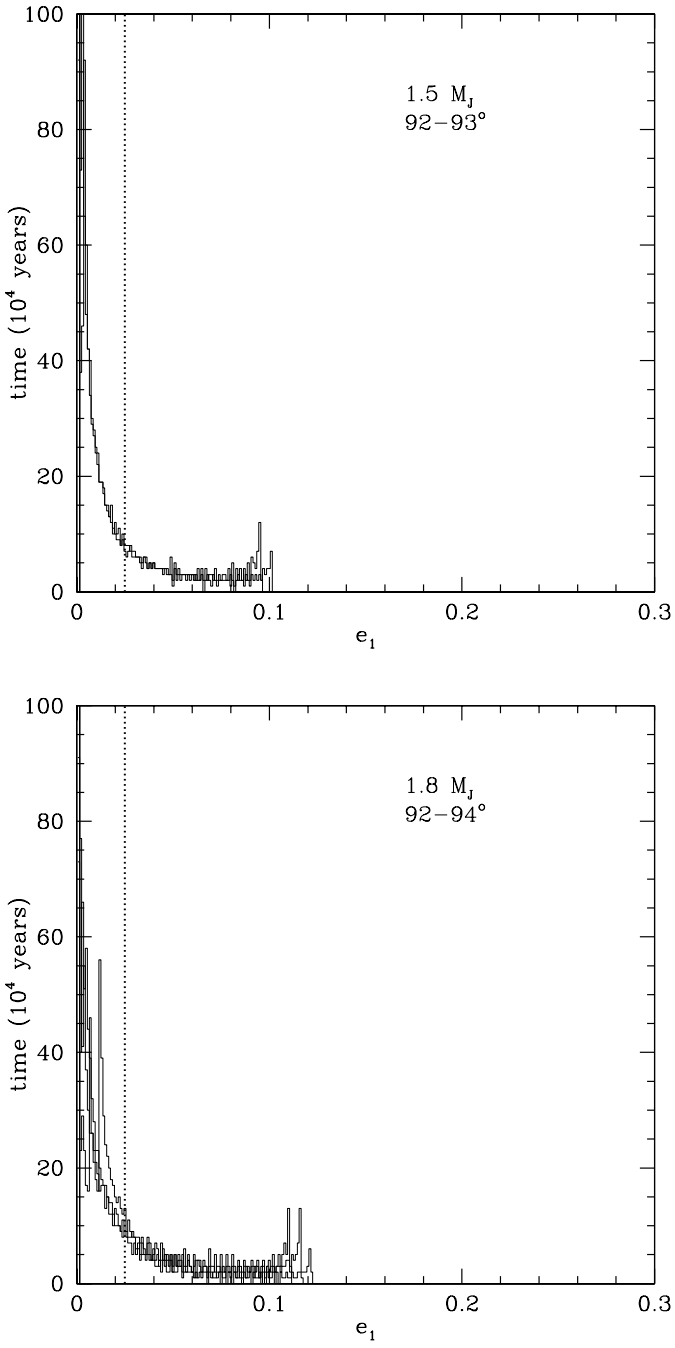

Fig. 3.15 Distribution of time spent at various eccentricities for a $1.5M_{Jup}$ object at 92 and 93 degrees (top plot) and a $1.8M_{Jup}$ object at 92, 93, and 94 degrees (bottom plot). The time spent near $e_{1,max}$ is much less pronounced than for prograde solutions. For the 92 degree solution in the bottom plot, the maximum for $e_{1,floor} \sim 0.015$ is visible, which is significantly higher than for the 88 degree solution with $m_2 = 1.8M_{Jup}$.

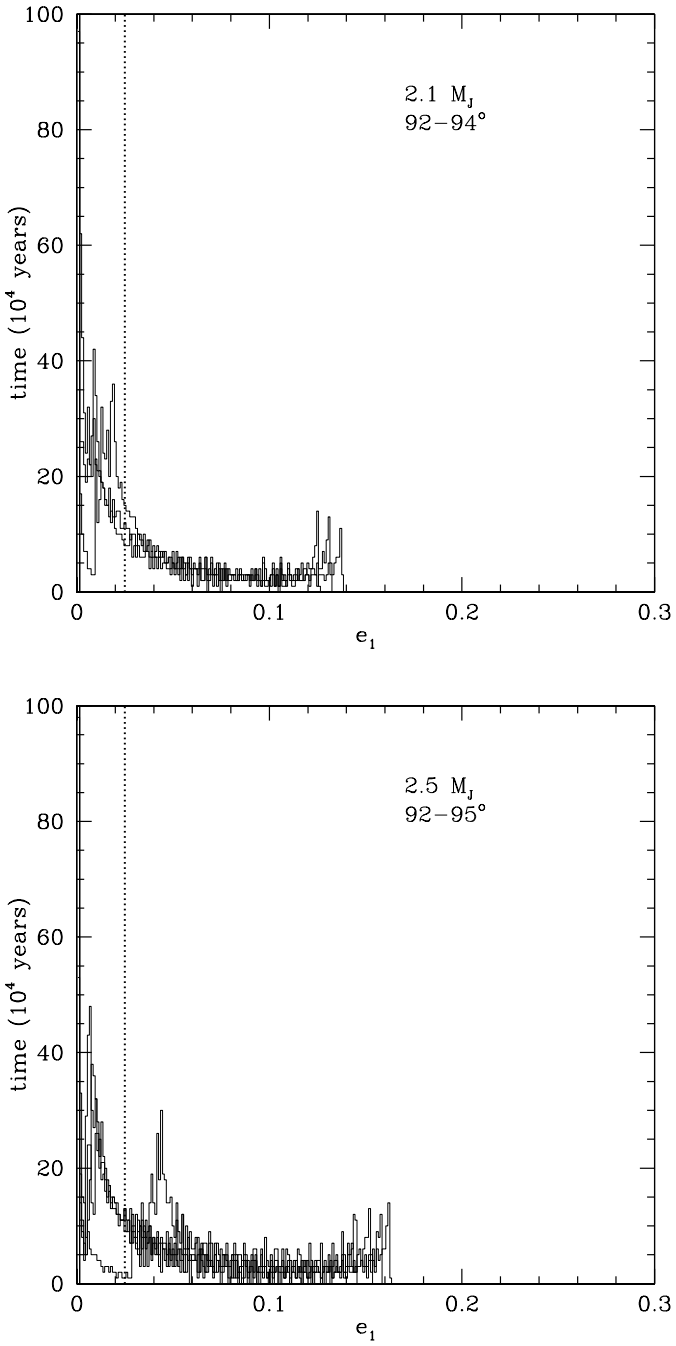

Fig. 3.16 Distribution of time spent at various eccentricities with m_2=2.1M_{Jup} and $i_0 = 92, 93, 94$ degrees in the top plot, and $2.5M_{Jup}$ and $i_0 = 92, 93, 94, 95$ degrees in the bottom plot. The value of $e_{1,floor}$ in the top plot is around 0.02, while the 95 degree soultion has a lower maximum of time spent at $e_1 = 0.042$.

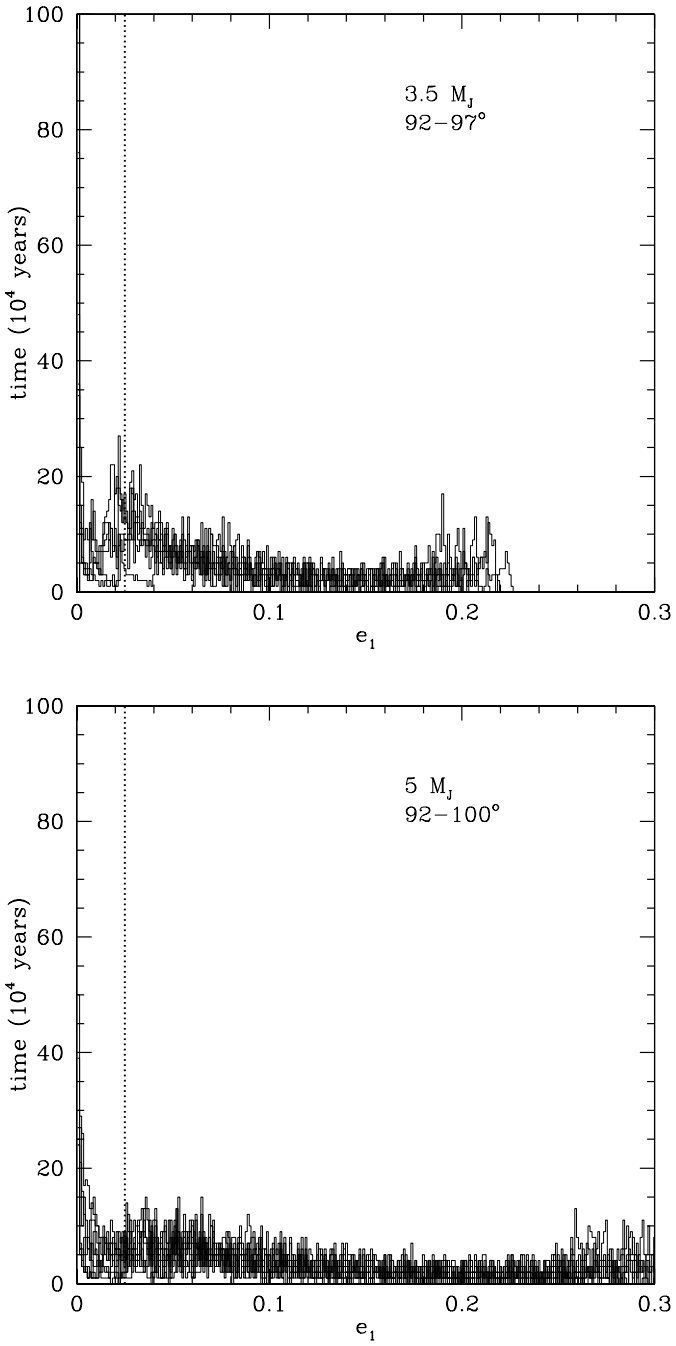

Fig. 3.17 Distribution of time spent at various eccentricities with m_2=3.5M_{Jup} in the top plot, and 5M_{Jup} in the bottom plot for inclinations of 92-100 degrees. The top plot shows values of $e_{1,floor}$ of 0.02-0.04 while the $e_{1,max}$ varies from 0.18-0.22.

Chapter 4

Eccentricity Pumping By a Planet at 50 AU

4.1 Introduction

The ongoing search for extrasolar planets has yielded 373 planets as of August 13 (according to the website exoplanet.eu), most of which have been a surprise to the traditional paradigm of planet formation based onthe solar system. One class in particular, the so-called warm Jupiters of which 70 Virginis is the archetype (Marcy & Butler 1996), is distinguished by their high eccentricity, which can be as high as over 0.9 (0.927 in the case of HD80606b found by Naef et al. (2001)). A few mechanisms have been proposed to explain orbits of high eccentricity include close stellar passages (de La Fuente Marcos & de La Fuente Marcos 1997; Laughlin & Adams 1998) or a companion to the star (Holman et al. 1997; Mazeh et al. 1997). The gravitational effect from other planets in the same system as the eccentric giant has been suggested as the cause by Weidenschilling & Marzari (1996b), Rasio & Ford (1996), Lin & Ida (1997), and Levison et al. (1998).

One other possible origin for high eccentricities of some planets seen in radial velocity studies could be angular momentum transfer with an object in a wider orbit. Dynamical simulations have been done by Adams et al. (2006) and Malmberg et al. (2007b) to examine the frequency of close passages of stars in young clusters. The consequences of the introduction of a companion star in a non-coplanar orbit have been done by direct integration of orbits (Malmberg et al. 2007a; Innanen et al. 1997), and show results consistent with the effect of the Kozai mechanism. Malmberg & Davies (2009) find that the distribution of eccentricities of some planets found in binaries fit their simulations. An exchange of a planet between stars while the stars are in the dense, low-velocity environment of the star forming region could also occur. Due to the isotropic nature of the interactions, the likely orbit of the new planet would be misaligned with the plane in which the inner system presumably formed. If the relative inclination of the two planes was larger than $\sim 40^{\circ}$, the Kozai effect could cause large eccentricities in the inner planets' orbits. An outer planet with a 40 AU orbit around a 1 $M_{\odot}$ star would not be visible on current radial velocity surveys as the period would be in the hundreds of years. Currently proposed astrometric searches would be best suited for determining the existence of such planets. Exchanges of smaller objects between stars still in their dense star-forming cluster have been proposed to explain objects in our solar system such as Sedna (Morbidelli & Levison 2004).

4.2 Description of Initial Conditions

I use the code described in Chapter 3 to integrate the octupole secular evolution equations. I use as initial conditions the Sun $m_0 = 1M_{\odot}$ with either the Earth ($m_1 =$

$3 \times 10^{-6} M_\odot = 1 M_E$, $a_1 = 1AU$) or Jupiter ($m_1 = 10^{-3} M_\odot = 1 M_J$, $a_1 = 5AU$) as the inner planet. Both types of planets are started with an initial eccentricity of $e_1 = 0.03$. Because of the recent spate of low-mass exoplanet discoveries (c.f. Udry et al. (2007)) we also performed runs with a 10 Earth-mass planet at 1AU as the inner body. For the properties of the outer planet, we vary the mass, initial eccentricity, and initial inclination over the following ranges: $m_2 = 0.01, 0.03, 0.1, 0.3, 1.0, 3.0, 10. M_J$, e_2=0.05, 0.1, 0.2, 0.4, and 0.7, and $i(0)$=40, 45, 50, 55, 60, 65, 70, 75, 80, 85, and 88 degrees. The outer planet is given a semimajor axis of 50 AU, excpet for one set where I vary a_2 to explore the effect of the size of the outer orbit. I integrate our models for 10^9 years, which is long enough to let us see all interesting behaviors of the eccentricity. General relativistic precession of the inner planet's orbit is modeled by adding the term

$$\left(\frac{dg_1}{dt}\right)_{GR} = \frac{6\pi G m_0}{a_1(1-e_1^2)Pc^2}$$

from Robertson (1938) to the dg_1/dt equation.

4.3 Results and Discussion

Table 4.1 shows the maximum eccentricities for the Jupiter as the inner planet as a function of mass and initial inclination of the outer planet having $e_2 = 0.05$. Figure 4.1 graphs these for selected eccentricities of the outer body. It is seen that, for even an outer object of 10 Earth-masses ($\log(m_2/M_\odot) = -4.5$)), the eccentricity of a Jupiter analog can reach values of over 0.1 for initial inclinations above 80 degrees. In comparison, the current value for the eccentricity of Jupiter is 0.03. Jupiter mass outer planets can produce extremely large maximum eccentricities. At the highest inclinations, these may perhaps be unbelievably large as above $e = 0.95$ for Jupiter, tidal circularization would become efficient. In the case of Jupiter as the inner body, an important threshold is reached when the mass of the outer body is above one-third of M_{Jup} when the ratio $L_2/L_1 > 1$ is reached. It is at that point where the outer body's influence changes from a perturbation of the inner body's orbit, to driving the eccentricity. Table 4.2 shows the data for changing e_2 with a 40 degree initial inclination. Other inclinations show a similar trend with increasing e_2. There is a slight increase in the maximum eccentricity, but the major effect is on the frequencies of the oscillations. The effect on the Earth analog by the outer planet is much less, as is shown in Figure 4.2. Figure 4.3 shows some example curves of the eccentricity with time. For low eccentricity of the outer body the curves show a simple oscillation. The curves have a more complex behavior for higher eccentricities of the outer body. The $e_1(t)$ curves can be projected as described in Chapter 3 to produce plots which show how long a planet stays at a particular eccentricity. Figure 4.7 and Figure 4.8 show this distribution for Jupiter under the influence of a $0.1 M_{Jup}$ outer planet with various initial inclinations (as indicated on the plots) and eccentricities (e_2=0.05 and 0.1 in Figure 4.7 and e_2=0.2 and 0.4 in Figure 4.8). These plots show the double horned distribution expected for an oscillating solution, but with some time at higher and lower eccentricities than the peaks due to secondary oscillations caused by the ocutpole solution.

In the solar system, the precession of Mercury's orbit has been used as evidence of general relativity. It is the closest planet to the Sun, and so experiences the strongest gravity. This makes it useful as a test particle for post-Newtonian dynamics. With the discovery of extrasolar planets in very tight orbits, there are many more planets in even stronger gravitational gradients than Mercury with which to test the predictions of GR. Direct observation of precession in extrasolar planets is difficult due to their circular orbits. Comparison of secular evolution in multi-planet systems with and without the effects of GR is one alternative method. Adams & Laughlin (2006) and Migaszewski & Goździewski (2009) perform simulations of the υ And and several other observed multi-planet systems as examples the copmetition between co-planar secular evolution and GR effects. For υ And, Adams et al. (2006) finds that GR precession supresses the eccentricity perturbations that would be produced on the inner planet. They find just the opposite for a different system.

The periods of precession due to general relativity (P_{GR}) and the Kozai mechanism (P_K) are shown in Figure 4.4. The GR precession period for Jupiter is 2.1 Gyr, while that for Earth is 33.7 Myr, and these are irrespective of the properties of the outer planet. The Kozai precession timescales are

$$P_{J,K} = 10.7 \text{ Myr} \left(\frac{M_J}{m_2}\right) \left(\frac{a_2}{50\text{AU}}\right)^3$$

$$P_{E,K} = 125 \text{ Myr} \left(\frac{M_J}{m_2}\right) \left(\frac{a_2}{50\text{AU}}\right)^3$$

When the precession from general relativity is slow ($P_{GR} >> P_K$), there is no effect on the Kozai mechanism and high eccentricities can be achieved. If the GR precession time is much shorter than the Kozai precession time, the perturbation on the inner orbit is washed out as GR precession advances the orbit faster than the eccentricity can be increased (Holman et al. 1997). For the Earth analog, the Kozai oscillation timescale (denoted in Figure 4.4 by the dotted lines) for masses of the outer body smaller than $m_2 = 10^{-2.5}\text{M}_\odot$ is much longer than the GR timescale. This is reflected in the fact that eccentricities for these solutions do not increase much beyond 0.035 even for high inclination initial conditions. Only when the outer body is given a mass more than a few times Jupiter is there a significant increase in eccentricity of the inner planet possible. For the Jupiter analog, the GR precession period is longer for all masses of the outer body studied, and even is the case for approximately Earth mass outer bodies. It is shown in Figure 4.5 how the eccentricity maximum varies with changing a_2 for a particular model. After a broad peak in the eccentricity exitation with an a_2 of from several tens of AU to about 150 AU, there is a sharp cutoff. It can be shown that, as a_2 increases, this cutoff is due to the Kozai precession period becoming longer than the GR precessional period. I intend to, in the near future, do a more complete study of the behavior of the inner planets as a response to outer bodies deposited into orbits of different size.

Current estimations of the stability of Jupiter's eccentricity are given in calculations by Kuznetsov & Kholshevnikov (2006) and simulations by Laskar (2008). They show that, absent any outside influence, Jupiter's eccentricity is capped at 0.05-0.06. Our solutions show a 10 Earth mass outer body produces a stronger perturbation at

moderately high inclinations ($\gtrsim$ 70 degrees), while larger bodies are ruled out entirely for inclinations above the critical value of ∼40 degrees for the Kozai mechanism. An effect of a much higher than observed eccentricity for Jupiter would most likely be a disturbing of the well ordered gaps in the asteroid belt due to resonances with Jupiter's orbit. The presence of the other outer planets in simualtions by Innanen et al. (1997) proved to be a stabilizing influence on the eccentricity, and so solutions which would only marginally perturb Jupiter's eccentricity ($e_{1,max} \sim 0.1$) might still be allowed.

Consider the object called Sedna, as discovered by Brown et al. (2004). It has a semimajor axis of over 500 AU and an eccentricity of about 0.9. Scenarios for the placement of this object in such an object were explored in Morbidelli & Levison (2004) and include interactions with Neptune, interactions between planetesimals in the early history of the solar system, close passages by other stars, and its capture from another star. If we were to suggest that there were a massive object farther out that is influencing Sedna's orbit via the Kozai mechanism, it is possible to estimate some of properties this outer object would have. By using the expression for the maximum eccentricity from the Kozai mechanism from Holman et al. (1997) $e_{1,max} \sim \sqrt{1 - 5/3 \cos^2 i_0}$, the inclination of the outer body should be about 60 degrees. To retain the assumption of a hierarchical triple, the outer body must have a semimajor axis at least a few times that of Sedna. The mass of the outer perturbing object and the eccentricity of its orbit are not amenable to simple calculation, but must be found through testing various initial conditions. Simulations of an outer body have been done by Legel et al. (2009).

Table 4.1. $e_{1,max}$ for Jovian inner planet versus mass of the outer planet. Outer planet has $e_2(0) = 0.05$.

i_0	$\log m_2(M_\odot)$						
	-5.0	-4.5	-4.0	-3.5	-3.0	-2.5	-2.0
40	0.03131	0.03381	0.04165	0.06319	0.10850	0.15962	0.19080
45	0.03295	0.03889	0.05590	0.10266	0.28442	0.37127	0.40484
50	0.03227	0.03702	0.06239	0.23010	0.44381	0.52286	0.55350
55	0.03296	0.03959	0.08144	0.36524	0.56457	0.64002	0.66882
60	0.03389	0.04336	0.15857	0.46558	0.66217	0.73559	0.76238
65	0.03523	0.04917	0.25768	0.55477	0.73913	0.81430	0.83893
70	0.03768	0.06759	0.34730	0.62997	0.81118	0.87704	0.90065
75	0.03886	0.08341	0.41719	0.69592	0.86988	0.92179	0.94841
80	0.04488	0.15252	0.47678	0.75518	0.91774	0.96111	0.98118
85	0.06331	0.22229	0.52918	0.80791	0.95316	0.98641	0.99177
88	0.08668	0.25440	0.55818	0.83636	0.97055	0.99399	0.99967

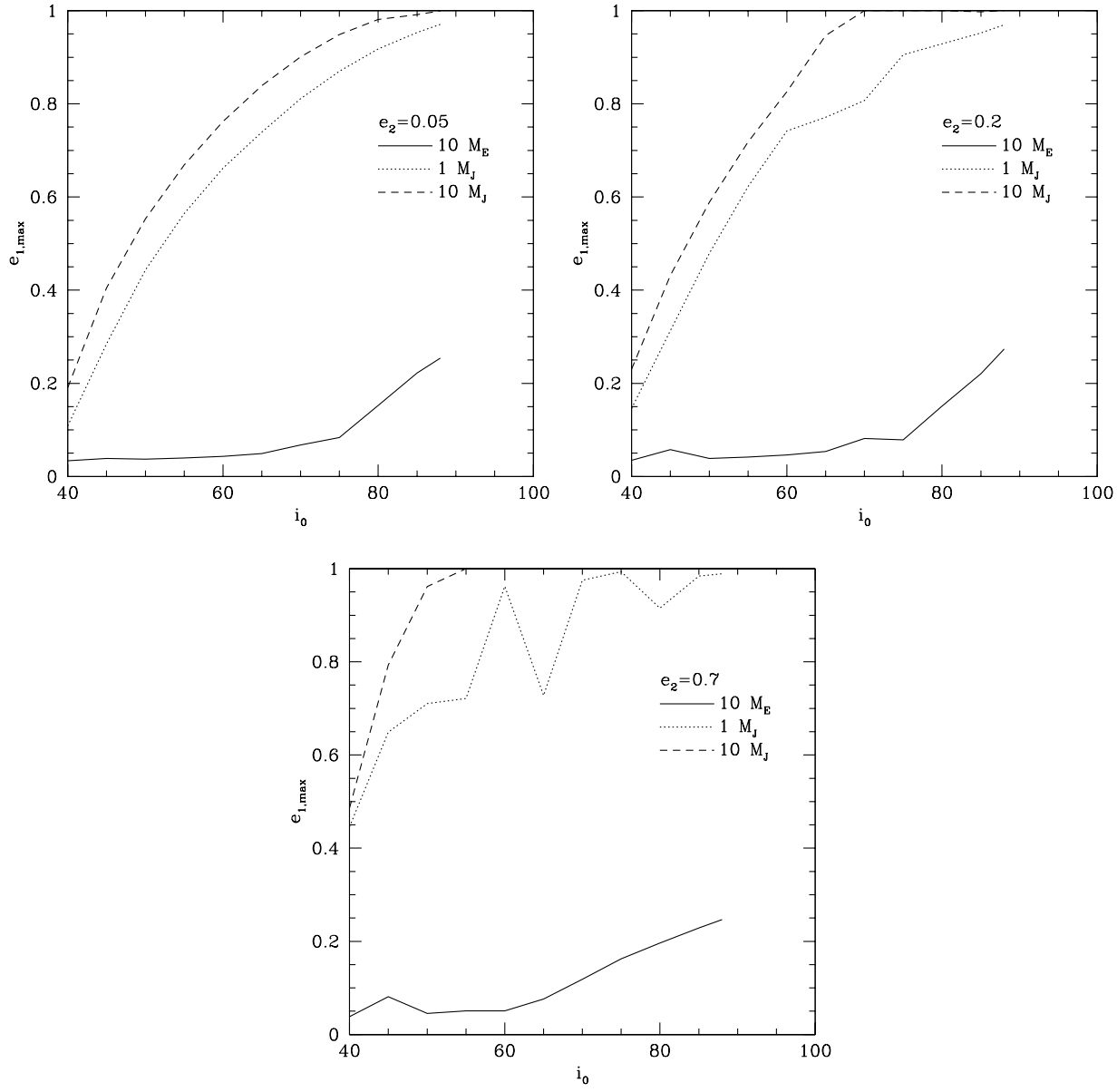

Fig. 4.1 Maximum eccentricity achieved by the Jupiter analog as a function of initial inclination of the outer object's orbit. Left plot is for a value of $e_2 = 0.05$, the right has $e_2 = 0.2$, bottom plot has $e_2 = 0.7$. Solid line is for an outer object having a mass of $10M_{Earth}$, dotted is for $1M_{Jupiter}$, and the dashed is for $10M_{Jupiter}$. Note that the increase in eccentricity of the outer body's orbit has two main effects: a slight increase in the maximum eccentricity, but mostly noticable at lower inclinations, and an increase of the maximum eccentricity seen at 45 degrees.

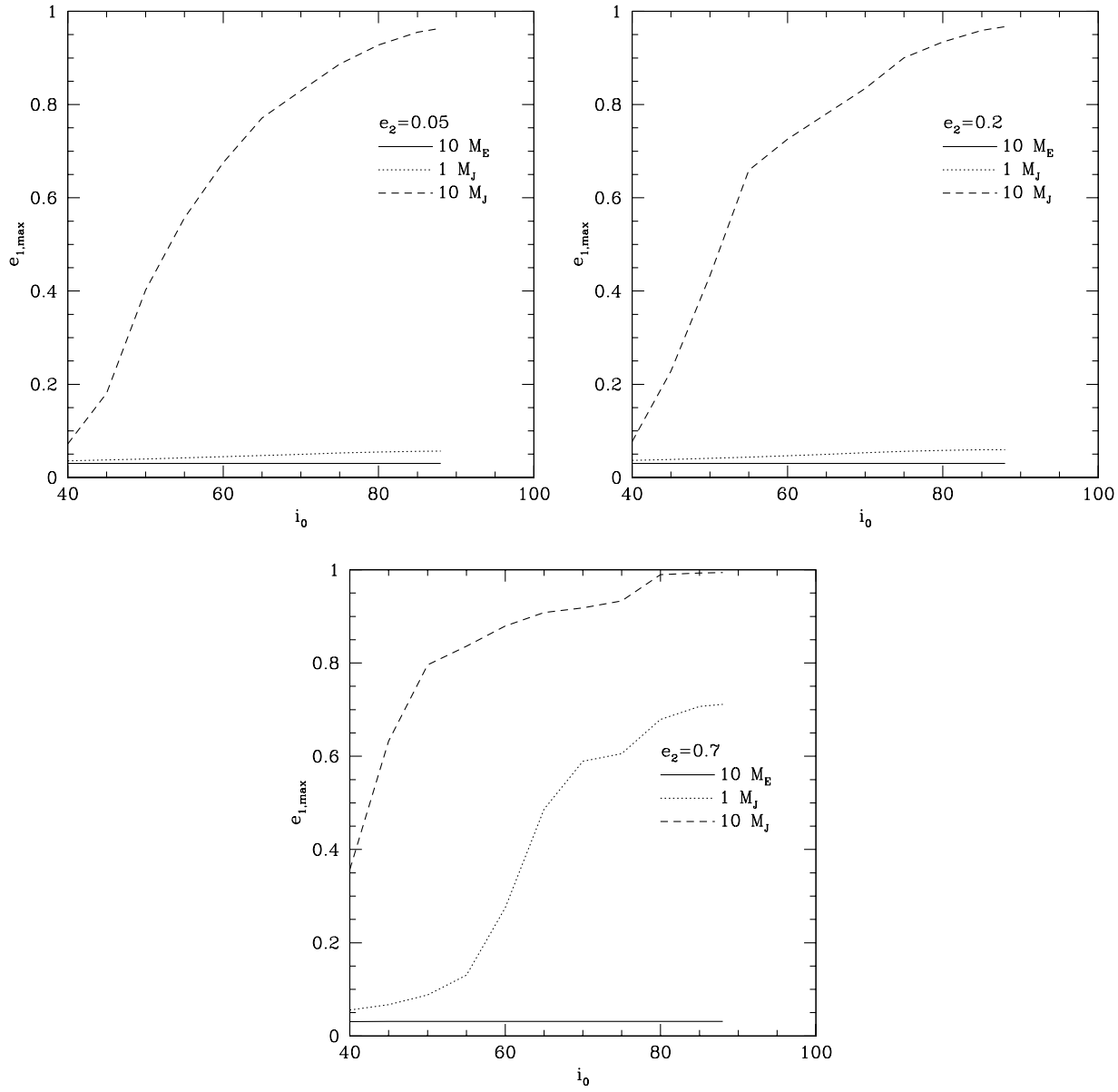

Fig. 4.2 Maximum eccentricity achieved by the Earth analog as a function of initial inclination of the outer object's orbit. Left plot is for a value of $e_2 = 0.05$, the right has $e_2 = 0.2$.

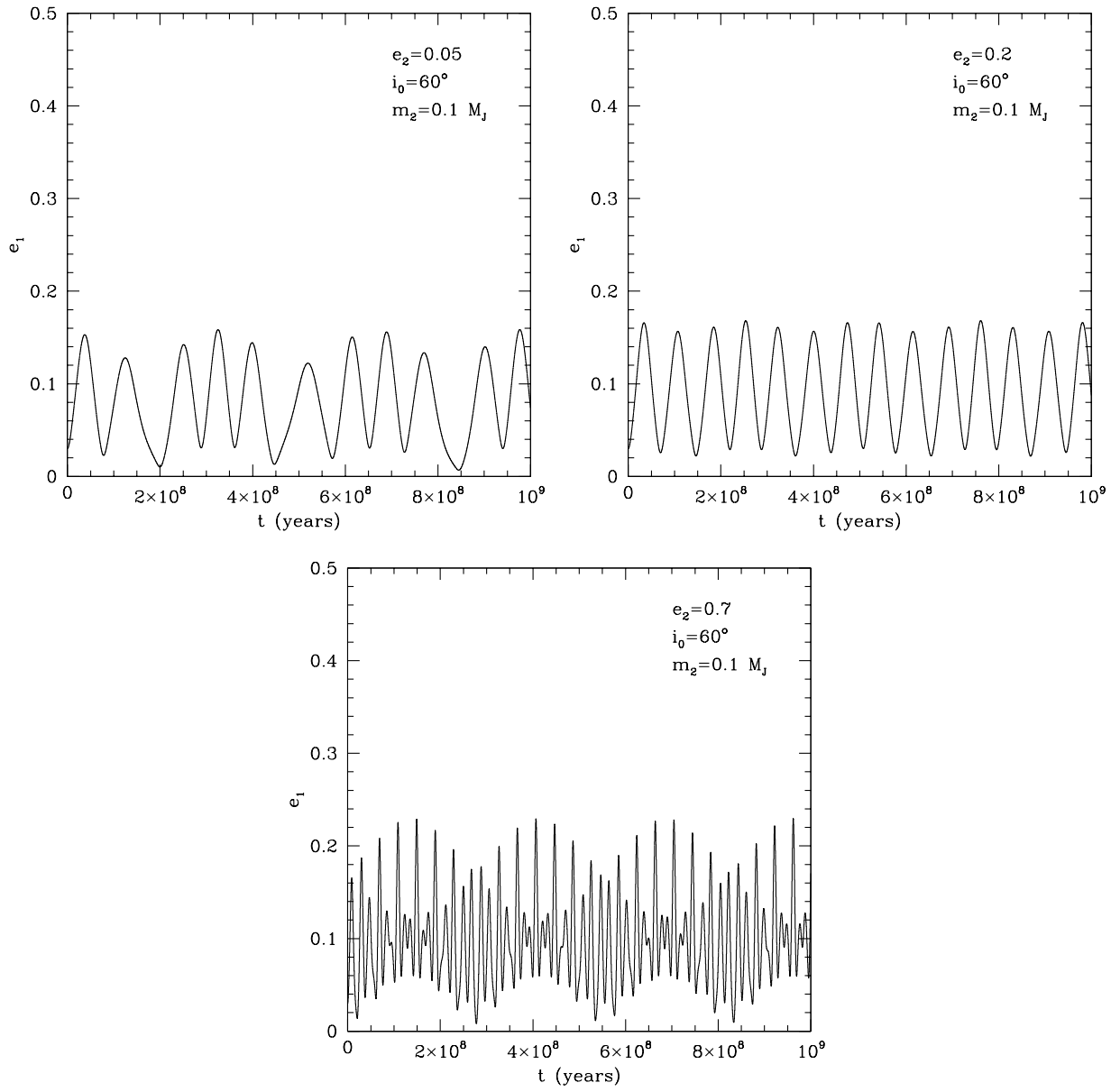

Fig. 4.3 Eccentricity as a function of time for the Jupiter analog. The top left plot has $e_2 = 0.05$, the right plot has $e_2 = 0.4$, and the bottom plot has $e_2 = 0.7$. The primary effect of increasing the outer body is to shorten the quasi-period of the eccentricity oscillations.

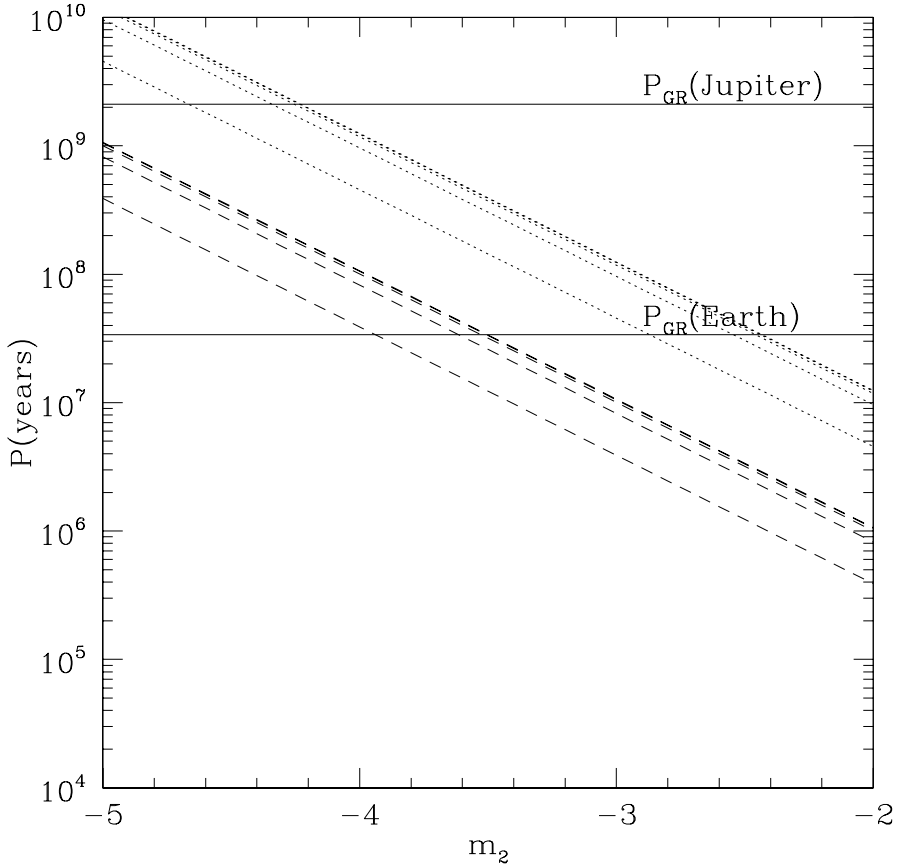

Fig. 4.4 Precessional timescales for general relativistic (GR) and Kozai precession. Horizontal lines are GR timescales as this is independent of the outer body. The dotted set of lines are for the Earth analog body, while the dashed set of lines are for the Jupiter analog. The outer eccentricity increases downward along the set having values $e_2 = \{0.05, 0.1, 0.2, 0.4, 0.7\}$.

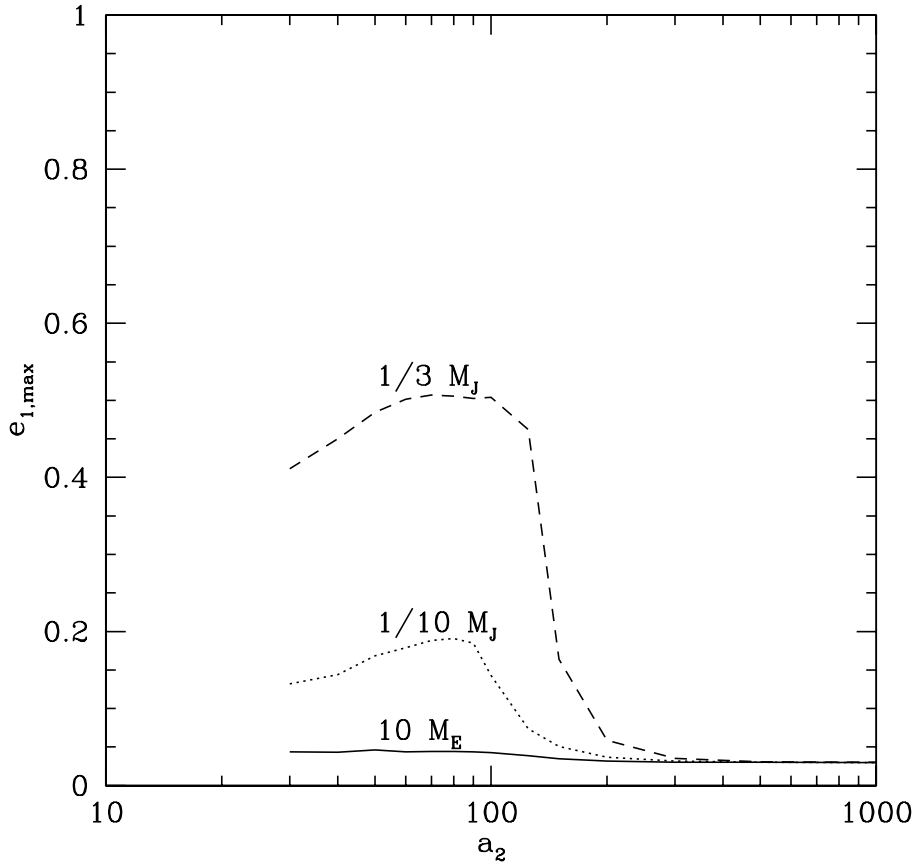

Fig. 4.5 Variation of the maximum eccentricity of the Jupiter-analog planet with different a_2 values. There is a broad peak of semi-major axes for which a significant increase of the eccentiricty occurs. We also see a sharp decline at 150 AU. The solid line is for a 10 Earth mass outer planet, the dotted has m_2 of 1/10th Jupiter's mass, the dashed line has m_2 of 1/3 Jupiter's mass. The initial inclination was 60 degrees, and the outer body's eccentricity started at 0.2.

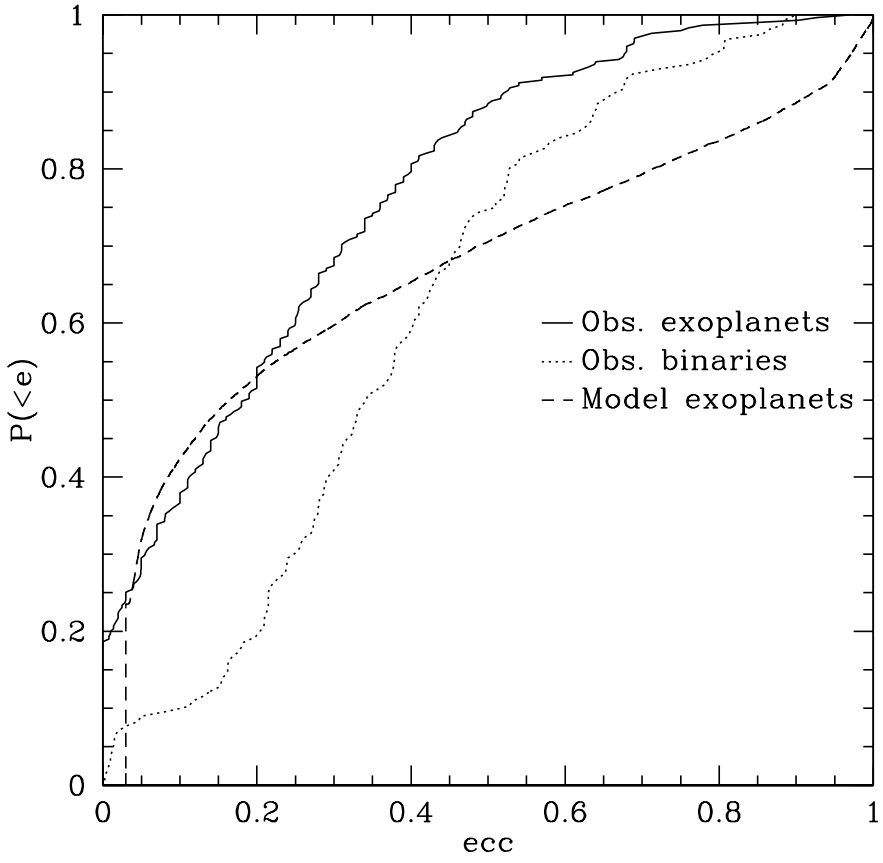

Fig. 4.6 Cumulative eccentricity distributions for observed exoplanets (solid line), a set of spectroscopic binaries found by Latham et al. (2002) (dotted line), and the set of planets chosen as described in the text (dashed line). As is described in Malmberg & Davies (2009), 23% of the planets do not have their eccentricities affected by the outer body. The observed exoplanet curve and our curve are close up to an eccentricity of 0.2, at which point high eccentricity ($e \geq 0.5$) systems are overproduced. This may be due to the fact we use the maximum eccentricity.

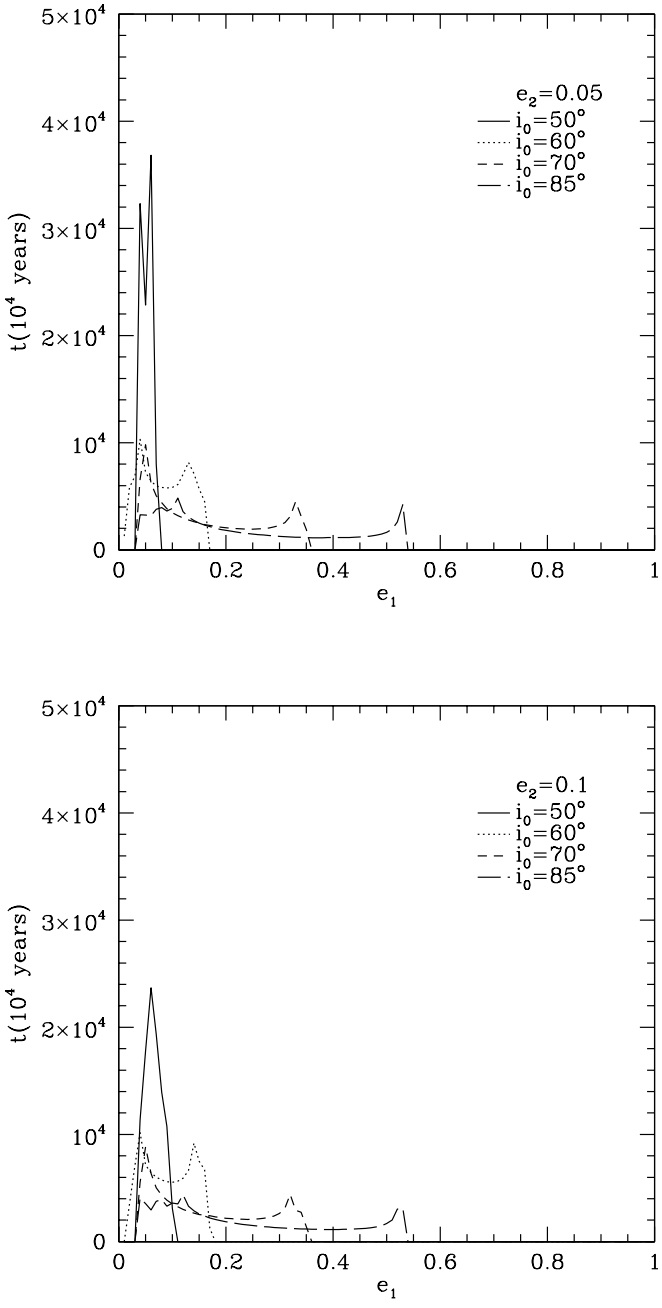

Fig. 4.7 Eccentriicty distributions for solutions with a 1/10 Jupiter mass outer body. Solid line has initial inclination of 50 degrees, dotted has $i(0)$ of 60, short dashed is 70, long dashed is 85. Top plot has $e_2 = 0.05$, bottom has $e_2 = 0.1$.

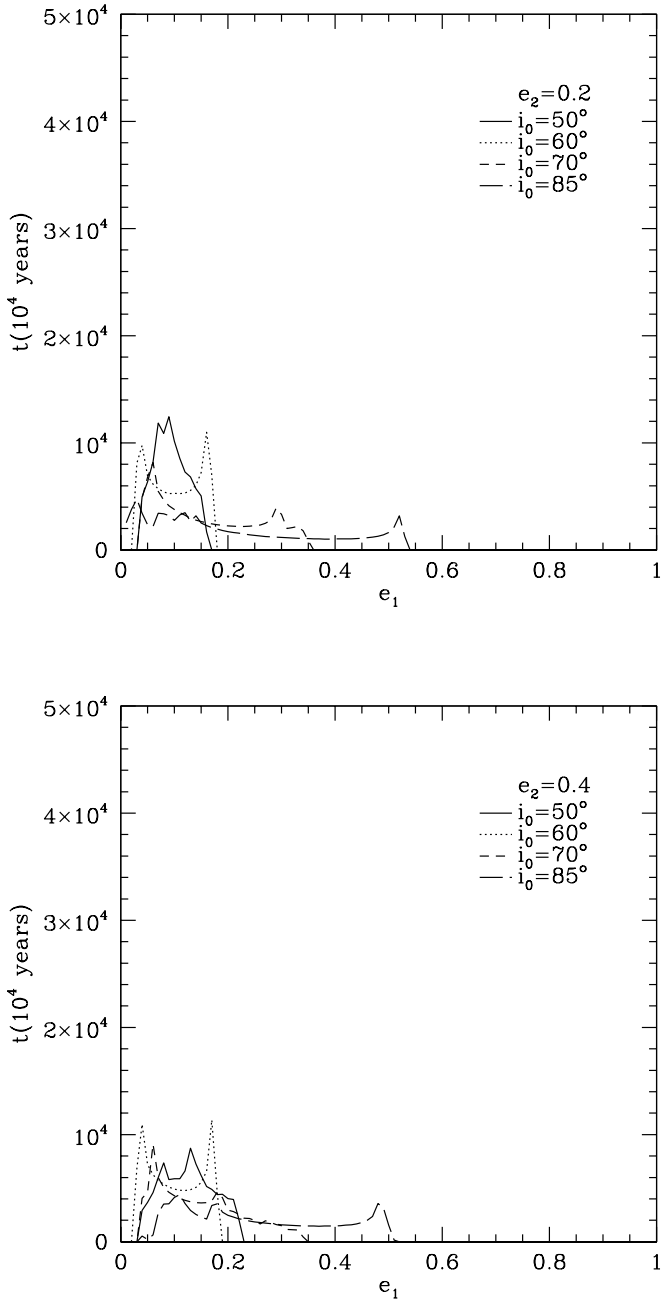

Fig. 4.8 Same as figure 6, but the top plot has $e_2 = 0.2$, bottom has $e_2 = 0.4$.

Table 4.2. $e_{1,max}$ for Jovian inner planet versus eccenricity of the outer orbit. Outer planet has $i(0) = 40$ degrees.

i_0	$\log m_2(M_\odot)$						
	-5.0	-4.5	-4.0	-3.5	-3.0	-2.5	-2.0
0.05	0.03131	0.03380	0.04165	0.06314	0.10846	0.15962	0.19079
0.1	0.03140	0.03408	0.04256	0.06924	0.12040	0.17280	0.20324
0.2	0.03158	0.03462	0.04434	0.08132	0.14573	0.20021	0.23005
0.4	0.03198	0.03576	0.04791	0.10485	0.20463	0.27267	0.30819
0.7	0.03280	0.03822	0.05547	0.12769	0.44572	0.47149	0.48569

Chapter 5

Summary and Conclusions

Three body dynamics are of particular interest in clusters where the density provides a greater opportunity for interactions. Globular clusters, which have had densities of tens to hundreds of thousands of stars per cubic parsec for billions of years, are the ideal laboratory for studying dynamics in systems which at best have solutions in only the mathematical sense of the word. It is also believed that most stars like the sun are formed in dense clusters (Lada et al. 1993), some of which it has just now become within our abililty to model (Hurley 2008). Modelling these systems in a realistic way which includes all stars individually represented, with their evolution and inclusion into a comparable number of binaries as is seen in observed clusters, has driven computer hardware and software for decades (Heggie & Hut 2003). In this thesis, I have used several techniques to answer the following questions: How many black hole binaries will a cluster produce, and will they have the required properties to be seen by our gravitational wave detectors? How often does the crowded environment of star forming cluster allow the exchange of a planet between stars? To answer these questions, I have studied three scenarios: the interaction of black holes in clusters, the effect of the Kozai mechanism on pulsars in clusters, and the effect of an exchanged planetary body on a planetary system.

In order to compare our models to the reality with which nature presents us, unusual objects have been identified such as pulsar binaries and blue stragglers in an attempt to reproduce their distributions and qualities in detail. The successfully vetted model can then be used to answer even deeper questions such as: how does an exchanged planet influence life on the native planets, i.e. those planets which form along with their host star?

In chapter 2, I examined the interactions of a system of black holes in a globular cluster. Previous studies had used the assumption that all black holes have the same mass, and as such when interacting tended to eject themselves to the very last one or two (Sigurdsson & Hernquist 1993; Kulkarni et al. 1993; Portegies Zwart & McMillan 2000). Since then, there has been progress in making a multi-mass distribution in initial black hole masses by Belczynski et al. (2004). This is important as getting away from equal mass black holes reduces the efficiency of three-body interactions in ejecting the binary (Sigurdsson & Phinney 1993). The previous paradigm for black holes was that all black holes were 10 solar masses. The distribution of masses now runs up to 50 or 80 $M_{\odot}$ depending on metallicity, which already makes it more difficult to eject the black hole (Miller & Hamilton 2002b). My new calculations have reduced the efficiency of three-body interactions in ejecting the binary due to their non-equal masses. One successful merger between two heavier black holes, which is preferred in three-body interactions, can already make an object over 100 $M_{\odot}$, which is in the intermediate mass black hole range. However, most observed candidates are thought to be in the $10^3 - 10^4 M_{\odot}$ range,

so further mergers or accretion of matter would be required. Work in the area of the second and subsequent mergers was done by Holley-Bockelmann et al. (2008).

Current population synthesis models leave much to be desired in terms of the understanding of physics which goes into the studies. In particular, close evolution of binaries and the common envelope phase, as well as mass loss through winds, are the areas that are most unsure, and yet they are also responsible for the most massive black holes. My new calculations have reduced the efficiency of three-body interactions in ejecting the binary due to their non-equal masses. I also use timescales derived from earlier simulations of clusters (Sigurdsson 1995) to determine the end state of individual binaries interacting with single black holes. While N-body simulations of black hole systems such as in O'Leary et al. (2006) are less model dependent, my method can easily adapt to advances in the understanding of the processes that make black holes and rapidly produce results on rates of binary black hole mergers for gravitational wave observations and the possibilities of intermediate mass black hole seeds.

Numerous black hole binaries are produced by clusters, they are hardened in the potential of the cluster, and the most massive black holes survive the interactions. Interactions with the other black holes preferentially produce binaries with higher eccentricities. Most are ejected. I found that as many as one in seven binaries will coalesce within a Hubble time, and with the strength of signal that their higher mass gives they would rival galactic black hole binaries as a background source. Compare this to the more pessimistic forecast in Kulkarni et al. (1993) that they would not be a significant background source. They suggest black hole binaries would be ejected with a separation of 1AU and a t_{GW} 10^{14}. With heavier binaries, the separation can be reduced to a few tenths of an AU before ejection, with a concommitant reduction in t_{GW} of 3 or 4 orders in magnitude. I also found that the binaries are ejected from the cluster with, for the most part, a velocity just above the escape speed of the cluster which is a few tens of km/sec. These gravitational wave sources are thus confined to their host galaxies as the galactic escape velocity is some hundreds of km/sec which only a very few binaries achieve in special cases (i.e. originally forming as a tight binary, their first three-body interaction liberates a large amount of kinetic energy). It is therefore fitting to perhaps take a census of galaxies and their clusters within the radius that the binaries would be visible to LIGO to estimate how many sources could be seen, especially considering the first extra-galactic black hole in a globular cluster being recently discovered (Maccarone et al. 2007). A similar project in a more general sense was done by Sadowski et al. (2008) using the simulations of O'Leary et al. (2006), but only in passing mentioning ejected cluster black hole binaries.

In Chapter 3, I studied the effect of the Kozai mechanism on two pulsars, one in the globular cluster M4, and the other J1903+0327. The M4 pulsar pulsar was found to have an unusually large orbital eccentricity and second derivative of the rotation period, given that it is in a binary with a period of nearly 200 days. This unusual behavior led to the conclusion that a planet-like third body of much less than a solar mass was orbiting the binary. Theories of the third object's formation, whether by gravitational collapse of circumstellar material (Beer et al. 2004; Livio et al. 1992) or by dynamical exchanges (Sigurdsson 1993; Ford et al. 2000a), can be differentiated by the inclination range for the planet which they predict. Scenarios which form the planet *in situ* tend

to leave it in a low inclination orbit and must rely on interactions with other stars to produce the observed eccentricity. Dynamical exchanges can deposit the planet in a highly inclined orbit, which can lead to eccentricity pumping by the Kozai effect. The Kozai effect requires a minimum inclination of the two orbits of about 40 degrees. Ford et al. (2000b) did a study of which values of mass and inclination could produce the observed eccentricity of this binary and a couple of other triple systems. I used my own code to integrate the secular evolution equations with a broad set of initial conditions to determine the first detailed properties of the third body; namely that the mass of the planet is about that of Jupiter.

As the dense environment of clusters should lead to many interactions, some hierarchical triples should form from binary-binary interactions. Miller & Hamilton (2002a) used this to produce another channel for black hole binary mergers. If one of the members of the inner binary is a pulsar, the Kozai effect could lead to periastron precession that would need to be separated from the expected post-Keplerian precession. Triple systems that are kicked out of the cluster upon formation would be free from the destructive influence of interactions from other stars and could wander far. The pulsar J1903+0327 found by Champion et al. (2008) consists of a 2.15ms pulsar and a near solar mass companion in an $e = 0.44$ orbit (the eccentricity of the pulsar binary in M4 is 0.025). A preliminary study of this pulsar showed that the high eccentricity can be reproduced by my models, and there are three candidate globular clusters from which this pulsar could have originated. My study of J1903+0327 provides a window onto possible formation scenaios of this interesting object. Radial velocity and proper motion study of this object could eventually identify the origin.

Other uses of the Kozai mechanism in clusters include the production of blue straggler stars. Blue stragglers are stars which, given a population, have a higher temperature and luminosity than should exist. Two main channels are thought to produce blue straggler stars, collisional interactions which would be enhanced in clusters, and mass transfer in close binaries. My idea, which I included in a Cycle 17 Hubble theory proposal, was that a third hybrid channel could exist by use of the Kozai mechanism. Main sequence binary-binary interactions which did not directly produce a collision could end in a hierarchical triple system which would periodically pump up the eccentricity of the inner binary and, through tidal circularization and drag, create a close binary that would merge into a blue straggler. These would have dynamical characteristics of collisional blue stragglers, but look spectroscopically like mass transfer blue stragglers. Perets & Fabrycky (2009) published work on this subject.

Chapter 4 describes my third project, which was a study of the effect of a planet at 50 AU on the inner solar system. The origin of this planet is assumed to be from an exchange with another solar system in the early stages of the sun's life while it was still in the dense star forming region where it was born. Planets have recently been directly imaged around Fomalhaut (Kalas et al. 2008) and HR8799 (Marois et al. 2008) in 100AU orbits which show that planets can form in orbits which are well placed to undergo exchange in the early history of a star. Similar studies have been done with the exchange of stars among binaries by Malmberg et al. (2007b). The exchange once again allows the Kozai effect to bring about drastic change in the inner system. A planet is chosen as the outer object as, unlike a stellar companion, it would remain unseen by

current radial velocity and direct observation methods, although it could be detected by upcoming astrometric missions. My study uses a outer body from the size of a super Earth to a brown dwarf, in various inclinations, and exerting its influence on an inner object modelled on the Earth or Jupiter. The 50 AU size of the outer orbit corresponds with the sharp drop off in Kuiper Belt objects. This result represents the first step in a much larger project to fully explore the parameter space. I found that the size of the outer orbit drastically affects the eccentricity obtained by the inner object due to the beating of the Kozai and general relativistic precessions. I also found that four-body calculation are needed for a full understanding of how the change in the outer native object's eccentricity is propagated to the inner native object. Simulations of young dense star forming clusters should illustrate how planetary sized objects are exchanged between stars.

In summary, I have explored the dynamics of exchanges between objects and the workings of the Kozai mechanism in my first two projects. These tools prepared me for work on a crucial issue in planet formation, that of how a peculiar subset of observed planets were formed. I have shown that exchanges and the Kozai mechanism can work together to produce the observed eccentricities of exoplanets. This is a new approach to the study of the dynamics of planet formation.

Bibliography

Aarseth, S. J. 1963, MNRAS, 126, 223

Aarseth, S. J. & Zare, K. 1974, Celestial Mechanics, 10, 185

Adams, F. C. & Laughlin, G. 2003, Icarus, 163, 290

—. 2006, International Journal of Modern Physics D, 15, 2133

Adams, F. C., Proszkow, E. M., Fatuzzo, M., & Myers, P. C. 2006, ApJ, 641, 504

Alpar, M. A., Cheng, A. F., Ruderman, M. A., & Shaham, J. 1982, Nature, 300, 728

Anosova, J. P., Orlov, V. V., & Aarseth, S. J. 1994, Celestial Mechanics and Dynamical Astronomy, 60, 365

Anosova, Z. P. 1990, Celestial Mechanics and Dynamical Astronomy, 48, 357

Backer, D. C., Foster, R. S., & Sallmen, S. 1993, Nature, 365, 817

Bahcall, J. N. & Ostriker, J. P. 1975, Nature, 256, 23

Bailyn, C. D. 1991, in Astronomical Society of the Pacific Conference Series, Vol. 13, The Formation and Evolution of Star Clusters, ed. K. Janes, 307–323

Bailyn, C. D. & Grindlay, J. E. 1990, ApJ, 353, 159

Barth, A. J., Ho, L. C., Rutledge, R. E., & Sargent, W. L. W. 2004, ApJ, 607, 90

Bate, M. R. 2009, MNRAS, 392, 590

Bate, M. R., Bonnell, I. A., & Bromm, V. 2003, MNRAS, 339, 577

Baumgardt, H., Hut, P., Makino, J., McMillan, S., & Portegies Zwart, S. 2003, ApJl, 582, L21

Beer, M. E., King, A. R., & Pringle, J. E. 2004, MNRAS, 355, 1244

Begelman, M. C. 2001, ApJ, 551, 897

Begelman, M. C. & Rees, M. J. 1978, MNRAS, 185, 847

Belczynski, K., Sadowski, A., & Rasio, F. A. 2004, ApJ, 611, 1068

Belczynski, K., Taam, R. E., Kalogera, V., Rasio, F. A., & Bulik, T. 2007, ApJ, 662, 504

Belczynski, K., Taam, R. E., Rantsiou, E., & van der Sluys, M. 2008, ApJ, 682, 474

Blaes, O., Lee, M. H., & Socrates, A. 2002, ApJ, 578, 775

Brown, M. E., Trujillo, C., & Rabinowitz, D. 2004, ApJ, 617, 645

Burrau, C. 1913, Astronomische Nachrichten, 195, 113

Burrows, A., Dessart, L., Livne, E., Ott, C. D., & Murphy, J. 2007, ApJ, 664, 416

Campanelli, M., Lousto, C., Zlochower, Y., & Merritt, D. 2007, ApJl, 659, L5

Champion, D. J., Ransom, S. M., Lazarus, P., Camilo, F., Bassa, C., Kaspi, V. M., Nice, D. J., Freire, P. C. C., Stairs, I. H., van Leeuwen, J., Stappers, B. W., Cordes, J. M., Hessels, J. W. T., Lorimer, D. R., Arzoumanian, Z., Backer, D. C., Bhat, N. D. R., Chatterjee, S., Cognard, I., Deneva, J. S., Faucher-Giguère, C.-A., Gaensler, B. M., Han, J., Jenet, F. A., Kasian, L., Kondratiev, V. I., Kramer, M., Lazio, J., McLaughlin, M. A., Venkataraman, A., & Vlemmings, W. 2008, Science, 320, 1309

Chernoff, D. F. & Weinberg, M. D. 1990, ApJ, 351, 121

Clairaut, A. C. 1760, Theorie du mouvement des cometes

Clark, G. W. 1975, ApJ, 199, L143

Clark, G. W., Markert, T. H., & Li, F. K. 1975, ApJ, 199, L93

Cordes, J. M. 1986, ApJ, 311, 183

Cresswell, P., Dirksen, G., Kley, W., & Nelson, R. P. 2007, A&A, 473, 329

de La Fuente Marcos, C. & de La Fuente Marcos, R. 1997, A&A, 326, L21

Euler, L. 1753, Theoria motus lunae : exhibens omnes eius inaequalitates : in additamento HOC idem argumentum aliter tractatur simulque ostenditur quemadmodum motus lunae cum omnibus inaequalitatibus innumeris aliis modis repraesentari atque AD calculum reuocari possit, ed. L. Euler

Fabbiano, G., Zezas, A., & Murray, S. S. 2001, ApJ, 554, 1035

Favata, M., Hughes, S. A., & Holz, D. E. 2004, ApJl, 607, L5

Filippenko, A. V. & Ho, L. C. 2003, ApJl, 588, L13

Ford, E. B., Joshi, K. J., Rasio, F. A., & Zbarsky, B. 2000a, ApJ, 528, 336

Ford, E. B., Kozinsky, B., & Rasio, F. A. 2000b, ApJ, 535, 385

Ford, E. B., Lystad, V., & Rasio, F. A. 2005, Nature, 434, 873

Freire, P. C. C., Ransom, S. M., Bégin, S., Stairs, I. H., Hessels, J. W. T., Frey, L. H., & Camilo, F. 2008a, ApJ, 675, 670

Freire, P. C. C., Wolszczan, A., van den Berg, M., & Hessels, J. W. T. 2008b, ApJ, 679, 1433

Freitag, M., Guerkan, M. A., & Rasio, F. A. 2007, in Astronomical Society of the Pacific Conference Series, Vol. 367, Massive Stars in Interactive Binaries, ed. N. St.-Louis & A. F. J. Moffat, 707–+

Fruchter, A. S., Stinebring, D. R., & Taylor, J. H. 1988, Nature, 333, 237

Fryer, C. L. & Kalogera, V. 2001, ApJ, 554, 548

Gebhardt, K., Rich, R. M., & Ho, L. C. 2002, ApJl, 578, L41

—. 2005, ApJ, 634, 1093

Gerssen, J., van der Marel, R. P., Gebhardt, K., Guhathakurta, P., Peterson, R. C., & Pryor, C. 2002, AJ, 124, 3270

Goldreich, P. & Tremaine, S. 1980, ApJ, 241, 425

González, J. A., Sperhake, U., Brügmann, B., Hannam, M., & Husa, S. 2007, Physical Review Letters, 98, 091101

Grindlay, J. & Gursky, H. 1976, ApJ, 205, L131

Grindlay, J. E. 1987, in IAU Symposium, Vol. 125, The Origin and Evolution of Neutron Stars, ed. D. J. Helfand & J.-H. Huang, 173–184

Grindlay, J. E., Hertz, P., Steiner, J. E., Murray, S. S., & Lightman, A. P. 1984, ApJ, 282, L13

Hagihara, Y. 1972, Celestial mechanics. Vol.2, pt.1: Perturbation theory; Vol.2, pt.2: Perturbation theory, ed. Y. Hagihara

Harrington, R. S. 1968, AJ, 73, 190

Harris, W. E. 1996, AJ, 112, 1487

Harrison, P. A., Lyne, A. G., & Anderson, B. 1993, MNRAS, 261, 113

Heggie, D. & Hut, P. 2003, The Gravitational Million-Body Problem: A Multidisciplinary Approach to Star Cluster Dynamics, ed. D. Heggie & P. Hut

Heggie, D. C. 1975, MNRAS, 173, 729

Heggie, D. C., Hut, P., & McMillan, S. L. W. 1996, ApJ, 467, 359

Heggie, D. C., Hut, P., Mineshige, S., Makino, J., & Baumgardt, H. 2007, PASJ, 59, L11

Hessels, J. W. T., Ransom, S. M., Stairs, I. H., Freire, P. C. C., Kaspi, V. M., & Camilo, F. 2006, Science, 311, 1901

Hills, J. G. 1975, AJ, 80, 809

Holley-Bockelmann, K., Gültekin, K., Shoemaker, D., & Yunes, N. 2008, ApJ, 686, 829

Holman, M., Touma, J., & Tremaine, S. 1997, Nature, 386, 254

Hurley, J. R. 2007, MNRAS, 379, 93

Hurley, J. R. 2008, in IAU Symposium, Vol. 246, IAU Symposium, ed. E. Vesperini, M. Giersz, & A. Sills, 89–98

Hurley, J. R. & Shara, M. M. 2002, ApJ, 565, 1251

Hut, P. 1983, AJ, 88, 1549

—. 1993, ApJ, 403, 256

Hut, P. & Bahcall, J. N. 1983, ApJ, 268, 319

Hut, P., Murphy, B. W., & Verbunt, F. 1991, A& A, 241, 137

Ibata, R. A., Gilmore, G., & Irwin, M. J. 1994, Nature, 370, 194

Innanen, K. A., Zheng, J. Q., Mikkola, S., & Valtonen, M. J. 1997, AJ, 113, 1915

Ivanova, N., Heinke, C. O., Rasio, F. A., Belczynski, K., & Fregeau, J. M. 2008, MNRAS, 386, 553

Jefferys, W. H. & Moser, J. 1966, AJ, 71, 568

Joshi, K. J. & Rasio, F. A. 1997, ApJ, 479, 948

Jurić, M. & Tremaine, S. 2008, ApJ, 686, 603

Kaaret, P., Prestwich, A. H., Zezas, A., Murray, S. S., Kim, D.-W., Kilgard, R. E., Schlegel, E. M., & Ward, M. J. 2001, MNRAS, 321, L29

Kalas, P., Graham, J. R., Chiang, E., Fitzgerald, M. P., Clampin, M., Kite, E. S., Stapelfeldt, K., Marois, C., & Krist, J. 2008, Science, 322, 1345

King, A. R., Davies, M. B., Ward, M. J., Fabbiano, G., & Elvis, M. 2001, ApJl, 552, L109

King, I. R. 1966, AJ, 71, 276

King, I. R. 1975, in IAU Symposium, Vol. 69, Dynamics of the Solar Systems, ed. A. Hayli, 99–+

Kozai, Y. 1962, AJ, 67, 591

Kramer, M., Bell, J. F., Manchester, R. N., Lyne, A. G., Camilo, F., Stairs, I. H., D'Amico, N., Kaspi, V. M., Hobbs, G., Morris, D. J., Crawford, F., Possenti, A., Joshi, B. C., McLaughlin, M. A., Lorimer, D. R., & Faulkner, A. J. 2003, MNRAS, 342, 1299

Kulkarni, S. R., Hut, P., & McMillan, S. 1993, Nature, 364, 421

Kustaanheimo, P. & Stiefel, E. 1965, Journal für die Reine und Angewandte Mathematik, 218, 204

Kuznetsov, E. D. & Kholshevnikov, K. V. 2006, Solar System Research, 40, 239

Lada, E. A., Strom, K. M., & Myers, P. C. 1993, in Protostars and Planets III, ed. E. H. Levy & J. I. Lunine, 245–277

Lagrange, J. L. 1772, Hist. de l'Acad. des Sci., 9

—. 1776, Mémoires des l'Academie Royale des Sciences et Belle-Lettres, 276

Landau, L. D. & Lifshitz, E. M. 1969, Mechanics, ed. L. D. Landau & E. M. Lifshitz

Laplace, P. S., Bowditch, N., & Bowditch, N. I. 1829, Mécanique céleste, ed. P. S. Laplace, N. Bowditch, & N. I. Bowditch

Larson, R. B. 1984, MNRAS, 210, 763

Laskar, J. 2008, Icarus, 196, 1

Latham, D. W., Stefanik, R. P., Torres, G., Davis, R. J., Mazeh, T., Carney, B. W., Laird, J. B., & Morse, J. A. 2002, AJ, 124, 1144

Lauer, T. R., Holtzman, J. A., Faber, S. M., Baum, W. A., Currie, D. G., Ewald, S. P., Groth, E. J., Hester, J. J., Kelsall, T., Light, R. M., Lynds, C. R., O'Neil, Jr., E. J., Schneider, D. P., Shaya, E. J., & Westphal, J. A. 1991, ApJL, 369, L45

Laughlin, G. & Adams, F. C. 1998, ApJl, 508, L171

Lee, H. M. 1995, MNRAS, 272, 605

Legel, L., Moody, K., & Sigurdsson, S. 2009, in preparation

Levison, H. F., Lissauer, J. J., & Duncan, M. J. 1998, AJ, 116, 1998

Lexell, A. J. 1778, Reflexions sur le temps periodique des cometes EN general

Lexell, J. A. & Maskelyne, N. 1779, Royal Society of London Philosophical Transactions Series I, 69, 68

Lin, D. N. C. & Ida, S. 1997, ApJ, 477, 781

Lineweaver, C. H. 2001, Icarus, 151, 307

Livio, M., Pringle, J. E., & Saffer, R. A. 1992, MNRAS, 257, 15P

Lorimer, D. R., Burgay, M., Freire, P. C. C., Lyne, A. G., Kramer, M., Possenti, A., McLaughlin, M. A., Camilo, F., Manchester, R. N., D'Amico, N., & Joshi, B. C. 2005, in Astronomical Society of the Pacific Conference Series, Vol. 328, Binary Radio Pulsars, ed. F. A. Rasio & I. H. Stairs, 113–+

Lyne, A. G., Biggs, J. D., Brinklow, A., McKenna, J., & Ashworth, M. 1988, Nature, 332, 45

Lyne, A. G., Brinklow, A., Middleditch, J., Kulkarni, S. R., & Backer, D. C. 1987, Nature, 328, 399

Lyne, A. G. & Lorimer, D. R. 1994, Nature, 369, 127

Maccarone, T. J., Kundu, A., Zepf, S. E., & Rhode, K. L. 2007, Nature, 445, 183

Mackey, A. D., Wilkinson, M. I., Davies, M. B., & Gilmore, G. F. 2007, MNRAS, 379, L40

—. 2008, MNRAS, 386, 65

Malmberg, D. & Davies, M. B. 2009, MNRAS, 394, L26

Malmberg, D., Davies, M. B., & Chambers, J. E. 2007a, MNRAS, 377, L1

Malmberg, D., de Angeli, F., Davies, M. B., Church, R. P., Mackey, D., & Wilkinson, M. I. 2007b, MNRAS, 378, 1207

Mapelli, M., Colpi, M., Possenti, A., & Sigurdsson, S. 2005, MNRAS, 364, 1315

Marchal, C. 1990, The three-body problem, ed. C. Marchal

Marcy, G. W. & Butler, R. P. 1996, ApJl, 464, L147+

Marois, C., Macintosh, B., Barman, T., Zuckerman, B., Song, I., Patience, J., Lafrenière, D., & Doyon, R. 2008, Science, 322, 1348

Matsumoto, H., Tsuru, T. G., Koyama, K., Awaki, H., Canizares, C. R., Kawai, N., Matsushita, S., & Kawabe, R. 2001, ApJ, 547, L25

Matsumura, S., Takeda, G., & Rasio, F. A. 2008, ApJL, 686, L29

Mayor, M. & Queloz, D. 1995, Nature, 378, 355

Mazeh, T., Krymolowski, Y., & Rosenfeld, G. 1997, ApJl, 477, L103+

McClintock, J. E., Shafee, R., Narayan, R., Remillard, R. A., Davis, S. W., & Li, L.-X. 2006, ApJ, 652, 518

McClure, R. D., Vandenberg, D. A., Smith, G. H., Fahlman, G. G., Richer, H. B., Hesser, J. E., Harris, W. E., Stetson, P. B., & Bell, R. A. 1986, ApJL, 307, L49

McKenna, J. & Lyne, A. G. 1988, Nature, 336, 226

Migaszewski, C. & Goździewski, K. 2009, MNRAS, 392, 2

Migliazzo, J. M., Gaensler, B. M., Backer, D. C., Stappers, B. W., Strom, R. G., & van der Swaluw, E. 2002, in Astronomical Society of the Pacific Conference Series, Vol. 271, Neutron Stars in Supernova Remnants, ed. P. O. Slane & B. M. Gaensler, 57–+

Miller, M. C. & Colbert, E. J. M. 2004, International Journal of Modern Physics D, 13, 1

Miller, M. C. & Hamilton, D. P. 2002a, ApJ, 576, 894

—. 2002b, MNRAS, 330, 232

Miocchi, P. 2007, MNRAS, 381, 103

Morbidelli, A. & Levison, H. F. 2004, AJ, 128, 2564

Murray, N., Hansen, B., Holman, M., & Tremaine, S. 1998, Science, 279, 69

Naef, D., Latham, D. W., Mayor, M., Mazeh, T., Beuzit, J. L., Drukier, G. A., Perrier-Bellet, C., Queloz, D., Sivan, J. P., Torres, G., Udry, S., & Zucker, S. 2001, A&A, 375, L27

Newton, H. A. 1893, Memoires of the Nationa Academy of Sciences, 6, 7

Norris, J. E., Freeman, K. C., Mayor, M., & Seitzer, P. 1997, ApJl, 487, L187+

Norris, J. E., Freeman, K. C., & Mighell, K. J. 1996, ApJ, 462, 241

Noyola, E., Gebhardt, K., & Bergmann, M. 2008, ApJ, 676, 1008

O'Leary, R. M., Rasio, F. A., Fregeau, J. M., Ivanova, N., & O'Shaughnessy, R. 2006, ApJ, 637, 937

O'Shaughnessy, R., Kalogera, V., & Belczynski, K. 2005a, ApJ, 620, 385

O'Shaughnessy, R., Kaplan, J., Kalogera, V., & Belczynski, K. 2005b, ApJ, 632, 1035

Papaloizou, J. C. B., Nelson, R. P., & Masset, F. 2001, A&A, 366, 263

Papaloizou, J. C. B. & Terquem, C. 2001, MNRAS, 325, 221

—. 2006, Reports on Progress in Physics, 69, 119

Perets, H. B. & Fabrycky, D. C. 2009, ApJ, 697, 1048

Peters, P. C. 1964, Physical Review, 136, 1224

Phinney, E. S. 1992, Royal Society of London Philosophical Transactions Series A, 341, 39

Piotto, G., Sosin, C., King, I. R., Djorgovski, S. G., Rich, R. M., Dorman, B., Renzini, A., Phinney, S., & Liebert, J. 1997, in Stellar Ecology: Advances in Stellar Evolution,, 84–91

Poisson, S. D. 1808, Journal de lEcole Polytechnique, 15, 1

Portegies Zwart, S. F. & McMillan, S. L. W. 2000, ApJl, 528, L17

—. 2002, ApJ, 576, 899

Pryor, C. & Meylan, G. 1993, in Astronomical Society of the Pacific Conference Series, Vol. 50, Structure and Dynamics of Globular Clusters, ed. S. G. Djorgovski & G. Meylan, 357–+

Quintana, E. V., Lissauer, J. J., Chambers, J. E., & Duncan, M. J. 2002, ApJ, 576, 982

Ransom, S. M. 2008, in American Institute of Physics Conference Series, Vol. 983, 40 Years of Pulsars: Millisecond Pulsars, Magnetars and More, ed. C. Bassa, Z. Wang, A. Cumming, & V. M. Kaspi, 415–423

Rappaport, S., Podsiadlowski, P., Joss, P. C., Di Stefano, R., & Han, Z. 1995, MNRAS, 273, 731

Rappaport, S., Putney, A., & Verbunt, F. 1989, ApJ, 345, 210

Rasio, F. A. 1994, ApJl, 427, L107

Rasio, F. A. & Ford, E. B. 1996, Science, 274, 954

Rich, R. M., Sosin, C., Djorgovski, S. G., Piotto, G., King, I. R., Renzini, A., Phinney, E. S., Dorman, B., Liebert, J., & Meylan, G. 1997, ApJl, 484, L25+

Robertson, H. P. 1938, Zeitschrift fur Astrophysik, 15, 69

Sadowski, A., Belczynski, K., Bulik, T., Ivanova, N., Rasio, F. A., & O'Shaughnessy, R. 2008, ApJ, 676, 1162

Sigurdsson, S. 1993, ApJl, 415, L43

—. 1995, ApJ, 452, 323

Sigurdsson, S. & Hernquist, L. 1993, Nature, 364, 423

Sigurdsson, S. & Phinney, E. S. 1993, ApJ, 415, 631

Sigurdsson, S., Richer, H. B., Hansen, B. M., Stairs, I. H., & Thorsett, S. E. 2003, Science, 301, 193

Sigurdsson, S. & Thorsett, S. E. 2005, in Astronomical Society of the Pacific Conference Series, Vol. 328, Binary Radio Pulsars, ed. F. A. Rasio & I. H. Stairs, 213–+

Silk, J. & Arons, J. 1975, ApJ, 200, L131

Soderhjelm, S. 1984, A&A, 141, 232

Spitzer, Jr., L. 1975, in IAU Symposium, Vol. 69, Dynamics of the Solar Systems, ed. A. Hayli, 3–26

Spitzer, L. J. 1969, ApJL, 158, L139+

Sundman, K. F. 1912, Acta MAthematica, 36, 105

Swank, J. H., Becker, R. H., Boldt, E. A., Holt, S. S., Pravdo, S. H., & Serlemitsos, P. J. 1977, ApJ, 212, L73

Szebehely, V. 1967, Theory of orbits. The restricted problem of three bodies, ed. V. Szebehely

Szebehely, V. & Peters, C. F. 1967, AJ, 72, 876

Takeda, G. & Rasio, F. A. 2005, ApJ, 627, 1001

Thorsett, S. E., Arzoumanian, Z., Camilo, F., & Lyne, A. G. 1999, ApJ, 523, 763

Thorsett, S. E., Arzoumanian, Z., & Taylor, J. H. 1993, ApJl, 412, L33

Tisserand, F. 1889, Bulletin Astronomique, Serie I, 6, 289

Trenti, M., Ardi, E., Mineshige, S., & Hut, P. 2007, MNRAS, 374, 857

Udry, S., Bonfils, X., Delfosse, X., Forveille, T., Mayor, M., Perrier, C., Bouchy, F., Lovis, C., Pepe, F., Queloz, D., & Bertaux, J.-L. 2007, A&A, 469, L43

Valtonen, M. & Karttunen, H. 2006, The Three-Body Problem, ed. M. Valtonen & H. Karttunen

Valtonen, M. J. & Aarseth, S. J. 1977, Revista Mexicana de Astronomia y Astrofisica, vol. 3, 3, 163

van den Bosch, R., de Zeeuw, T., Gebhardt, K., Noyola, E., & van de Ven, G. 2006, ApJ, 641, 852

van der Marel, R. P., Gerssen, J., Guhathakurta, P., Peterson, R. C., & Gebhardt, K. 2002, AJ, 124, 3255

Veras, D. & Armitage, P. J. 2004, Icarus, 172, 349

—. 2005, ApJL, 620, L111

Verbunt, F. & Hut, P. 1987, in IAU Symposium, Vol. 125, The Origin and Evolution of Neutron Stars, ed. D. J. Helfand & J.-H. Huang, 187–+

Ward, P. & Brownlee, D. 2000, Rare earth : why complex life is uncommon in the universe, ed. P. Ward & D. Brownlee

Weidenschilling, S. J. & Marzari, F. 1996a, Nature, 384, 619

—. 1996b, Nature, 384, 619

Wolszczan, A. & Frail, D. A. 1992, Nature, 355, 145

Wyller, A. A. 1970, ApJ, 160, 443

Zakamska, N. L. & Tremaine, S. 2004, AJ, 128, 869

Vita
Kenneth Moody

Education

The Pennsylvania State University State College, Pennsylvania 2002–Present

Ph.D. in Astronomy & Astrophysics, expected in December 2009

Indiana University Bloomington, Indiana 1998–2002

B.S. in Astronomy, *summa cum laude* with distinction in the major

Awards and Honors

Indiana University Astronomy Excellence 2002

Zaccheus Daniel Foundation for Astronomical Science Grant 2005, 2006

Research Experience

Doctoral Research The Pennsylvania State University 2004–Present

Thesis Advisor: Prof. Steinn Sigurdsson

Black hole binariy mergers. Kozai mechanism by jovian mass objects.

Graduate Research The Pennsylvania State University 2003–2005

Research Advisor: Prof. George G. Pavlov

Visible and near-infrared photometry of the field near pulsar 1E1207.

Teaching Experience

Teaching Assistant The Pennsylvania State University 2002

Astro 11 lab.